5 q T

NASA CONTRACTOR REPORT

NASA CR-141419

ALTIMETER WAVEFORM SOFTWARE DESIGN

G. S. Hayne
L. S. Miller
G. S. Brown

FINAL REPORT

Prepared Under Contract No. NAS6-2520 by

Applied Science Associates, Inc.
105 East Chatham Street
Apex, North Carolina 27502

National Aeronautics and
Space Administration

Wallops Flight Center
Wallops Island, Virginia 23337
AC 804 824-3411

June 1977

1. Report No.	2. Government Accession No.	3. Recipient's Catalog No.
NASA CR-141419		

4. Title and Subtitle	5. Report Date
ALTIMETER WAVEFORM SOFTWARE DESIGN	June 1977
	6. Performing Organization Code

7. Author(s)	8. Performing Organization Report No.
G. S. Hayne, L. S. Miller, and G. S. Brown	
	10. Work Unit No.

9. Performing Organization Name and Address	11. Contract or Grant No.
Applied Science Associates, Inc. 105 East Chatham Street Apex, North Carolina 27502	NAS 6-2520
	13. Type of Report and Period Covered
12. Sponsoring Agency Name and Address	Final Report, Task 3.1
NASA, Wallops Flight Center Wallops Island, Virginia 23337	14. Sponsoring Agency Code

15. Supplementary Notes

16. Abstract

This report covers the subject of preprocessing techniques for raw return waveform data from the GEOS-3 radar altimeter. Specifically it contains sections on: (1) general altimeter data preprocessing to be done at the Wallops Flight Center GEOS-3 Data Processing Center to correct altimeter waveform data for temperature calibrations, to convert between engineering and final data units and to convert telemetered parameter quantities to more appropriate final data distribution values: (2) time "tagging" of altimeter return waveform data quantities to compensate for various delays, misalignments and calculational intervals; (3) data processing procedures for use in estimating spacecraft attitude from altimeter waveform sampling gates, and (4) feasibility of use of a ground-based reflector or transponder to obtain in-flight calibration information on GEOS-3 altimeter performance.

17. Key Words (Suggested by Author(s))	18. Distribution Statement
Radar Altimeters Radar Data Radar Altimeter Calibration Radar Altimeter Evaluation	Unclassified, Unlimited Star Category 19

19. Security Classif. (of this report)	20. Security Classif. (of this page)	21. No. of Pages	22. Price*
Unclassified	Unclassified	128	

*For sale by the National Technical Information Service, Springfield, Virginia 22151

TABLE OF CONTENTS

TABLE OF CONTENTS (Cont.)

LIST OF FIGURES

LIST OF TABLES

1.0 INTRODUCTION AND SUMMARY

This is the final technical report on Task 3.1 of NASA Contract No. NAS6-2520. Task 3.1 covers the subject of preprocessing techniques for raw data from the GEOS-C radar altimeter, and the major portion of our work on this task has been concerned with first assuring that adequate pre-flight calibration data were obtained and then assisting the NASA Wallops Flight Center data processing personnel in properly using these calibration data for the GEOS-C radar altimeter Flight Model. Our work on the subject of pre-flight calibration data continues activity of an earlier contract [1]. In addition to the work described in the present report, there have been several visits to the GEOS-C radar altimeter testing, both at GE in Utica, N. Y., and at APL in Silver Spring, Maryland; several informal memoranda have been written on the subject of altimeter testing. One of these memoranda is reproduced in Appendix A because it relates to tests not yet conducted. Some of these tests could be done post-launch using the altimeter Protoflight Model, if experience with the satellite data indicates the need for such additional information.

Chapter 2 of this report discusses the general data preprocessing to be done at the NASA Wallops Flight Center and then the relationship between Telemetry Counts, Engineering Units, and Functional Units and radar altimeter temperatures (these various quantities to be defined in Chapter 2) as this relationship is implemented by the Wallops preprocessing programs. A number of tables are provided, each indicating a best estimate, based on the calibration data available to us during the period of Task 3.1, of the calibration data to be used in the Wallops altimeter data conversion and correction process.

Chapter 3 examines the question of what time to associate with a given radar altimeter altitude output, both for the "instantaneous" ~ 100 per second altitudes out of the Telemetry Mode 3 (the second of the two high-data-rate telemetry modes) and for the "average" ~ 10 per second altitudes from Telemetry Modes 1 and 2.

Chapter 4 provides information on the estimation procedure which uses the "Average Plateau Gate" and the "Average Attitude/Specular Gate" outputs

of the radar altimeter to form an estimate of the attitude, the angle by which the altimeter's antenna beam axis is off nadir. The attitude estimation curve is derived, and estimates are obtained for the pointing angle estimation error which arises from the statistical nature of the gate outputs. Chapter 4 concludes with a discussion of effects of several practical factors such as gate nonlinearities, saturation, etc.

Chapter 5 examines the feasibility of using a ground-based reflector, or else a ground-based transponder, to obtain additional in-flight calibration information on the GEOS-C altimeter. The conclusion is that a passive reflector is not practical but that an active transponder might be, and that this question should be re-examined following the GEOS-C post-launch evaluation period.

In the work summarized in this report, G. S. Brown has been primarily responsible for the contents of Chapter 4 and for the major portion of the monitoring of the radar altimeter testing when it was in progress. L. S. Miller has contributed Chapters 3 and 5, and G. S. Hayne was responsible for Chapter 2 and for the final organization of this report.

2.0 GEOS-C CALIBRATION PROCEDURES AND DATA

Our principal activity in this area has been to assist in developing the NASA/WFC data processing operations and in obtaining and using pre-flight calibration data for the GEOS-C radar altimeter. Some degree of general "best engineering judgement" has been involved in selecting and editing the data. In this report chapter we present a variety of calibration tables for the various altimeter quantities of interest after discussing the general relationship between telemetry counts, "Engineering Units", and "Functional Units" and then discussing the type of interpolation which should be employed. First we define the sources for the data presented later in this chapter.

The key documents, from which the altimeter Flight Model calibration data in Chapter 2 were derived, are listed as References 2-4. Reference 2 defines the Electrical Performance Test Procedure (EPTP) followed in obtaining the Flight Unit data given in these references. There also exist as well EPTP data for the Engineering Model and the Protoflight Model of the altimeter, and any post-launch testing on the Protoflight Model (to clarify some of the Flight Model's properties) will require study of the Protoflight Model's equivalent of the Flight Model's References 3 and 4. A variety of other data, not specifically part of the EPTP set, also exists for the different altimeter models and these data have in general been microfilmed for (and are thus obtainable from) the Applied Physics Laboratory; at the end of Chapter 4 of this report, one possible use for the Protoflight Model data is described.

The calibration data tables in this chapter are based only upon the data that we had as of February and March 1975; that is, these tables are derived only from References 2-4. We expect that some of these tables may change as a result of further examination of data from the Flight Model further testing at APL or at Goddard, but this is information not yet available to us.

2.1 General Relationship Between Telemetry Counts, Engineering Units, and Functional Units.

The GEOS-C radar altimeter presents a number of signals as voltage levels to the telemetry interface aboard the spacecraft; these voltages are converted (by either high-speed or by low-speed analog-to-digital converters, as appropriate to the individual quantities) to telemetry counts and then transmitted to Earth-based receiving stations. The major exception to this is the 32 bit altitude word (or the cumulative altitude word, depending upon telemetry mode) which is transmitted as four separate 8-bit words. The voltage levels of the spacecraft's altimeter-telemetry interface are functions of other fundamental quantities and we will say that these fundamental quantities are in Functional Units (FU). The signal presented (in volts) to the altimeter-telemetry interface will be said to be in Engineering Units (EU), and the information will be transmitted in Telemetry Counts (TM). One name will designate a given quantity but the quantity will be in FU, EU, or TM depending upon where one is looking in the overall data flow.

As a specific example, look at the receiver AGC voltage designated as RAGC.* RAGC is ultimately a measure of the peak signal power level into the radar altimeter receiver and the Functional Units for RAGC are dBm. The Engineering Units for RAGC are volts. Instead of "Engineering Units", this might just as well have been designated as "Telemetry Volts" or anything else as long as one was consistent. Many of the altimeter quantities of interest have Functional Units of volts and it seemed inadvisable to have two different kinds of volts in a discussion of given signal. The label "Engineering Units" has come to denote the altimeter signal's voltage as applied to the altimeter-telemetry interface and we continue that usage in this report.

*This signal designation is used by the Applied Physics Laboratory and by NASA/Wallops Flight Center. Unfortunately the General Electric Company has an entirely different signal nomenclature and the APL-designated RAGC is designated by GE as V(AGC). We will use the APL & WFC designation in all of this report.

Figure 2-1 provides a brief summary of relevant portions of the NASA/WFC processing of altimeter quantities. The magnetic tapes out of the three programs CALIMERGE, GAP, and ARC have exactly the same data format but different operations on parts of the data are performed in these programs. Program CALIMERGE in general converts from TM to EU by "scaling", by applying the appropriate scale factor. Some quantities in CALIMERGE are converted directly to FU; the larger number of quantities are converted from EU to FU in program GAP which follows CALIMERGE. CALIMERGE also performs some limit checks on quantities in EU to verify that those are within the known calibration range.

Table 2-1 summarizes the quantities converted directly from TM to FU in CALIMERGE; the conversion in general uses a table look-up procedure already implemented at NASA/WFC and we will not repeat in this report those tables. Notice that we indicate the Range Servo Error RSE in Table 2-1 as a signal which could have been converted directly from TM→FU in a one-step process. It happens that RSE is now being handled by the two-step procedure TM→EU→FU, and the discussion of RSE in sub-section 2.3.2 will supply proper conversion recipes for both the one-step and the two-step conversion of RSE from TM to FU.

Table 2-2 lists altimeter quantities converted by the two-step procedure; conversion from TM→EU occurs in CALIMERGE using the scaling or conversion rules in the table, and then conversion from EU→FU occurs in GAP. Each quantity's telemetry count (TM) can range from 0 counts to a maximum of 255 counts, and the EU limits corresponding to these TM limits are shown in the next two columns in the table. Most of the EU→FU conversions are temperature-dependent, and the relevant temperatures are noted in the rightmost column of Table 2-2.

Notice that a major problem not treated in this report is the question of which altimeter quantities are to be converted and printed out in each mode or submode of the radar altimeter. For example RAGC has a high value during BIT/CAL steps Video #1 and Video #2, but this high value is of no practical significance and hence there is no point in carrying out the TM→EU→FU conversion process in CALIMERGE and GAP for RAGC in these two steps of BIT/CAL. To avoid meaningless error messages from out-of-range but

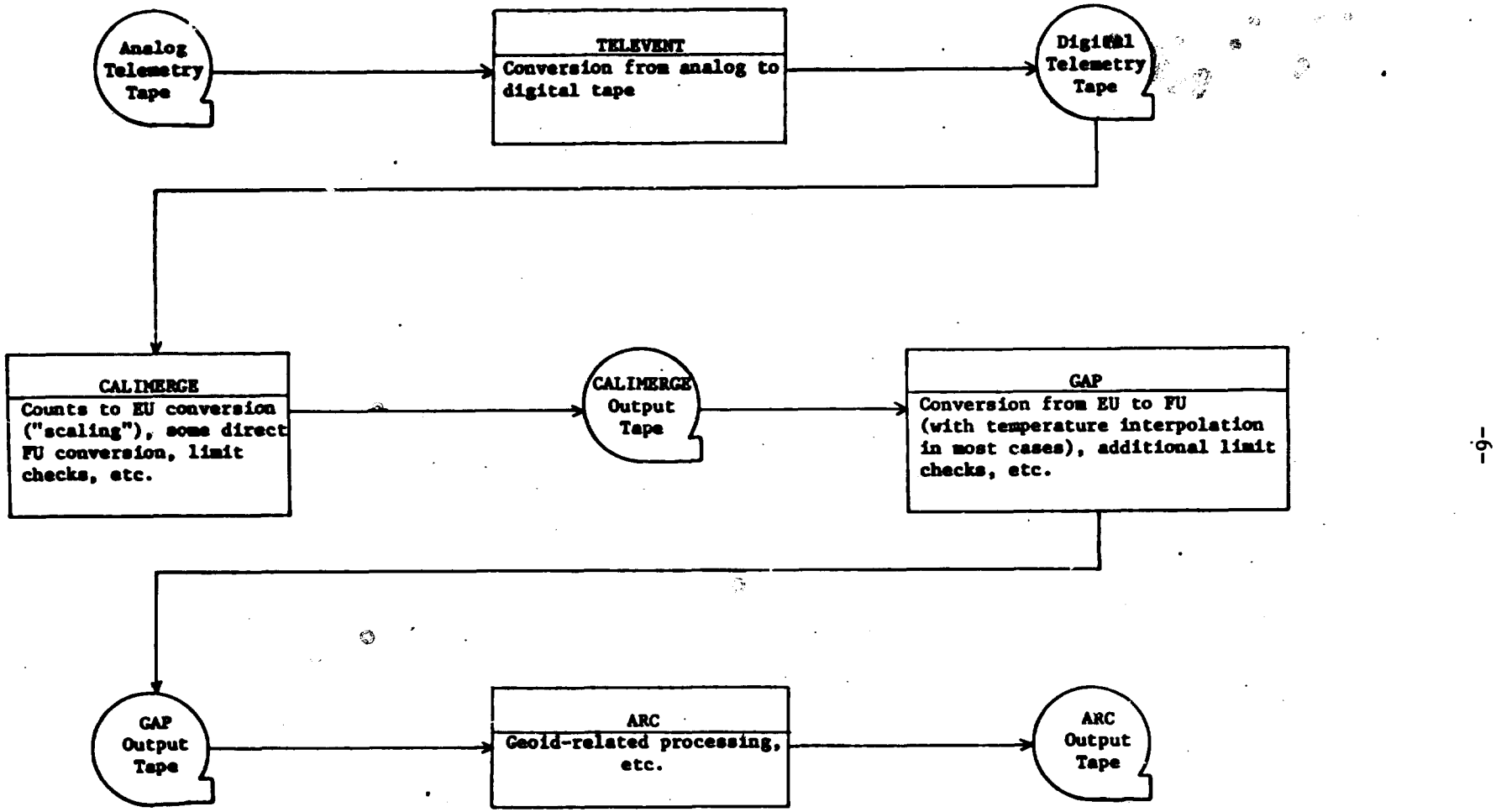

Figure 2-1. Partial Summary of Data Flow for Altimeter Quantities

Table 2-1. Altimeter Quantities Directly Converted TM→FU (TM=Telemetry Counts, FU=Functional Units).

Nomenclature APL	Nomenclature GE	Altimeter Signal	Functional Units	Notes
RTT	TT1	Transmitter Temperature	^{o}C	a
RRT	TT2	Receiver Temperature	^{o}C	a
GTT	TT3	Global Tracker Temperature	^{o}C	a
ITT	TT4	Intensive Tracker Temperature	^{o}C	a
WST	TT5	Waveform Sampler Temperature	^{o}C	a
BCT	TT6	BIT/CAL Temperature	^{o}C	a
RMI	$V(I_x)$	Receiver Mixer Current	volts	b
ALT		Altitude	meters	c
CALT		Cumulative Altitude	meters	d
RSE	$V(T_j)$	Range Servo Error	centimeters	e

Notes:

a - The same conversion table relating counts to degrees centigrade, applies to all six temperatures from the altimeter.

b - The "receiver mixer current" actually is a monitor voltage which is related to the current in the receiver mixer.

c - In the Intensive Mode of the tracker, the least significant bit of the 32 bit altitude word is 1.56257813 ns, and in the Global Mode the least significant bit is four times as great, or 6.25031252 ns. These bit weights must be multiplied by the speed of light (in m/ns) and then applied to the 32 bit altitude word after the four appropriately bit-reversed 8 bit words from the telemetry system are reassembled into the 32 bit altitude.

d - The cumulative altitude word is the sum of 10 successive individual altitudes and the result must be divided by 10; otherwise note c applies.

e - It would be possible to directly convert RSE from counts to centimeters. Because of the way Wallops data processing programs are implemented however, RSE is now being converted via the Engineering Units two-step procedure. RSE is listed in this table only because of the (not implemented) direct conversion possibility.

Table 2-2. Altimeter Quantities Processed by TM→EU→FU (TM=Telemetry Counts, EU=Engineering Units, and FU=Functional Units).

Nomenclature APL	Nomenclature GE	Altimeter Signal	Tracker Mode(s)	TM→EU Conversion, EU in Volts, TM in Counts	EU Limits TM=0	EU Limits TM=255	Functional Units	Temperature Dependence
ARG	V(R)	Average Ramp Gate	G	.03247TM	0. V	8.280V	volts	a
"	"	" " "	I	"	"	"	volts	ITT
APG	V(P)	Average Plateau Gate	G	.03233TM	"	8.244	volts	a
"	"	" " "	I	"	0.	"	volts	ITT
IPG	$V(P_i)$	Instantaneous Plateau Gate	G	.032025TM-4.0844375	-4.084	4.082	volts	a
"	"	" " "	I	" "	"	"	volts	ITT
IFTA	V(IF/C)	IF Test Signal Amplitude	I&G	.03248TM	0.	8.282	volts	b
VTA	V(V/C)	Video Test Signal Amplitude	I&G	.03257TM	"	8.305	volts	c
RSA	V(CL)	Reference Signal Amplitude	I&G	.03252TM	"	8.293	volts	c
ANG	V(N)	Average Noise Gate	I&G	.03261TM	"	8.316	volts	GTT
AASG	V(A/S)	Average Attitude/ Specular Gate	I&G	.03250TM	"	8.288	volts	GTT
RSE	V(Tj)	Range Servo Error	I&G	.032025TM-4.0844375	-4.084		centimeters	d

Notes: a - Calibration data available at only one temperature; if more data can be found from the APL or Goddard testing, this altimeter signal may be dependent upon temperature GTT.

b - This BIT/CAL quantity may be dependent upon temperature BCT, but we have inadequate information for now.

c - To within relatively broad tolerances, this signal is simply present or absent and hence there is no practical temperature dependence.

d - Any temperature dependence disappears within the $\pm$ 20 millivolt limits discussed in the text.

Table 2-2. Altimeter Quantities Processed by TM→EU→FU (TM=Telemetry Counts, EU=Engineering Units, and FU=Functional Units). (Continued)

Nomenclature APL	Nomenclature GE	Altimeter Signal	Tracker Mode(s)	TM→EU Conversion, EU in Volts, TM in Counts	EU Limits TM=0	EU Limits TM=255	Functional Units	Temperature Dependence
RTP	$V(P_T)$	Transmitter Power	I&G	.03250TM	0. V	8.288V	dBm	RTT
RAGC	V(AGC)	Receiver AGC Voltage	I&G	.032025TM-4.0844375 Note e	-4.084	4.082	dBm	RRT
ARS1	IAW1	Average Return Sample #1	I&G	.03245TM	0.	8.275	volts	WST
ARS2	IAW2	" " #2	"	.03251TM	"	8.290	"	"
ARS3	IAW3	" " #3	"	.03260TM	"	8.313	"	"
ARS4	IAW4	" " #4	"	.03238TM	"	8.257	"	"
ARS5	IAW5	" " #5	"	.03255TM	"	8.300	"	"
ARS6	IAW6	" " #6	"	.03248TM	"	8.282	"	"
ARS7	IAW7	" " #7	"	.03246TM	"	8.277	"	"
ARS8	IAW8	" " #8	"	.03233TM	"	8.244	"	"
ARS9	IAW9	" " #9	"	.03255TM	"	8.300	"	"
ARS10	IAW10	" " #10	"	.03251TM	"	8.290	"	"
ARS11	IAW11	" " #11	"	.03239TM	"	8.259	"	"
ARS12	IAW12	" " #12	"	.03263TM	"	8.321	"	"
ARS13	IAW13	" " #13	"	.03221TM	"	8.214	"	"
ARS14	IAW14	" " #14	"	.03254TM	"	8.298	"	"
ARS15	IAW15	" " #15	"	.03245TM	"	8.275	"	"
ARS16	IAW16	Average Return Sample #16	I&G	.03240TM	0.	8.262	volts	WST

Note e - There are actually two AGC telemetry channels, RAGC-LO and RAGC-HI. The TM→EU conversion given here is for RAGC-LO; RAGC-HI has about twice the scale, from about -8 to +8 volts.

Table 2-2. Altimeter Quantities Processed by TM→EU→FU (TM=Telemetry Counts, EU=Engineering Units, and FU=Functional Units). (Continued)

Nomenclature APL	Nomenclature GE	Altimeter Signal	Tracker Mode(s)	TM→EU Conversion, EU in Volts, TM in Counts	EU Limits TM=0	EU Limits TM=255	Functional Units	Temperature Dependence
IRS1	IIW1	Instantaneous Return Sample #1	I	.032025TM-4.0844375	-4.084	4.082	volts	WST
IRS2	IIW2	" " " #2	"	" "	"	"	"	"
.	.	. . . .	.	. .	.	.	.	.
.	.	. . . .	.	. .	.	.	.	.
.	.	. . . .	.	. .	.	.	.	.
IRS16	IIW16	Instantaneous Return Sample#16	I	.032025TM-4.0844375	-4.084	4.082	volts	WST

meaningless altimeter quantities, the NASA/WFC processing must "know" what submode the altimeter is in and must process only the quantities of importance or significance to that altimeter submode.

2.2 Interpolation in Temperature and Engineering Units to Obtain Functional Units.

As shown in Table 2-2, many of the altimeter quantities of interest have a temperature dependence. Typical calibration data consist of sample points obtained for an Engineering Units (EU) vs. Functional Units (FU) curve at one altimeter temperature (T) with the entire process being repeated for several different temperatures. In this section we discuss the interpolation procedure to be used for all the temperature dependent quantities of Table 2-2.

Two informal memoranda* in 1974 had independently proposed use of a least-squares-fitted polynomial surface; the coefficients were to be determined by the least-squares fitting process and any other point on the surface could then be determined. The surface referred to here is of course FU as a function of EU and T, and the coefficients plus any given EU and T pair would produce a FU value. We subsequently† rejected the least-squares-fitted surface and proposed instead that simple linear interpolation in both EU and T be used. We summarize below some of our conclusions which were based upon various calculations using the radar altimeter Engineering Model data, the only data available at that time. We will not reproduce those numerical results which are of no use to the Flight Model with which this report is concerned. (We should indicate though that the Flight Model data is generally better behaved than the Engineering Model data.)

Briefly, the problems with the least-squares-determined polynomial coefficients lies in the different allowed range of EU for the different temperature curves and in the curvature between data points contributed by

---

*Informal memoranda to NASA/WFC: 1) from G. S. Hayne, Applied Science Associates, dated 7 August 1974, and 2) from J. Zarur, Wolf Research and Development, undated (probably middle August 1974).

†Letter to C. Leitao, NASA/WFC from G. S. Hayne, Applied Science Associates, dated 4 November 1974.

the polynomial fit which tends, outside the region for which data points are supplied, to go to plus or minus infinity. In general an interpolation polynomial fitted by least-squares methods will act as a smoothing function when the polynomial degree is much lower than the number of input data points. However when the polynomial degree is comparable to the number of input data points, the polynomial can exhibit severe oscillations between individual data values. For some of the altimeter quantities there are calibration data at only three different temperatures and even a second degree polynomial in temperature builds in a curvature between temperature pairs even though a linear behavior would seem more appropriate.

For these various reasons it seemed clear to us that a better procedure was to use linear interpolation between the different temperature curves. Moreover even for the curves of FU vs. EU at test temperatures, we should use linear interpolation between known points. Without a considerably larger number of data points (more densely sampled in both EU and T), we have no realistic basis for anything but the assumption of linear line segments between known data points.

Some judicious data editing should also be used. The FU vs. EU cannot be allowed to be multiple-valued in FU at any given EU; if a multiple-valued behavior appears at extremes of EU, the data points for the larger absolute values of FU should be simply deleted since this behavior is probably a saturation effect in the testing. Should the multiple values of FU occur near zero EU it will be necessary to adjust the data so that FU is restored to monotonic behavior with EU. (If this type of behavior does occur near the middle of the range of EU, we are probably in trouble anyhow and more calibration data would be warranted near this region of improper behavior.)

Figure 2-2 summarizes the procedure recommended for carrying out linear interpolation in both EU and T to produce a FU value. This was proposed as one processing step to be carried out for any temperature-dependent altimeter quantity; the same subroutine is used in all cases with only the tables of input data changing for different altimeter quantities. The remainder of Chapter 2 presents these tables of input data based upon the pre-flight Flight Model data available to us in References 3 and 4. Appendix B presents

Figure 2-2. Summary of Linear-Linear Interpolation Procedure.

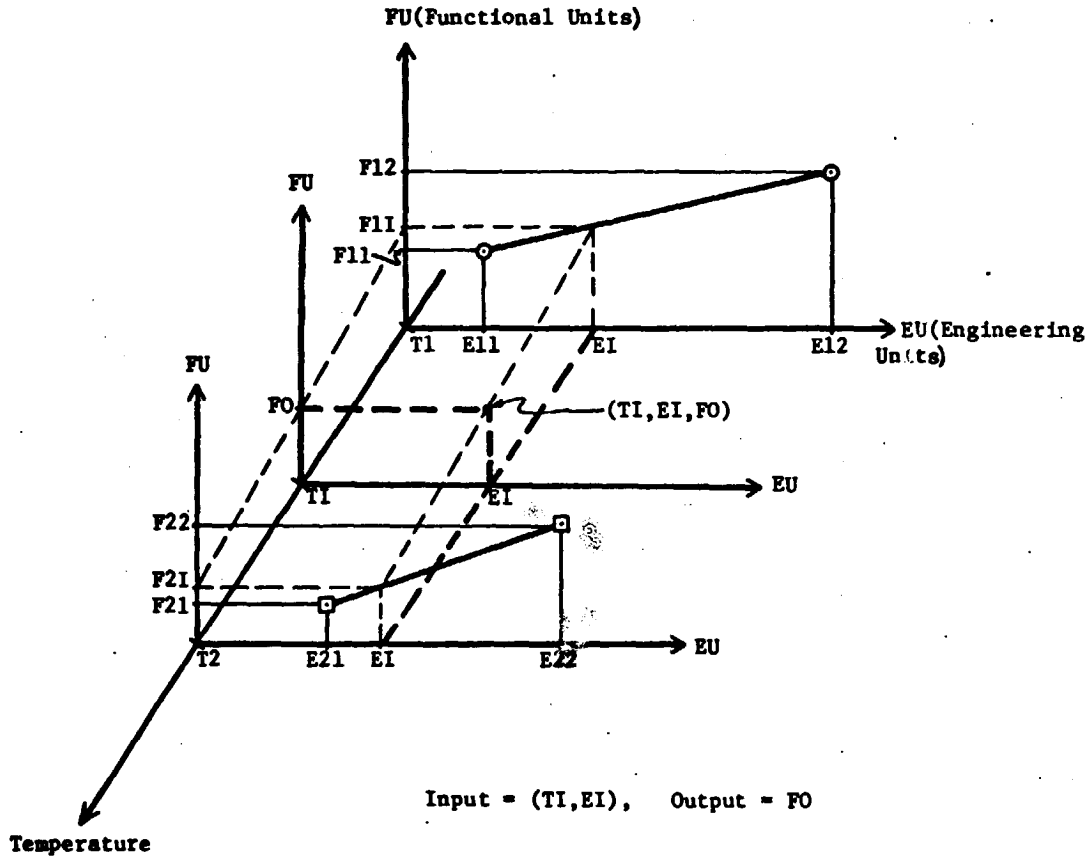

Input = (TI,EI), Output = FO

Procedure:

1. Find temperatures T1,T2 such that T1<TI<T2
2. Find points E11 and E12 on T1 curve such that E11<EI<E12
3. Find points E21 and E22 on T2 curve such that E21<EI<E22
4. $F1I = F11+(F12-F11)\times\frac{(EI-E11)}{(E12-E11)}$

   $F2I = F21+(F22-F21)\times\frac{(EI-E21)}{E(22-E21)}$

   $FO = F1I+(F2I-F1I)\times\frac{(TI-T1)}{(T2-T1)}$

a sample FORTRAN subroutine to carry out the linear-linear interpolation procedure of Figure 2-2 and also presents sample output from the subroutine based on data for the average waveform sample #1, ARS1.

These preceding paragraphs have discussed the double interpolation in EU and T. It should be obvious that for the simpler case of a single set of EU vs. FU points for an altimeter quantity with no known* temperature dependence the interpolation procedure to be used is based upon simple straight-line segments connecting successive pairs of input data points (i.e., simple linear interpolation).

2.3 Altimeter Data Quantities Whose Calibration Data Shows No Temperature Dependence.

The sub-sections of Section 2.3 present the available calibration data for those quantities of Table 2-1 and 2-2 which are identified as having no known temperature dependence.

2.3.1 Temperatures RTT, RRT, GTT, ITT, WST, and BCT.

These six temperatures (identified individually in Table 2-1) are measured by six different thermistors within the altimeter, and the direct conversion from telemetry counts to degrees centigrade is already implemented in the NASA/WFC programs. We will not reproduce that conversion table here. We do, however, present in Table 2-3 the conversion table for these thermistors from volts to degrees centigrade. This table is directly from Reference 4 and is reprinted here for the convenience of anyone analyzing various TAMS data (TAMS = GE's Test and Monitor System; see Reference 2); the TAMS output (and hence much of the pre-flight data taken at GE, APL or NASA/GSFC) records temperatures from these six thermistors in volts (EU).

2.3.2 The Range Servo Error RSE.

The Range Servo Error, RSE, voltage at the GEOS-C radar altimeter output

---

*The word "known" is important here. For instance we are now treating the Global Mode quantities ARG, APG, and IPG as having no temperature dependence because we have only data at one temperature (see sub-section 2.3.3).

Table 2-3. Thermistor Volts/Temperature Characteristics

Voltage	Temp., °C	Voltage	Temp., °C	Voltage	Temp., °C
-0.324V	-28.89°C	-.221V	- 7.78°C	-.065V	13.33°C
- .322	-28.33	-.218	- 7.22	-.060	13.89
- .320	-27.78	-.214	- 6.67	-.056	14.44
- .318	-27.22	-.210	- 6.11	-.052	15.00
- .316	-26.67	-.206	- 5.56	-.047	15.56
- .314	-26.11	-.203	- 5.00	-.043	16.11
- .312	-25.56	-.199	- 4.44	-.039	16.67
- .310	-25.00	-.195	- 3.89	-.035	17.22
- .308	-24.44	-.191	- 3.33	-.030	17.78
- .306	-23.89	-.187	- 2.78	-.026	18.33
- .304	-23.33	-.183	- 2.22	-.022	18.89
- .302	-22.78	-.179	- 1.67	-.018	19.44
- .300	-22.22	-.175	- 1.11	-.013	20.00
- .297	-21.67	-.171	- 0.56	-.009	20.56
- .295	-21.11	-.167	0.00	-.005	21.11
- .293	-20.56	-.163	0.56	-.001	21.67
- .290	-20.00	-.159	1.11	0.003	22.22
- .288	-19.44	-.155	1.67	.007	22.78
- .285	-18.89	-.151	2.22	.011	23.23
- .283	-18.33	-.146	2.78	.016	23.89
- .280	-17.78	-.142	3.33	.020	24.44
- .277	-17.22	-.138	3.89	.024	25.00
- .274	-16.67	-.134	4.44	.028	25.56
- .271	-16.11	-.130	5.00	.031	26.11
- .268	-15.56	-.125	5.56	.035	26.67
- .265	-15.00	-.121	6.11	.039	27.22
- .262	-14.44	-.117	6.67	.043	27.78
- .259	-13.89	-.112	7.22	.047	28.33
- .256	-13.33	-.108	7.78	.051	28.89
- .252	-12.78	-.104	8.33	.055	29.44
- .249	-12.22	-.099	8.89	.059	30.00
- .246	-11.67	-.095	9.44	.062	30.56
- .242	-11.11	-.091	10.00	.066	31.11
- .239	-10.56	-.086	10.55	.070	31.67
- .235	-10.00	-.082	11.11	.073	32.22
- .232	- 9.44	-.078	11.67	.077	32.78
- .228	- 8.89	-.073	12.22	.081	33.33
- .225	- 8.33	-.069	12.78	.084	33.89

Table 2-3. Thermistor Volts/Temperature Characteristics (Continued)

Voltage	Temp., °C	Voltage	Temp., °C	Voltage	Temp., °C
+.088V	34.44°C	+.160V	47.22	+.214	60.00°C
.091	35.00	.162	47.78	.216	60.56
.095	35.56	.165	48.33	.218	61.11
.098	36.11	.168	48.89	.220	61.67
.101	36.67	.170	49.44	.222	62.22
.105	37.22	.173	50.00	.224	62.78
.108	37.78	.175	50.56	.225	63.33
.111	38.33	.178	51.11	.227	63.89
.115	38.89	.180	51.67	.229	64.44
.118	39.44	.183	52.22	.231	65.00
.121	40.00	.185	52.78	.233	65.56
.124	40.56	.188	53.33	.234	66.11
.127	41.11	.190	53.89	.236	66.67
.131	41.67	.192	54.44	.238	67.22
.134	42.22	.195	55.00	.239	67.78
.137	42.78	.197	55.56	.241	68.33
.140	43.33	.199	56.11	.243	68.89
.143	43.89	.201	56.67	.244	69.44
.145	44.44	.204	57.22	.246	70.00
.148	45.00	.206	57.78	.247	70.57
.151	45.56	.208	58.33	.249	71.11
.154	46.11	.210	58.89		
.157	46.67	.212	59.44		

is sampled by the high-speed A/D of the telemetry system. In this section we will summarize the relationship between telemetry counts (as received for processing at NASA/WFC, for example) and the actual number of bits added to the Altitude Register (designation used by GE) which is the tracking loop altitude accumulator. While the Altitude Register Correction is a binary number, a discrete number of bits being added to or subtracted from the Altitude Register for each transmitted radar altimeter pulse, this correction is converted by a 7-bit D/A in the altimeter to an analog voltage RSE.

Table 2-4 summarizes the important relationships within the altimeter.* The first column specifies the voltage threshold value for the tracking loop A/D, and the second column in Table 2-4 gives the resulting A/D output for any given pair of threshold values. Table 2-4 lists only the endpoints and the range of input voltages near-zero; the near-zero region is the important region for normal altimeter tracking for which the Altitude Register Correction will be only a few bits either side of zero. The third column in Table 2-4 gives the Range Servo Error voltage produced by the 7-bit D/A within the altimeter; the fourth and fifth columns give the corresponding I-Mode and G-Mode Altitude Register Corrections. Finally, to keep information on this problem together, the last column gives the TAMS output (either I- or G-Mode); the TAMS software contained a minor error which resulted in a shift by one and a sign change of the TAMS output relative to the I-Mode Altitude Register Corrections. This effect is important for any detailed analysis of TAMS output but is irrelevant to this report's purpose.

We designate the I-Mode Altitude Register Correction as MI, and the G-Mode Correction as MG. MI and MG are signed integers and MG can be directly derived from MI. Since $-63 \leq MI + 64$, one way to write this relationship is

$$MG = [MI - (MI + 64) \bmod 4]/4 \qquad (2\text{-}1)$$

---

*Based on telephone conversations with E. L. Hofmeister, GE-Utica, early March 1975.

Input Voltage Threshold Levels (Filtered Error Signal in Tracking Loop)	Resulting 7 Bit word from Tracking Loop A/D	Tracker Error Voltage Out of Altimeter, RSE	Number of Bits in Actual Correction Applied to Altitude Register		TAMS Output, in Testing
		(Allow ±.020V)	I-Mode	G-Mode	
3.969 V	0 111 111	3.969 V	-63	-16	+64
3.096	⋮	⋮	⋮	⋮	⋮
⋮	⋮	⋮	⋮	⋮	⋮
0.344	0 000 101	0.344	-5	-2	+6
0.281	0 000 100	0.281	-4	-1	+5
0.219	0 000 011	0.219	-3	-1	+4
0.156	0 000 010	0.156	-2	-1	+3
0.094	0 000 001	0.094	-1	-1	+2
0.031	0 000 000	0.031	0	0	+1
-0.031	1 111 111	-0.031	+1	0	0
-0.094	1 111 110	-0.094	+2	0	-1
-0.156	1 111 101	-0.156	+3	0	-2
-0.219	1 111 100	-0.219	+4	+1	-3
-0.281	1 111 011	-0.281	+5	+1	-4
-0.344	⋮	⋮	⋮	⋮	⋮
⋮	⋮	⋮	⋮	⋮	⋮
-3.969	1 000 000	-3.969	+64	+16	-63
-4.031					
			1.s.b.=1.5625 ns	1.s.b.= 6.25 ns	

It is important to remember that the Altitude Register's least significant bit (l.s.b.) has different value in the G-Mode and the I-Mode. The G-Mode l.s.b. is 6.25 ns and the I-Mode l.s.b. is 1.5625 ns (neglecting the 50 ppm nominal oscillator offset which is unimportant for the present purpose). These l.s.b. values are 93.750 cm and 23.4375 cm, respectively, in satellite altitude (where c=30 cm/ns has been used, since the error in this value is again not significant for this purpose).

The counts/volts conversion of RSE for the high-speed A/D channel of the telemetry system is

$$RSE = .032025JTC - 4.08444 \qquad (2\text{-}2)$$

where JTC is the (integer) number of telemetry counts, $0 \leq JTC \leq 255$, and RSE is in volts. The value of RSE in 2-2 is the mid-voltage; for a given JTC, the value from 2-2 is at the center of the voltage range of .032025 volts full width. We can rewrite 2-2 and indicate by TC the number of telemetry counts for a given RSE voltage,

$$TC = (RSE + 4.08444)/.032025 \qquad (2\text{-}3)$$

JT is not necessarily integer in Equation 2-3, and using the truncation of floating-point to integer conversions in FORTRAN, we can produce the integer telemetry count value JTC (for any allowed RSE in) by

$$JTC = INT(0.5 + TC) \qquad (2\text{-}4)$$

$$= INT(0.5 + (RSE+4.08444)/.032025)$$

We need also to characterize the RSE out of the altimeter for a given value of MI. Using Table 2-4, we see that the total voltage range is 2*(3.969)V and that the 7 bit D/A will have (2^7-1) intervals so that the individual step is 7.938/127 = 0.0624039. The MI to RSE relation can be written as

$$= (64-MI) * .0625039 - 3.969 \text{ volts} \qquad (2\text{-}5)$$

Finally, combining Equations 2-3 and 2-5, eliminating RSE, and redesignating the I-Mode correction MI by ACC, we find

$$ACC = 65.8469 - 0.51273 * JTC \qquad (2\text{-}6)$$

To produce the integer MI from ACC above, we must algebraically round ACC to the nearest integer. A rounding-off operation within a computer for positive and negative quantities is slightly more awkward than is rounding off of numbers which are zero or positive only [this latter rounding was done in Equation 2-4 for the positive JTC]. A whole-value-only signed floating-point quantity XMI can be produced from ACC above using the following FORTRAN statement.

$$XMI = SIGN(FLOAT(INT(ABS(ACC) + 0.5)),ACC), \qquad (2\text{-}7)$$

and for a given telemetry count value JTC, Equations 2-6 and 2-7 produce the best estimate of MI,

$$MI = XMI$$

The estimate of MI must be done in either G- or I-Mode. If in I-Mode, multiply MI by 23.4375 cm to obtain the final I-Mode Tracker Altitude Register Correction in cm. If, instead, in G-Mode, first obtain MG from MI by equating Equation 2-1 and then multiply MG by 93.75 cm to obtain the G-Mode Altitude Register correction in cm.

The entire procedure just described is summarized in Figure 2-3 which provides the (FORTRAN-like) steps to obtain a final Altitude Register correction in cm from an input number of telemetry counts related to RSE. This is the procedure which would be followed if the direct Telemetry Counts→Functional Units process of Table 2-1 were being done. However, because of the way Wallops Flight Center processing is carried out (Figure 2-1), RSE is already converted from counts to Engineering Units in CALIMERGE. For this reason we supply Figure 2-4 which follows in an obvious way from the preceding discussion and which summarizes the procedure which should be used at Wallops in the GAP program to obtain the Altitude Register

Figure 2-3. Summary of Conversion from RSE Telemetry Counts to Altitude Register Correction in Centimeters.

Define: JTC=Telemetry Counts From RSE
ALTCOR=Altitude Register Correction in Centimeters

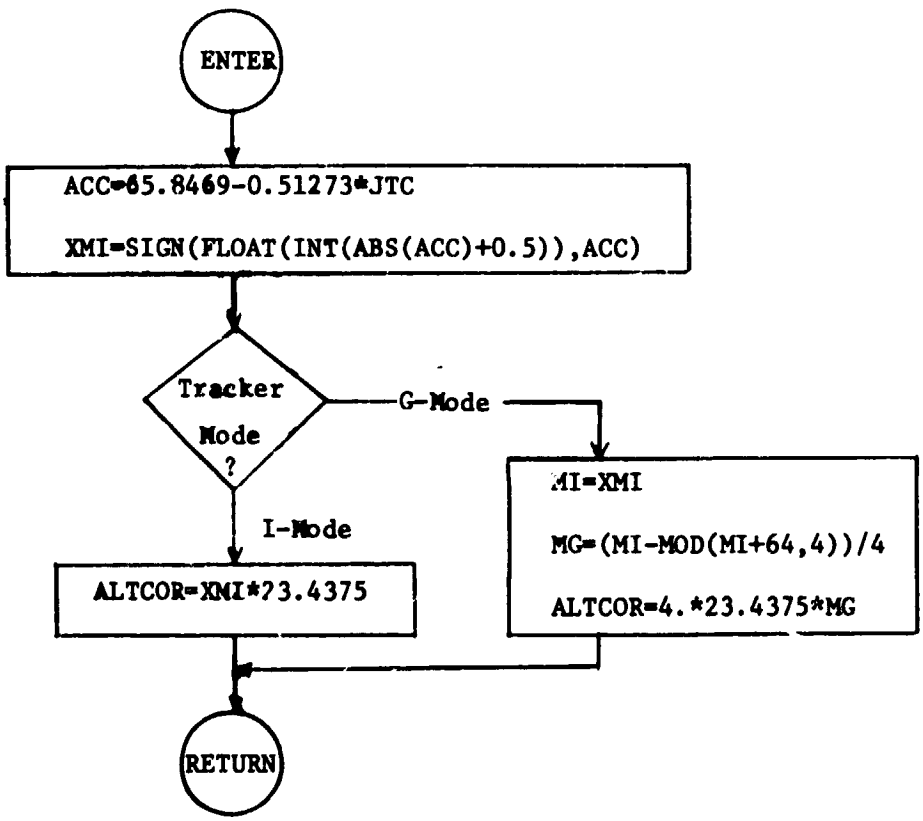

Figure 2-4. Summary of Conversion from RSE Engineering Units (Volts) to Altitude Register Correction in Centimeters.

Define: ALTCOR=Altitude Register Correction in Centimeters
RSE=CALIMERGE Output, in Volts, for Range Servo Error

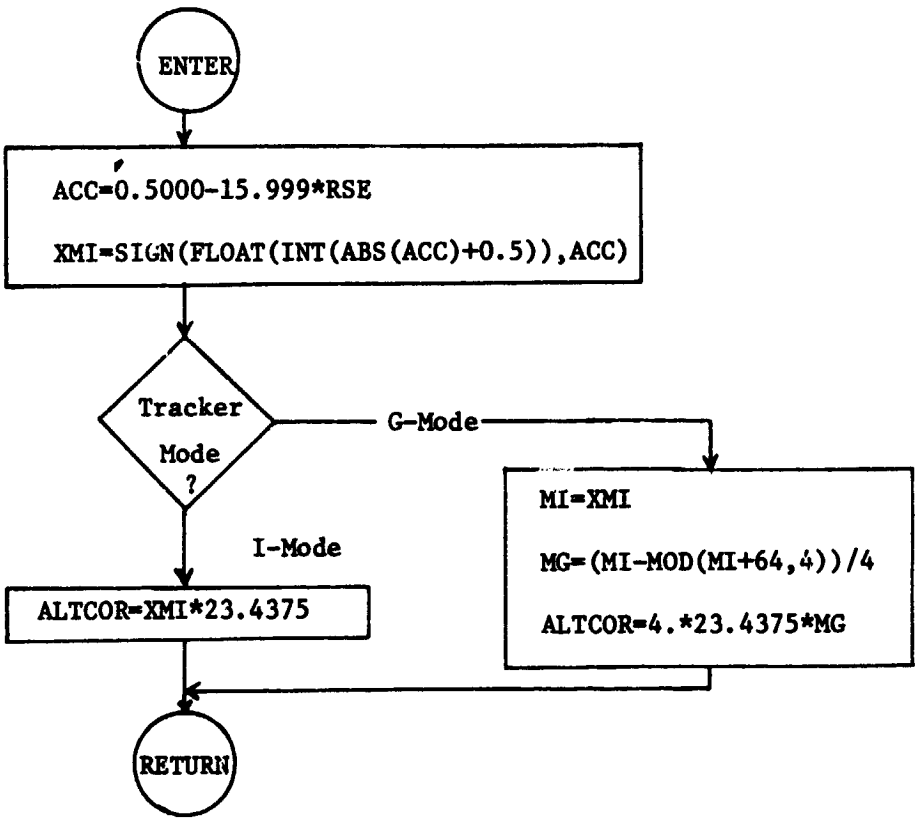

correction in cm from an input value of RSE in Engineering Units (volts). Note that in both Figures 2-3 and 2-4, the expression XMI=SIGN(...) is merely the algebraic rounding operation already described in the discussion of equation 2-7. There are probably better, more compact ways of doing this rounding but this method accomplishes the purpose.

The next couple of pages will examine the effects of error in the MI→RSE conversion. That is, what if the numbers in the third column of Table 2-4 are incorrect? (Temperature-dependence might be one possibility.) According to E. Hofmeister, the values of RSE in Table 2-4 are good to $\pm$ 20 millivolts, and the question we must consider is whether a 20 millivolt uncertainty in RSE leads to any ambiguities in the JTC↔MI relationship. The simplest check is just to add $\pm$ 20 mv to RSE values and examine the consequences. A simple FORTRAN program was written to accomplish this, and Table 2-5 is the data printed out by the program. The following paragraph discusses each column in Table 2-5, from left to right.

We start on the left with the 128 possible values of MI, the I-Mode Altitude Register Correction, in bits. By equation 2-5), we generate RSE (in mv in Table 2-5). Then equations 2-3) and 2-4) are used to produce the two columns TC-HI and TC-LO; TC-HI is the telemetry system count for RSE+20 mv and TC-LO is the telemetry count for RSE-20 mv. MI-HI is the predicted value of MI, given a telemetry count TC-HI, and is calculated by equations 2-6) and 2-7). MI-LO is similarly calculated from TC-LO.

MI-HI and MI-LO should agree with each other and with the input MI if there are no ambiguities introduced by the $\pm$ 20 mv RSE uncertainty. The asterisks immediately to the right of MI-LO point out those places in this conversion process where there <u>are</u> ambiguities. Finally, we use equation 2-1) to produce the MG estimate MG-HI from MI-HI and MG-LO from MI-LO. Again asterisks highlight regions of ambiguity.

The conclusion from Table 2-5 is that there <u>are</u> regions of ambiguity in which the $\pm$ 20 mv uncertainty in RSE value leads to the possibility of being off in MI by one bit. However, the altitude tracker will never, in normal tracking operation, get outside the range of 0 $\pm$ 6 bits for MI. Even for the fine search mode during acquisition, the value of MI will be within this range. In the Peak Detect or the Coarse Sweep modes the MI

can be out of this range but the one count MI ambiguity is of no practical significance at these times. Notice that in Table 2-5 the region $-8 \leq MI \leq +7$ is an unambiguous region and that even a full 20 mv uncertainty in the RSE values [from equation 2-5)] will cause no problem. If in the future it could be determined that the RSE uncertainty is significantly less than $\pm$ 20 mv, then it would be possible to narrow the regions of ambiguity in Table 2-5; however, it has already been argued above that the current situation presents no problems for the GEOS-C altimeter and its expected 0 ± 6 count range in MI.

Table 2-5. Relationships of Altitude Register Correction, RSE, and Telemetry Counts. Quantities TC-HI and TC-LO in Counts, RSE in Millivolts, Other Entries in Bits.

MI	RSE	TC-HI	TC-LO	MI-HI	MI-LO	MG-HI	MG-LO
-63	3969.	252	251	-63	-63	-16	-16
-62	3906.	250	249	-62	-62	-16	-16
-61	3844.	248	247	-61	-61	-16	-16
-60	3781.	246	245	-60	-60	-15	-15
-59	3719.	244	243	-59	-59	-15	-15
-58	3656.	242	241	-58	-58	-15	-15
-57	3594.	240	239	-57	-57	-15	-15
-56	3531.	238	237	-56	-56	-14	-14
-55	3469.	236	235	-55	-55	-14	-14
-54	3406.	235	233	-55	-54◆◆◆◆	-14	-14
-53	3344.	233	231	-54	-53◆◆◆◆	-14	-14
-52	3281.	231	229	-53	-52◆◆◆◆	-14	-13◆◆◆◆
-51	3219.	229	227	-52	-51◆◆◆◆	-13	-13
-50	3156.	227	225	-51	-50◆◆◆◆	-13	-13
-49	3094.	225	224	-50	-49◆◆◆◆	-13	-13
-48	3031.	223	222	-48	-48	-12	-12
-47	2969.	221	220	-47	-47	-12	-12
-46	2906.	219	218	-46	-46	-12	-12
-45	2844.	217	216	-45	-45	-12	-12
-44	2781.	215	214	-44	-44	-11	-11
-43	2719.	213	212	-43	-43	-11	-11
-42	2656.	211	210	-42	-42	-11	-11
-41	2594.	209	208	-41	-41	-11	-11
-40	2531.	207	206	-40	-40	-10	-10
-39	2469.	205	204	-39	-39	-10	-10
-38	2406.	203	202	-38	-38	-10	-10
-37	2344.	201	200	-37	-37	-10	-10
-36	2281.	199	198	-36	-36	-9	-9
-35	2219.	197	196	-35	-35	-9	-9
-34	2156.	195	194	-34	-34	-9	-9
-33	2094.	194	192	-34	-33◆◆◆◆	-9	-9
-32	2031.	192	190	-33	-32◆◆◆◆	-9	-8◆◆◆◆
-31	1969.	190	188	-32	-31◆◆◆◆	-8	-8
-30	1906.	188	186	-31	-30◆◆◆◆	-8	-8
-29	1844.	186	184	-30	-28◆◆◆◆	-8	-7◆◆◆◆
-28	1781.	184	183	-28	-28	-7	-7
-27	1719.	182	181	-27	-27	-7	-7
-26	1656.	180	179	-26	-26	-7	-7
-25	1594.	178	177	-25	-25	-7	-7
-24	1531.	176	175	-24	-24	-6	-6
-23	1469.	174	173	-23	-23	-6	-6
-22	1406.	172	171	-22	-22	-6	-6
-21	1344.	170	169	-21	-21	-6	-6
-20	1281.	168	167	-20	-20	-5	-5
-19	1219.	166	165	-19	-19	-5	-5
-18	1156.	164	163	-18	-18	-5	-5
-17	1094.	162	161	-17	-17	-5	-5
-16	1031.	160	159	-16	-16	-4	-4
-15	969.	158	157	-15	-15	-4	-4
-14	906.	156	155	-14	-14	-4	-4
-13	844.	155	153	-14	-13◆◆◆◆	-4	-4
-12	781.	153	151	-13	-12◆◆◆◆	-4	-3◆◆◆◆
-11	719.	151	149	-12	-11◆◆◆◆	-3	-3

Table 2-5 (continued)

-10	656.	149	147	-11	-10◆◆◆◆	-3	-3
-9	594.	147	145	-10	-8◆◆◆◆	-3	-2◆◆◆◆
-8	531.	145	144	-8	-8	-2	-2
-7	469.	143	142	-7	-7	-2	-2
-6	406.	141	140	-6	-6	-2	-2
-5	344.	139	138	-5	-5	-2	-2
-4	281.	137	136	-4	-4	-1	-1
-3	219.	135	134	-3	-3	-1	-1
-2	156.	133	132	-2	-2	-1	-1
-1	94.	131	130	-1	-1	-1	-1
0	31.	129	128	0	0	0	0
1	-31.	127	126	1	1	0	0
2	-94.	125	124	2	2	0	0
3	-156.	123	122	3	3	0	0
4	-219.	121	120	4	4	1	1
5	-281.	119	118	5	5	1	1
6	-344.	117	116	6	6	1	1
7	-406.	115	114	7	7	1	1
8	-469.	114	112	7	8◆◆◆◆	1	2◆◆◆◆
9	-531.	112	110	8	9◆◆◆◆	2	2
10	-594.	110	108	9	10◆◆◆◆	2	2
11	-656.	108	106	10	11◆◆◆◆	2	2
12	-719.	106	104	11	13◆◆◆◆	2	3◆◆◆◆
13	-781.	104	103	13	13	3	3
14	-844.	102	101	14	14	3	3
15	-906.	100	99	15	15	3	3
16	-969.	98	97	16	16	4	4
17	-1031.	96	95	17	17	4	4
18	-1094.	94	93	18	18	4	4
19	-1156.	92	91	19	19	4	4
20	-1219.	90	89	20	20	5	5
21	-1281.	88	87	21	21	5	5
22	-1344.	86	85	22	22	5	5
23	-1406.	84	83	23	23	5	5
24	-1469.	82	81	24	24	6	6
25	-1531.	80	79	25	25	6	6
26	-1594.	78	77	26	26	6	6
27	-1656.	76	75	27	27	6	6
28	-1719.	74	73	28	28	7	7
29	-1781.	73	71	28	29◆◆◆◆	7	7
30	-1844.	71	69	29	30◆◆◆◆	7	7
31	-1906.	69	67	30	31◆◆◆◆	7	7
32	-1969.	67	65	31	33◆◆◆◆	7	8◆◆◆◆
33	-2031.	65	63	33	34◆◆◆◆	8	8
34	-2094.	63	62	34	34	8	8
35	-2156.	61	60	35	35	8	8
36	-2219.	59	58	36	36	9	9
37	-2281.	57	56	37	37	9	9
38	-2344.	55	54	38	38	9	9
39	-2406.	53	52	39	39	9	9
40	-2469.	51	50	40	40	10	10
41	-2531.	49	48	41	41	10	10
42	-2594.	47	46	42	42	10	10
43	-2656.	45	44	43	43	10	10

Table 2-5 (continued)

44	-2719.	43	42	44	44	11	11
45	-2781.	41	40	45	45	11	11
46	-2844.	39	38	46	46	11	11
47	-2906.	37	36	47	47	11	11
48	-2969.	35	34	48	48	12	12
49	-3031.	34	32	48	49♦♦♦♦	12	12
50	-3094.	32	30	49	50♦♦♦♦	12	12
51	-3156.	30	28	50	51♦♦♦♦	12	12
52	-3219.	28	26	51	53♦♦♦♦	12	13♦♦♦♦
53	-3281.	26	24	53	54♦♦♦♦	13	13
54	-3344.	24	22	54	55♦♦♦♦	13	13
55	-3406.	22	21	55	55	13	13
56	-3469.	20	19	56	56	14	14
57	-3531.	18	17	57	57	14	14
58	-3594.	16	15	58	58	14	14
59	-3656.	14	13	59	59	14	14
60	-3719.	12	11	60	60	15	15
61	-3781.	10	9	61	61	15	15
62	-3844.	8	7	62	62	15	15
63	-3906.	6	5	63	63	15	15
64	-3969.	4	3	64	64	16	16

2.3.3 Average Ramp Gate ARG, Average Plateau Gate APG, and Instantaneous Plateau Gate IPG, Global Mode Only.

As already noted in Table 2-1, we include these Global Mode gates in the temperature independent category because of the lack of data at any temperature other than GTT = 32.4°C; if these three Global Mode quantities ARG, APG, and IPG do have a temperature dependence, the Global Tracker Temperature GTT would be the relevant temperature. The only data we have is from the APL Special Tests* conducted at a single temperature. These data are supplied in Table 2-6 of our report.

Referring to Table 2-2, we see that ARG and APG are never less than zero volts and that their upper limit is about +8 volts whereas IPG can range from about -4 to +4 volts. Suitable Engineering Units lower and upper limits respectively for these three gates are: 0. and 5. volts for ARG; the same for APG; and -1.347 and 3.510 volts for IPG.

2.3.4 Other

We supply no conversion tables here for other quantities which are either temperature-independent or for which we haven't sufficient data. We merely list them below with a few general remarks.

RMI - The Receiver Mixer Current, is converted from telemetry counts to volts by a conversion table already implemented at NASA/WFC. The resulting voltage is useful as a monitor of receiver "health" and should be checked for agreement with the range of RMI generally seen during pre-flight testing.

ALT or CALT - The Altitude, or the Cumulative Altitude, is a 32 bit word telemetered in four separate 8 bit words and reassembled into the 32 bit word by NASA/WFC.

IFTA - The IF Test Signal is related to the BIT/CAL Mode and we have insufficient information about its use or its temperature dependence at present. It may be possible to relate IFTA quantitatively to IF#1 and IF#2 levels within BIT/CAL at

*APL Special Test Data GEOS-C Flight Model, dated 13 November 1974 (obtained from C. L. Purdy NASA/WFC).

Table 2-6. Flight Model Average Ramp Gate ARG, Average Plateau Gate APG, and Instantaneous Plateau Gate, IPG, Global Mode Only

GE designation →	V(R)	V(P)	V(Pi)
APL designation →	ARG	APG	IPG
(Functional Units) Input in Volts	(Engineering Units) Output in Volts		
-0.2V	-3.233V	-3.295V	-1.347V
-.1	-1.606	-1.633	-0.750
.0	0.017*	0.045*	-0.004*
.1	1.612	1.677	1.022
.2	3.205	3.305	1.854
.3	5.000	5.000	2.719
.35	"	"	2.965
.4	"	"	3.232
.45	"	"	3.320
.5	"	"	3.472
.6	"	"	3.510
Above Results for Single Temperature Only, Nominal Ambient Chamber. Average GTT (TT3) During Test = 32.4°C.			

Notes: * - Two sets of data were taken at this input, for two different DDG settings. The values here are from the second setting, for DDG = 3654540.

some time in the future based upon information which is scheduled to appear in the GE Design Error Analysis.

VTA - The Video Test Signal Amplitude is either present or absent in the BIT/CAL mode.

RSA - This signal is either present or absent depending upon correct operation of the altimeter internal clock.

2.4 Altimeter Quantities With Temperature-Dependent Calibration

As in section 2.3 , separate sub-sections of 2.4 list the calibration tables and the general remarks for those altimeter quantities of Table 2-2 having specific temperature dependence and for which the linear-linear interpolation of section 2.2 is to be used. The bar over a temperature designation (such as $\overline{WST}$ below) denotes the average temperature for the time interval over which the TAMS system acquired the EU vs. FU data.

2.4.1 The Instantaneous Waveform Samplers IRS1,...,16

The double interpolation, in Engineering Units (volts) and in the waveform sampler temperature WST (in ^{o}C), will be used for the 16 Instantaneous Waveform Sample values. On following pages Table 2-7 provides the calibration data as taken from References 4a, 4b and 4c.

We indicate in Table 2-7 where data values have been generated by interpolation between pairs of input data points in order to put all IRS1,...,16 data on a common Functional Units scale. Because the satellite in orbit may run colder than the lowest $\overline{WST}$ value of ~ $20^{o}C$ under which waveform sampler data were taken during GE testing and calibration, we have duplicated the $\overline{WST}=20^{o}C$ column in each part of Table 2-7 and labelled the result as $\overline{WST}=0^{o}C$. If this were not done, there is a good chance that an appreciable amount of the waveform sampler data would not be converted at all in the Wallops Flight Center processing but instead would flag an out-of-calibration error message. To avoid this loss of data and because the temperature dependence of the IRS1,...,16 results is not too strong at the lower WST values, this duplication of the $\overline{WST}$ low column has been chosen as a simplest, fastest temporary fix. It is conceivable that data already existing from Flight Model testing at APL or at Goddard will allow us to replace the leftmost $\overline{WST}$ column in Table 2-7 with actual measured data, but

this will involve a detailed search of the microfilmed test data.

For the desired (EU) limit checks in CALIMERGE, we have indicated in each section of Table 2-7 the upper and lower limits on EU. The upper limit is taken as the maximum EU value at the maximum FU value and the lower EU limit is chosen as the maximum EU value for the minimum FU value. Only IRS13, the Instantaneous Waveform Sampler #13, is an exception to this rule; since there is clearly some type of breakdown at the highest $\overline{WST}$ value in this sampler, the Engineering Unit upper limit has been taken from the $\overline{WST} = 44.7^{o}C$ column, and we suggest that any data for $WST > 44.7^{o}C$ be considered out of the calibration range and thus invalid.

Table 2-7(a). Waveform Sampler Calibration Data (IRS)

Flight Model Waveform Sampler IRS1 ,

the Instantaneous Return Waveform Sample #1

(Functional Units) Input Amplitude, in Volts	(Engineering Units) Output, in Volts			
	$\overline{WST}=0^{o}C$ Note a	$\overline{WST}=20.0^{o}$ TV/$-2^{o}C$	$\overline{WST}=44.7^{o}$ Ambient	$\overline{WST}=63.1^{o}$ TV/$+42^{o}$
-0.2V	-0.886V	-0.886	-0.821	-0.819
- .1	-0.440	-0.440	-0.421	-0.356
0.0	0.003	0.003	0.000	0.008
.1	0.446	0.446	0.429	0.445
.2	0.876	0.876	0.848	0.847
.3	1.258	1.258	1.248	1.184
.35	1.412	1.412[b]	1.420	1.288[b]
.4	1.567	1.567	1.505	1.391
.45	1.575	1.575[b]	1.539	1.402[b]
.5	1.583	1.583	1.545	1.413
.6	1.600	1.600	1.547	1.423

Engineering Units Lower Limit = -0.819V
Engineering Units Upper Limit = 1.423V

- - - - - - - -

Table 2-7(b). Waveform Sampler Calibration Data (IRS)

Flight Model Waveform Sampler IRS2 ,

the Instantaneous Return Waveform Sample #2

(Functional Units) Input Amplitude, in Volts	(Engineering Units) Output, in Volts			
	$\overline{WST}=0^{o}$ Note a	$\overline{WST}=20.0^{o}$ TV/$-2^{o}C$	$\overline{WST}=44.7^{o}$ Ambient	$\overline{WST}=63.1^{o}$ TV/$+42^{o}$
-0.2V	-0.874V	-0.874	-0.815	-0.816
- .1	-0.451	-0.451	-0.417	-0.405
0.0	-0.019	-0.019	0.000	0.000
.1	0.417	0.417	0.411	0.430
.2	0.841	0.841	0.825	0.793
.3	1.217	1.217	1.219	1.159
.35	1.375	1.375[b]	1.412	1.211[b]
.4	1.533	1.533[c]	1.433	1.263
.45	"	"	1.446[c]	1.269[b]
.5	"	"	"	1.275
.6	"	"	"	1.284

Engineering Units Lower Limit = -0.815V
Engineering Units Upper Limit = 1.284V

Notes: a - $\overline{WST}=20.^{o}$ column duplicated; see text.
b - Not in original test data, supplied by linear interpolation.
c - Last data point before a reversal in Output vs Input data.

Table 2-7(c). Waveform Sampler Calibration Data (IRS, continued)

Flight Model Waveform Sampler IRS3 ,
the Instantaneous Return Waveform Sample #3

(Functional Units) Input Amplitude, in Volts	(Engineering Units) Output, in Volts			
	$\overline{WST}=0^{o}C$ Note a	$\overline{WST}=20.0^{o}$ TV/$-2^{o}C$	$\overline{WST}=44.7^{o}$ Ambient	$\overline{WST}=63.1^{o}$ TV/$+42^{o}$
-0.2V	-0.875V	-0.875	-0.812	-0.778
- .1	-0.445	-0.445	-0.426	-0.400
0.0	-0.003	-0.003	0.001	-0.004
.1	0.434	0.434	0.422	0.429
.2	0.860	0.860	0.830	0.802
.3	1.237	1.237	1.228	1.085
.35	1.356	1.356[b]	1.347	1.118[b]
.4	1.475	1.475[c]	1.367[c]	1.152
.45	"	"	"	1.155[b]
.5	"	"	"	1.158[c]
.6	"	"	"	"

Engineering Units Lower Limit = -0.778V
Engineering Units Upper Limit = 1.158V

Table 2-7(d). Waveform Sampler Calibration Data (IRS)

Flight Model Waveform Sampler IRS4 ,
the Instantaneous Return Waveform Sample #4

(Functional Units) Input Amplitude, in Volts	(Engineering Units) Output, in Volts			
	$\overline{WST}=0^{o}$ Note a	$\overline{WST}=20.0^{o}$ TV/$-2^{o}C$	$\overline{WST}=44.7^{o}$ Ambient	$\overline{WST}=63.1^{o}$ TV/$+42^{o}$
-0.2V	-0.848V	-0.848	-0.784	-0.769
- .1	-0.433	-0.433	-0.400	-0.400
0.0	-0.014	-0.014	-0.015	-0.013
.1	0.405	0.405	0.396	0.419
.2	0.832	0.832	0.805	0.780
.3	1.196	1.196	1.193	1.049
.35	1.373	1.373[b]	1.374	1.148[b]
.4	1.550	1.550	1.434	1.246
.45	1.557	1.557[b]	1.439	1.253[b]
.5	1.564	1.564[c]	1.445	1.260
.6	"	"	1.451	1.264

Engineering Units Lower Limit = -0.769V
Engineering Units Upper Limit = 1.264V

Notes: a - $\overline{WST}=20.^{o}$ column duplicated; see text.
b - Not in original test data, supplied by linear interpolation.
c - Last data point before a reversal in Output vs Input data.

Table 2-7(e). Waveform Sampler Calibration Data (IRS, continued)

Flight Model Waveform Sampler IRS5 ,
the Instantaneous Return Waveform Sample #5

(Functional Units) Input Amplitude, in Volts	(Engineering Units) Output, in Volts			
	$\overline{WST}=0^{o}C$ Note a	$\overline{WST}=20.0^{o}$ TV/$-2^{o}C$	$\overline{WST}=44.7^{o}$ Ambient	$\overline{WST}=63.1^{o}$ TV/$+42^{o}$
-0.2V	-0.865V	-0.865	-0.806	-0.815
- .1	-0.447	-0.447	-0.421	-0.407
0.0	0.012	0.012	-0.006	0.019
.1	0.444	0.444	0.419	0.434
.2	0.865	0.865	0.837	0.765
.3	1.251	1.251	1.228	1.142
.35	1.420	1.420[b]	1.422	1.260[b]
.4	1.589	1.589	1.512	1.378
.45	1.602	1.602[b]	1.560	1.380[b]
.5	1.616	1.616[c]	1.563	1.383[c]
.6	"	"	1.571	"

Engineering Units Lower Limit = -0.806V
Engineering Units Upper Limit = 1.383V

Table 2-7(f). Waveform Sampler Calibration Data (IRS)

Flight Model Waveform Sampler IRS6 ,
the Instantaneous Return Waveform Sample #6

(Functional Units) Input Amplitude, in Volts	(Engineering Units) Output, in Volts			
	$\overline{WST}=0^{o}$ Note a	$\overline{WST}=20.0^{o}$ TV/$-2^{o}C$	$\overline{WST}=44.7^{o}$ Ambient	$\overline{WST}=63.1^{o}$ TV/$+42^{o}$
-0.2V	-0.878V	-0.878	-0.816	-0.809
- .1	-0.455	-0.455	-0.417	-0.410
0.0	-0.008	-0.008	-0.020	0.013
.1	0.408	0.408	0.406	0.416
.2	0.834	0.834	0.823	0.792
.3	1.214	1.214	1.218	1.153
.35	1.370	1.370[b]	1.413	1.258[b]
.4	1.527	1.527	1.503	1.364
.45	1.536	1.536[b]	1.525[c]	1.367[b]
.5	1.544	1.544[c]	"	1.370
.6	"	"	"	"

Engineering Units Lower Limit = -0.809V
Engineering Units Upper Limit = 1.370V

Notes: a - $\overline{WST}=20.^{o}$ column duplicated; see text.
b - Not in original test data, supplied by linear interpolation.
c - Last data point before a reversal in Output vs Input data.

Table 2-7(g). Waveform Sampler Calibration Data (IRS, continued)

Flight Model Waveform Sampler IRS7 ,

the Instantaneous Return Waveform Sample #7

(Functional Units) Input Amplitude, in Volts	(Engineering Units) Output, in Volts			
	$\overline{WST}$=0°C Note a	$\overline{WST}$=20.0° TV/-2°C	$\overline{WST}$=44.7° Ambient	$\overline{WST}$=63.1° TV/+42°
-0.2V	-0.913V	-0.913	-0.856	-0.904
- .1	-0.501	-0.501	-0.471	-0.446
0.0	-0.046	-0.046	-0.054	-0.167
.1	0.363	0.363	0.354	0.368
.2	0.797	0.797	0.771	0.748
.3	1.188	1.188	1.168	1.086
.35	1.376	1.376[b]	1.357	1.132[b]
.4	1.563	1.563	1.491	1.177
.45	1.580	1.580[b]	1.510[c]	1.192[b]
.5	1.596	1.596	"	1.208
.6	1.604	1.604	"	1.223

Engineering Units Lower Limit = -0.856V
Engineering Units Upper Limit = 1.223V

Table 2-7(h). Waveform Sampler Calibration Data (IRS)

Flight Model Waveform Sampler IRS8 ,

the Instantaneous Return Waveform Sample #8

(Functional Units) Input Amplitude, in Volts	(Engineering Units) Output, in Volts			
	$\overline{WST}$=0° Note a	$\overline{WST}$=20.0° TV/-2°C	$\overline{WST}$=44.7° Ambient	$\overline{WST}$=63.1° TV/+42°
-0.2V	-0.828V	-0.828	-0.771	-0.778
- .1	-0.415	-0.415	-0.400	-0.382
0.0	-0.001	-0.001	-0.006	-0.001
.1	0.405	0.405	0.406	0.416
.2	0.827	0.827	0.799	0.800
.3	1.187	1.187	1.174	1.099
.35	1.332	1.332[b]	1.324	1.130[b]
.4	1.478	1.478[c]	1.351	1.162[c]
.45	"	"	1.359[c]	"
.5	"	"	"	"
.6	"	"	"	"

Engineering Units Lower Limit = -0.771V
Engineering Units Upper Limit = 1.162V

Notes: a - $\overline{WST}$=20.° column duplicated; see text.
b - Not in original test data, supplied by linear interpolation.
c - Last data point before a reversal in Output vs Input data.

Table 2-7(i). Waveform Sampler Calibration Data (IRS, continued)

Flight Model Waveform Sampler IRS9 ,

the Instantaneous Return Waveform Sample #9

(Functional Units)	(Engineering Units) Output, in Volts			
Input Amplitude, in Volts	$\overline{WST}$=0°C Note a	$\overline{WST}$=20.0° TV/-2°C	$\overline{WST}$=44.7° Ambient	$\overline{WST}$=63.1° TV/+42°
-0.2V	-0.921V	-0.921	-0.852	-0.858
- .1	-0.462	-0.462	-0.440	-0.444
0.0	-0.004	-0.004	-0.010	-0.009
.1	0.439	0.439	0.418	0.433
.2	0.880	0.880	0.838	0.843
.3	1.259	1.259	1.250	1.153
.35	1.406	1.406[b]	1.409	1.214[b]
.4	1.552	1.552[c]	1.436	1.274
.45	"	"	1.452	1.280[b]
.5	"	"	1.459[c]	1.285
.6	"	"	"	1.291

Engineering Units Lower Limit = -0.852V
Engineering Units Upper Limit = 1.291V

Table 2-7(j). Waveform Sampler Calibration Data (IRS)

Flight Model Waveform Sampler IRS10,

the Instantaneous Return Waveform Sample #10

(Functional Units)	(Engineering Units) Output, in Volts			
Input Amplitude, in Volts	$\overline{WST}$=0° Note a	$\overline{WST}$=20.0° TV/-2°C	$\overline{WST}$=44.7° Ambient	$\overline{WST}$=63.1° TV/+42°
-0.2V	-0.867V	-0.867	-0.812	-0.809
- .1	-0.444	-0.444	-0.411	-0.369
0.0	-0.007	-0.007	0.003	-0.006
.1	0.435	0.435	0.423	0.445
.2	0.870	0.870	0.849	0.817
.3	1.245	1.245	1.239	1.182
.35	1.411	1.411[b]	1.452	1.288[b]
.4	1.577	1.577	1.538	1.394
.45	1.582	1.582[b]	1.555[c]	1.408[b]
.5	1.588	1.588[c]	"	1.423[c]
.6	"	"	"	"

Engineering Units Lower Limit = -0.809V
Engineering Units Upper Limit = 1.423V

Notes: a - $\overline{WST}$=20.° column duplicated; see text.
b - Not in original test data, supplied by linear interpolation.
c - Last data point before a reversal in Output vs Input data.

Table 2-7(k). Waveform Sampler Calibration Data (IRS, continued)

Flight Model Waveform Sampler IRS11,
the Instantaneous Return Waveform Sample #11

(Functional Units) Input Amplitude, in Volts	(Engineering Units) Output, in Volts			
	$\overline{WST}$=0°C Note a	$\overline{WST}$=20.0° TV/-2°C	$\overline{WST}$=44.7° Ambient	$\overline{WST}$=63.1° TV/+42°
-0.2V	-0.867V	-0.867	-0.815	-0.809
- .1	-0.440	-0.440	-0.411	-0.428
0.0	0.012	0.012	0.008	0.008
.1	0.449	0.449	0.433	0.445
.2	0.876	0.876	0.855	0.820
.3	1.257	1.257	1.252	1.187
.35	1.440	1.440[b]	1.452	1.281[b]
.4	1.623	1.623	1.551	1.375[c]
.45	1.633	1.633[b]	1.574	"
.5	1.643	1.643	1.575	"
.6	1.660	1.660	1.584	"

Engineering Units Lower Limit = -0.809V
Engineering Units Upper Limit = 1.375V

Table 2-7(l). Waveform Sampler Calibration Data (IRS)

Flight Model Waveform Sampler IRS12,
the Instantaneous Return Waveform Sample #12

(Functional Units) Input Amplitude, in Volts	(Engineering Units) Output, in Volts			
	$\overline{WST}$=0° Note a	$\overline{WST}$=20.0° TV/-2°C	$\overline{WST}$=44.7° Ambient	$\overline{WST}$=63.1° TV/+42°
-0.2V	-0.844V	-0.844	-0.780	-0.767
- .1	-0.438	-0.438	-0.396	-0.394
0.0	-0.010	-0.010	-0.001	0.006
.1	0.408	0.408	0.405	0.429
.2	0.825	0.825	0.811	0.800
.3	1.196	1.196	1.188	1.164
.35	1.368	1.368[b]	1.374	1.208[b]
.4	1.539	1.539	1.440[c]	1.251
.45	1.541	1.541[b]	"	1.256[b]
.5	1.544	1.544	"	1.260
.6	1.546	1.546	"	1.262

Engineering Units Lower Limit = -0.767V
Engineering Units Upper Limit = 1.262V

Notes: a - $\overline{WST}$=20.° column duplicated; see text.
b - Not in original test data, supplied by linear interpolation.
c - Last data point before a reversal in Output vs Input data.

Table 2-7(m). Waveform Sampler Calibration Data (IRS, continued)

Flight Model Waveform Sampler IRS13,

the Instantaneous Return Waveform Sample #13

(Functional Units) Input Amplitude, in Volts	(Engineering Units) Output, in Volts			
	$\overline{WST}$=0°C Note a	$\overline{WST}$=20.0° TV/-2°C	$\overline{WST}$=44.7° Ambient	$\overline{WST}$=63.1° TV/+42°
-0.2V	-0.842V	-0.842	-0.789	-0.535
- .1	-0.429	-0.429	-0.397	-0.397
0.0	0.017	0.017	-0.001	0.020
.1	0.416	0.416	0.397	0.416
.2	0.838	0.838	0.802	0.549
.3	1.214	1.214	1.188	0.567
.35	1.310	1.310[b]	1.231	0.598[b]
.4	1.407	1.407	1.254	0.629
.45	1.415	1.415[b]	1.262	0.642[b]
.5	1.423	1.423	1.271	0.655
.6	1.430	1.430	1.275	0.695

Engineering Units Lower Limit = -0.789V
Engineering Units Upper Limit = 1.275V

} EU Limits from Ambient Chamber results; see text.

Table 2-7(n). Waveform Sampler Calibration Data (IRS)

Flight Model Waveform Sampler IRS14,

the Instantaneous Return Waveform Sample #14

(Functional Units) Input Amplitude, in Volts	(Engineering Units) Output, in Volts			
	$\overline{WST}$=0° Note a	$\overline{WST}$=20.0° TV/-2°C	$\overline{WST}$=44.7° Ambient	$\overline{WST}$=63.1° TV/+42°
-0.2V	-0.875V	-0.875	-0.820	-0.802
- .1	-0.450	-0.450	-0.413	-0.405
0.0	-0.008	-0.008	0.000	-0.003
.1	0.422	0.422	0.421	0.426
.2	0.847	0.847	0.830	0.815
.3	1.221	1.221	1.221	1.162
.35	1.373	1.373[b]	1.414	1.219[b]
.4	1.525	1.525[c]	1.442[c]	1.276
.45	"	"	"	1.278[b]
.5	"	"	"	1.280[c]
.6	"	"	"	"

Engineering Units Lower Limit = -0.802V
Engineering Units Upper Limit = 1.280V

Notes: a - $\overline{WST}$=20.° column duplicated; see text.
b - Not in original test data, supplied by linear interpolation.
c - Last data point before a reversal in Output vs Input data.

Table 2-7(o). Waveform Sampler Calibration Data (IRS, continued)

Flight Model Waveform Sampler IRS15,
the Instantaneous Return Waveform Sample #15

(Functional Units) Input Amplitude, in Volts	(Engineering Units) Output, in Volts			
	$\overline{WST}=0^{\circ}C$ Note a	$\overline{WST}=20.0^{\circ}$ TV/-2°C	$\overline{WST}=44.7^{\circ}$ Ambient	$\overline{WST}=63.1^{\circ}$ TV/+42°
-0.2V	-0.875V	-0.875	-0.811	-0.791
- .1	-0.445	-0.445	-0.421	-0.405
0.0	-0.007	-0.007	-0.003	0.002
.1	0.422	0.422	0.412	0.458
.2	0.854	0.854	0.827	0.814
.3	1.248	1.248	1.217	1.163
.35	1.430	1.430[b]	1.428	1.256[b]
.4	1.611	1.611	1.535	1.350
.45	1.626	1.626[b]	1.550	1.356[b]
.5	1.640	1.640[c]	1.564[c]	1.362
.6	"	"	"	1.374

Engineering Units Lower Limit = -0.791V
Engineering Units Upper Limit = 1.374V

Table 2-7(p). Waveform Sampler Calibration Data (IRS)

Flight Model Waveform Sampler IRS16,
the Instantaneous Return Waveform Sample #16

(Functional Units) Input Amplitude, in Volts	(Engineering Units) Output, in Volts			
	$\overline{WST}=0^{\circ}$ Note a	$\overline{WST}=20.0^{\circ}$ TV/-2°C	$\overline{WST}=44.7^{\circ}$ Ambient	$\overline{WST}=63.1^{\circ}$ TV/+42°
-0.2V	-0.820V	-0.820	-0.762	-0.766
- .1	-0.412	-0.412	-0.389	-0.372
0.0	0.010	0.010	0.003	0.000
.1	0.415	0.415	0.400	0.434
.2	0.814	0.814	0.789	0.792
.3	1.174	1.174	1.170	1.119
.35	1.349	1.349[b]	1.354	1.178[b]
.4	1.524	1.524	1.414	1.236
.45	1.531	1.531[b]	1.451[c]	1.244[b]
.5	1.538	1.538	"	1.251
.6	1.541	1.541	"	1.267

Engineering Units Lower Limit = -0.762V
Engineering Units Upper Limit = 1.267V

Notes: a - $\overline{WST}=20.^{\circ}$ column duplicated; see text.
b - Not in original test data, supplied by linear interpolation.
c - Last data point before a reversal in Output vs Input data.

2.4.2 The Average Waveform Sampler ARS1,...,16

Many of the remarks for IRS1,...,16 apply here as well. We have again supplied a "fictitious" $\overline{WST} = 0^{o}C$ column, and ARS13 shows a spurious behavior at higher WST just as did IRS13. The ARS1,...,16 calibration data are supplied in Table 2-8 on the following pages.

For the CALIMERGE EU limits, we indicate again on Table 2-8 the EU upper limit using the same recipe as in ARS1,...,16. The EU lower limit for all these Average Waveform Samplers may be taken as 0. volts however; this is because ARS1,...,16 are sampled by a different A/D converter for telemetry than were IRS1,...,16, and so the EU value for any individual ARS can only be zero or positive. Negative EU values appear in Table 2-8 for ARS1,...,16 only so as to encompass the value EU = 0.

Each ARS value is an average over something of the order of one second. The receiver AGC circuit is supposed to set the receiver gain so that the average plateau region has a Functional Units mean value of about 0.1 volt. To the degree that the point sample value on the return waveform has a standard deviation equal to its mean value and that the averaging is a one-second rectangular average (over 100 individual returns), the plateau region ARS values should be about 0.1 ± 0.01. This is not exact; for example the averaging process is not rectangular but is instead an RC=1 second process. However, this argument should be adequate to indicate that it would be highly unlikely under normal altimeter operation to have ARS Functional Units values exceeding 0.2 volts, and hence by Table 2-8 to have ARS Engineering Units values exceeding 4.0 volts.

Table 2.8(a). Waveform Sampler Calibration Data (ARS)

Flight Model Waveform Sampler ARS1 ,
the Average Return Waveform Sample #1

(Functional Units) Input Amplitude, in Volts	(Engineering Units) Output, in Volts			
	$\overline{WST}$=0°C Note a	$\overline{WST}$=20.0° TV/-2°C	$\overline{WST}$=44.7° Ambient	$\overline{WST}$=63.1° TV/+42°
- .1V	-1.752V	-1.752	-1.655	-1.596
0.0	0.024	0.024	0.017	0.024
.1	1.754	1.754	1.701	1.765
.2	3.457	3.457	3.332	3.232
.3	4.975	4.975	4.949	4.653
.35	4.986	4.986[b]	4.998	4.826[b]
.4	4.998	4.998	"	4.998
.45	"	"	"	"
.5	"	"	"	"
.6	"	"	"	"

Engineering Units Upper Limit = 4.998V

Table 2.8(b). Waveform Sampler Calibration Data (ARS)

Flight Model Waveform Sampler ARS2 ,
the Average Return Waveform Sample #2

(Functional Units Input Amplitude, in Volts	(Engineering Units) Output, in Volts			
	$\overline{WST}$=0°C Note a	$\overline{WST}$=20.0° TV/-2°C	$\overline{WST}$=44.7° Ambient	$\overline{WST}$=63.1° TV/+42°
- .1V	-1.754V	-1.754	-1.630	-1.607
0.0	-0.043	-0.043	-0.026	-0.026
.1	1.650	1.650	1.622	1.683
.2	3.328	3.328	3.262	3.165
.3	4.808	4.808	4.816	4.539
.35	4.903	4.903[b]	4.998	4.757[b]
.4	4.998	4.998	"	4.975
.45	"	"	"	4.986[b]
.5	"	"	"	4.998
.6	"	"	"	"

Engineering Units Upper Limit = 4.998V

Notes: a - $\overline{WST}$=20.° column duplicated; see text.
b - Not in original test data, supplied by linear interpolation.

Table 2.8(c). Waveform Sampler Calibration Data (ARS, continued)

Flight Model Waveform Sampler ARS3 ,

the Average Return Waveform Sample #3

(Functional Units)	(Engineering Units) Output, in Volts			
Input Amplitude, in Volts	$\overline{WST}$=0°C Note a	$\overline{WST}$=20.0° TV/-2°C	$\overline{WST}$=44.7° Ambient	$\overline{WST}$=63.1° TV/+42°
- .1V	-1.754V	-1.754	-1.651	-1.591
0.0	0.001	0.001	-0.001	0.003
.1	1.717	1.717	1.680	1.727
.2	3.395	3.395	3.302	3.188
.3	4.916	4.916	4.857	4.326
.35	4.957	4.957[b]	4.998	4.417[b]
.4	4.998	4.998	"	4.508
.45	"	"	"	4.536[b]
.5	"	"	"	4.564
.6	"	"	"	4.595

Engineering Units Upper Limit = 4.595V

Table 2.8(d). Waveform Sampler Calibration Data (ARS)

Flight Model Waveform Sampler ARS4 ,

the Average Return Waveform Sample #4

(Functional Units	(Engineering Units) Output, in Volts			
Input Amplitude, in Volts	$\overline{WST}$=0°C Note a	$\overline{WST}$=20.0° TV/-2°C	$\overline{WST}$=44.7° Ambient	$\overline{WST}$=63.1° TV/+42°
- .1V	-1.694V	-1.694	-1.580	-1.569
0.0	-0.015	-0.015	-0.017	-0.026
.1	1.629	1.629	1.585	1.644
.2	3.278	3.278	3.183	3.084
.3	4.765	4.765	4.705	4.420
.35	4.882	4.882[b]	4.998	4.667[b]
.4	4.998	4.998	"	4.914
.45	"	"	"	4.942[b]
.5	"	"	"	4.971
.6	"	"	"	4.995

Engineering Units Upper Limit = 4.995V

Notes: a - $\overline{WST}$=20.° column duplicated; see text.
b - Not in original test data, supplied by linear interpolation.

Table 2.8(e). **Waveform Sampler Calibration Data** (ARS, continued)

Flight Model Waveform Sampler ARS5 ,

the Average Return Waveform Sample #5

(Functional Units)	(Engineering Units) Output, in Volts			
Input Amplitude, in Volts	$\overline{WST}$=0°C Note a	$\overline{WST}$=20.0° TV/-2°C	$\overline{WST}$=44.7° Ambient	$\overline{WST}$=63.1° TV/+42°
- .1V	-1.721V	-1.721	-1.639	-1.613
0.0	0.034	0.034	0.003	-0.008
.1	1.738	1.738	1.672	1.718
.2	3.446	3.446	3.317	3.206
.3	4.938	4.938	4.863	4.554
.35	4.968	4.968[b]	4.998	4.776[b]
.4	4.998	4.998	"	4.998
.45	"	"	"	"
.5	"	"	"	"
.6	"	"	"	"

Engineering Units Upper Limit = 4.998V

Table 2.8(f). Waveform Sampler Calibration Data (ARS)

Flight Model Waveform Sampler ARS6 ,

the Average Return Waveform Sample #6

(Functional Units	(Engineering Units) Output, in Volts			
Input Amplitude, in Volts	$\overline{WST}$=0°C Note a	$\overline{WST}$=20.0° TV/-2°C	$\overline{WST}$=44.7° Ambient	$\overline{WST}$=63.1° TV/+42°
- .1V	-1.771V	-1.771	-1.643	-1.625
0.0	-0.052	-0.052	-0.042	-0.047
.1	1.634	1.634	1.601	1.671
.2	3.306	3.306	3.240	3.166
.3	4.783	4.783	4.776	4.528
.35	4.890	4.890[b]	4.998	4.763[b]
.4	4.998	4.998	"	4.998
.45	"	"	"	"
.5	"	"	"	"
.6	"	"	"	"

Engineering Units Upper Limit = 4.998V

Notes: a - $\overline{WST}$=20.° column duplicated; see text.
b - Not in original test data, supplied by linear interpolation.

Table 2.8(g). **Waveform Sampler Calibration Data** (ARS, continued)

Flight Model Waveform Sampler ARS7 ,

the Average Return Waveform Sample #7

(Functional Units) Input Amplitude, in Volts	(Engineering Units) Output, in Volts			
	$\overline{WST}$=0°C Note a	$\overline{WST}$=20.0° TV/-2°C	$\overline{WST}$=44.7° Ambient	$\overline{WST}$=63.1° TV/+42°
- .1V	-1.973V	-1.973	-1.879	-1.829
0.0	-0.231	-0.231	-0.236	-0.241
.1	1.456	1.456	1.418	1.474
.2	3.151	3.151	3.062	2.999
.3	4.694	4.694	4.627	4.287
.35	4.846	4.846[b]	4.998	4.467[b]
.4	4.998	4.998	"	4.647
.45	"	"	"	4.711[b]
.5	"	"	"	4.775
.6	"	"	"	4.842

Engineering Units Upper Limit = 4.842V

- - - - - - - -

Table 2.8(h). Waveform Sampler Calibration Data (ARS)

Flight Model Waveform Sampler ARS8 ,

the Average Return Waveform Sample #8

(Functional Units Input Amplitude, in Volts	(Engineering Units) Output, in Volts			
	$\overline{WST}$=0°C Note a	$\overline{WST}$=20.0° TV/-2°C	$\overline{WST}$=44.7° Ambient	$\overline{WST}$=63.1° TV/+42°
- .1V	-1.658V	-1.658	-1.542	-1.535
0.0	-0.008	-0.008	0.000	-0.001
.1	1.612	1.612	1.583	1.660
.2	3.236	3.236	3.143	3.061
.3	4.661	4.661	4.605	4.328
.35	4.830	4.830[b]	4.998	4.436[b]
.4	4.998	4.998	"	4.544
.45	"	"	"	4.568[b]
.5	"	"	"	4.592
.6	"	"	"	4.598

Engineering Units Upper Limit = 4.598V

Notes: a - $\overline{WST}$=20.° column duplicated; see text.
b - Not in original test data, supplied by linear interpolation.

Table 2.8(i). Waveform Sampler Calibration Data (ARS, continued)

Flight Model Waveform Sampler ARS9 ,

the Average Return Waveform Sample #9

(Functional Units) Input Amplitude, in Volts	(Engineering Units) Output, in Volts			
	$\overline{WST}$=0°C Note a	$\overline{WST}$=20.0° TV/-2°C	$\overline{WST}$=44.7° Ambient	$\overline{WST}$=63.1° TV/+42°
- .1V	-1.837V	-1.837	-1.751	-1.723
0.0	-0.026	-0.026	-0.041	-0.058
.1	1.735	1.735	1.669	1.746
.2	3.468	3.468	3.331	3.223
.3	4.998	4.998	4.940	4.570
.35	"	" [b]	4.998	4.784[b]
.4	"	"	"	4.998
.45	"	"	"	"
.5	"	"	"	"
.6	"	"	"	"

Engineering Units Upper Limit = 4.998V

Table 2.8(j). Waveform Sampler Calibration Data (ARS)

Flight Model Waveform Sampler ARS10 ,

the Average Return Waveform Sample #10

(Functional Units Input Amplitude, in Volts	(Engineering Units) Output, in Volts			
	$\overline{WST}$=0°C Note a	$\overline{WST}$=20.0° TV/-2°C	$\overline{WST}$=44.7° Ambient	$\overline{WST}$=63.1° TV/+42°
- .1V	-1.732V	-1.732	-1.624	-1.594
0.0	0.017	0.017	0.019	0.006
.1	1.728	1.728	1.695	1.752
.2	3.435	3.435	3.347	3.264
.3	4.953	4.953	4.924	4.658
.35	4.976	4.976[b]	4.998	4.828[b]
.4	4.998	4.998	"	4.998
.45	"	"	"	"
.5	"	"	"	"
.6	"	"	"	"

Engineering Units Upper Limit = 4.998V

Notes: a - $\overline{WST}$=20.° column duplicated; see text.
b - Not in original test data, supplied by linear interpolation.

Table 2.8(k). Waveform Sampler Calibration Data (ARS, continued)

Flight Model Waveform Sampler ARS11 ,
the Average Return Waveform Sample #11

(Functional Units)	(Engineering Units) Output, in Volts			
Input Amplitude, in Volts	$\overline{WST}$=0°C Note a	$\overline{WST}$=20.0° TV/-2°C	$\overline{WST}$=44.7° Ambient	$\overline{WST}$=63.1° TV/+42°
- .1V	-1.708V	-1.708	-1.628	-1.599
0.0	0.069	0.069	0.046	0.007
.1	1.783	1.783	1.717	1.740
.2	3.481	3.481	3.356	3.225
.3	4.964	4.964	4.910	4.602
.35	4.981	4.981[b]	4.998	4.800[b]
.4	4.998	4.998	"	4.998
.45	"	"	"	"
.5	"	"	"	"
.6	"	"	"	"

Engineering Units Upper Limit = 4.998V

Table 2.8(l). Waveform Sampler Calibration Data (ARS)

Flight Model Waveform Sampler ARS12 ,
the Average Return Waveform Sample #12

(Functional Units	(Engineering Units) Output, in Volts			
Input Amplitude, in Volts	$\overline{WST}$=0°C Note a	$\overline{WST}$=20.0° TV/-2°C	$\overline{WST}$=44.7° Ambient	$\overline{WST}$=63.1° TV/+42°
- .1V	-1.724V	-1.724	-1.600	-1.557
0.0	-0.032	-0.032	-0.020	-0.009
.1	1.621	1.621	1.597	1.677
.2	3.275	3.275	3.198	3.145
.3	4.770	4.770	4.719	4.464
.35	4.884	4.884[b]	4.998	4.688[b]
.4	4.998	4.998	"	4.912
.45	"	"	"	4.946[b]
.5	"	"	"	4.979
.6	"	"	"	4.980

Engineering Units Upper Limit = 4.980V

Notes: a - $\overline{WST}$=20.° column duplicated; see text.
b - Not in original test data, supplied by linear interpolation.

Table 2.8(m). Waveform Sampler Calibration Data (ARS, continued)

Flight Model Waveform Sampler ARS13 ,
the Average Return Waveform Sample #13

(Functional Units) Input Amplitude, in Volts	(Engineering Units) Output, in Volts			
	$\overline{WST}$=0°C Note a	$\overline{WST}$=20.0° TV/-2°C	$\overline{WST}$=44.7° Ambient	$\overline{WST}$=63.1° TV/+42°
- .1V	-1.689V	-1.689	-1.599	-1.552
0.0	0.009	0.009	0.000	0.096
.1	1.666	1.666	1.580	1.639
.2	3.314	3.314	3.178	2.142
.3	4.825	4.825	4.725	2.264
.35	4.912	4.912[b]	4.903	2.370[b]
.4	4.998	4.998	4.964	2.476
.45	"	"	4.998	2.558[b]
.5	"	"	"	2.640
.6	"	"	"	2.711

Engineering Units Upper Limit = 4.998V; taken from Ambient Chamber results.

- - - - - - - -

Table 2.8(n). Waveform Sampler Calibration Data (ARS)

Flight Model Waveform Sampler ARS14 ,
the Average Return Waveform Sample #14

(Functional Units Input Amplitude, in Volts	(Engineering Units) Output, in Volts			
	$\overline{WST}$=0°C Note a	$\overline{WST}$=20.0° TV/-2°C	$\overline{WST}$=44.7° Ambient	$\overline{WST}$=63.1° TV/+42°
- .1V	-1.751V	-1.751	-1.639	-1.584
0.0	-0.014	-0.014	-0.006	0.006
.1	1.674	1.674	1.651	1.735
.2	3.359	3.359	3.277	3.217
.3	4.859	4.859	4.840	4.580
.35	4.928	4.928[b]	4.998	4.789[b]
.4	4.998	4.998	"	4.998
.45	"	"	"	"
.5	"	"	"	"
.6	"	"	"	"

Engineering Units Upper Limit = 4.998V

Notes: a - $\overline{WST}$=20.° column duplicated; see text.
b - Not in original test data, supplied by linear interpolation.

Table 2.8(o). Waveform Sampler Calibration Data (ARS, continued)

Flight Model Waveform Sampler ARS15 ,
the Average Return Waveform Sample #15

(Functional Units) Input Amplitude, in Volts	(Engineering Units) Output, in Volts			
	$\overline{WST}=0^{o}C$ Note a	$\overline{WST}=20.0^{o}$ TV/$-2^{o}C$	$\overline{WST}=44.7^{o}$ Ambient	$\overline{WST}=63.1^{o}$ TV/$+42^{o}$
- .1V	-1.772V	-1.772	-1.658	-1.551
0.0	-0.009	-0.009	-0.001	0.030
.1	1.690	1.690	1.644	1.755
.2	3.389	3.389	3.282	3.232
.3	4.897	4.897	4.819	4.589
.35	4.948	4.948[b]	4.998	4.794[b]
.4	4.998	4.998	"	4.998
.45	"	"	"	"
.5	"	"	"	"
.6	"	"	"	"

Engineering Units Upper Limit = 4.998V

Table 2.8(p). Waveform Sampler Calibration Data (ARS)

Flight Model Waveform Sampler ARS16 ,
the Average Return Waveform Sample #16

(Functional Units Input Amplitude, in Volts	(Engineering Units) Output, in Volts			
	$\overline{WST}=0^{o}C$ Note a	$\overline{WST}=20.0^{o}$ TV/$-2^{o}C$	$\overline{WST}=44.7^{o}$ Ambient	$\overline{WST}=63.1^{o}$ TV/$+42^{o}$
- .1V	-1.628V	-1.628	-1.506	-1.457
0.0	0.020	0.020	0.029	0.063
.1	1.633	1.633	1.597	1.716
.2	3.218	3.218	3.134	3.105
.3	4.641	4.641	4.592	4.384
.35	4.820	4.820[b]	4.998	4.624[b]
.4	4.998	4.998	"	4.864
.45	"	"	"	4.908[b]
.5	"	"	"	4.952
.6	"	"	"	4.954

Engineering Units Upper Limit = 4.954V

Notes: a - $\overline{WST}=20.^{o}$ column duplicated; see text.
b - Not in original test data, supplied by linear interpolation.

2.4.3 The Peak Transmitter Power RTP

The calibration curves for RTP[V(P_T) in GE nomenclature] were generated during subassembly test of the A2 RF SWITCH ASS'Y. The measured coupling value for the A2DC1 50 dB coupler used in these tests was 50.7 dB. This number is necessary because the peak transmit power is defined as

$$P_T = \text{Measured Coupling Value} + \text{Detected Peak Power (dBm)}$$

where Detected Peak Power refers to the power measured by the transmit power monitor.

Two calibration tables are used; the choice of which table of calibration values to use depends upon whether the tracker is operating in the Global or the Intensive mode. These tables are from Reference 4, and are the input data for the linear-linear interpolation in EU and T as already described. The subassembly results from the Flight Model for the pulse-burst (the Global Mode of the tracker) are given in Table 2-9, and Table 2-10 presents the Flight Model subassembly results for the single-pulse mode (the Intensive Mode of the tracker). For both of these tables, the temperature to use under altimeter operating conditions is RTT (GE's TT1), the transmitter temperature. The Peak Transmitter Power (in dBm) is the quantity in Functional Units, and the Output Voltage is the Engineering Units quantity for this process.

2.4.4 Average Noise Gate ANG and Average Attitude/Specular Gate AASG

These two averaging gates are common to both the Global and the Intensive Modes of the Altimeter. They are physically located in the Global Tracker portion of the altimeter and their calibration data vary with temperature GTT, the Global Tracker Temperature. The Attitude/Specular gate output is used in the attitude estimation procedure discussed in Chapter 4 of this report, and Tables 2-11 and 2-12 give the input data for the linear-linear interpolation for ANG and AASG respectively.

2.4.5 Average Ramp Gate ARG, Average Plateau Gate APG, and Instantaneous Plateau Gate IPG, For Intensive Mode Only.

These three gates are physically separate elements from the corresponding three Global Mode gates discussed in section 2.3.3; the calibration data for

Table 2-9. Peak Transmitter Power RTP Calibration for the Global Mode (Pulse-Burst Mode) of the Tracker.

P_T, Peak Transmit Power in dBm (Functional Units)	Output Voltage RTP, in Volts (Engineering Units)			
	TT1=-25°C	+25°C	+50°C	+75°C
+54.7 dBm	-0.016V	+0.199	0.216	0.219
57.7	+0.386	0.587	0.600	0.599
58.7	0.561	0.758	0.769	0.759
59.7	0.759	0.943	0.956	0.944
60.7	0.982	1.172	1.170	1.153
61.7	1.235	1.417	1.414	1.389
62.7	1.520	1.693	1.693	1.660
63.7	1.840	2.000	1.992	1.958
64.7	2.194	2.350	2.330	2.292
65.7	2.574	2.720	2.694	2.641
66.7	2.933	3.060	3.052	2.964

Engineering Units Lower Limit = +0.219 V, Upper Limit = +2.933 V.

Table 2-10. Peak Transmitter Power RTP Calibration for the Intensive Mode (Single-Pulse Mode) of the Tracker.

P_T, Peak Transmit Power in dBm (Functional Units)	Output Voltage RTP, in Volts (Engineering Units)			
	TT1=-25°C	+25°C	+50°C	+75°C
+54.7 dBm	-0.038V	+0.167	0.180	0.179
57.7	+0.363	0.555	0.563	0.536
58.7	0.539	0.724	0.732	0.693
59.7	0.729	0.914	0.922	0.877
60.7	0.956	1.134	1.130	1.084
61.7	1.207	1.380	1.374	1.316
62.7	1.497	1.660	1.642	1.577
63.7	1.855	1.979	1.947	1.893
64.7	2.192	2.322	2.282	2.218
65.7	2.570	2.690	2.644	2.572
66.7	2.918	3.032	2.991	2.901

Engineering Units Lower Limit = +0.180 V, Upper Limit = +2.901 V.

Table 2-11. Flight Model Average Noise Gate ANG,
(Common to Intensive and Global Mode)

(Functional Units)	(Engineering Units) Output, in Volts			
Input Amplitude, in Volts	$\overline{GTT}$=0°C Note a	$\overline{GTT}$=12.2°C TV/-2°C	$\overline{GTT}$=39.4°C TV/Ambient	$\overline{GTT}$=56.3°C TV/+42°C
.0V	-0.012V	-0.012	-0.009	-0.013
.1	2.038	2.038	2.022	0.662
.2	4.039	4.039	3.992	1.236
.3	4.998	4.998	4.998	1.799
.35	"	"	"	2.552[b]
.4	"	"	"	3.305[c]
+.45	"	"	"	"

Notes: a - $\overline{GTT}$=12.2°C Column duplicated; see text.

b - Not in original test data, supplied by linear interpolation.

c - Last data point before a reversal in Output vs. Input.

Table 2-12. Flight Model Average Attitude/Specular Gate AASG, (Common to Intensive and Global Modes).

(Functional Units)	(Engineering Units) Output, in Volts			
Input Amplitude, in Volts	$\overline{GTT}=0^{o}C$ Note a	$\overline{GTT}=12.2^{o}C$ TV/$-2^{o}C$	$\overline{GTT}=39.4^{o}C$ TV/Ambient	$\overline{GTT}=56.3^{o}C$ TV/$+42^{o}C$
.0V	-0.043V	-0.043	-0.025	-0.015
.1	2.114	2.114	2.106	2.244
.2	4.191	4.191	4.144	4.108
.3	4.998	4.998	4.998	4.998
.35	"	"	"	"

Notes: a - $\overline{GTT}=12.2^{o}C$ Column duplicated; see text.

Table 2-13. Flight Model Average Ramp Gate ARG, Intensive Mode Only.

(Functional Units)	(Engineering Units) Output, in Volts			
Input Amplitude, in Volts	$\overline{ITT}$=0°C Note a	$\overline{ITT}$=20.8°C TV/-2°C	$\overline{ITT}$=45.6°C TV/Ambient	$\overline{ITT}$=65.3°C TV/+42°C
-.1V	-1.195V	-1.195	-1.093	-0.993
.0	-0.072	-0.072	-0.031	0.046
.1	1.043	1.043	1.059	1.154
.2	2.014	2.014	2.017	2.042
.3	2.897	2.897	3.020	3.052
.35	3.480	3.480[b]	3.531	3.919[b]
.4	4.063	4.063	4.144	4.786
+.45	4.530	4.530[b]	4.985	4.892[b]
.5	4.998	4.998	4.998	4.998
.6	"	"	"	"

Notes: a - $\overline{ITT}$=20.8°C column duplicated; see text.

b - Not in original test data, supplied by linear interpolation.

Table 2-14. Flight Model Average Plateau Gate APG, Intensive Mode Only.

(Functional Units)	(Engineering Units) Output in Volts			
Input Amplitude, in Volts	$\overline{ITT}$=0°C Note a	$\overline{ITT}$=20.8°C TV/-2°C	$\overline{ITT}$=45.6°C TV/Ambient	$\overline{ITT}$=65.3°C TV/+42°C
-.1	-1.203V	-1.203	-1.121	-1.031
.0	-0.110	-0.110	-0.086	0.010
.1	0.970	0.970	0.951	1.088
.2	1.945	1.945	1.903	1.983
.3	2.887	2.887	2.926	3.076
.35	3.728	3.728[b]	3.702	4.037[b]
.4	4.570	4.570	4.685	4.998
+.45	4.784	4.784[b]	4.998	"
.5	4.998	4.998	"	"
.6	"	"	"	"

Notes: a - $\overline{ITT}$=20.8°C column duplicated; see text.

b - Not in original test data, supplied by linear interpolation.

Table 2-15. Flight Model Instantaneous Plateau Gate IPG, Intensive Mode Only.

(Functional Units)	(Engineering Units) Output in Volts			
Input Amplitude, in Volts	$\overline{ITT}$=0°C Note a	$\overline{ITT}$=20.8°C TV/-2°C	$\overline{ITT}$=45.6°C TV/Ambient	$\overline{ITT}$=65.3°C TV/+42°C
-.2V	-0.969V	-0.969	-0.924	-0.931
-.1	-0.555	-0.555	-0.498	-0.426
.0	-0.017	-0.017	0.026	0.065
.1	0.549	0.549	0.560	0.603
.2	1.048	1.048	1.040	1.064
.3	1.528	1.528	1.541	1.599
.35	1.952	1.952[b]	1.938	2.161[b]
.4	2.376	2.376	2.435	2.723
+.45	2.870	2.870[b]	3.087	3.218[b]
.5	3.363	3.363	3.485	3.714
.6	3.659	3.659	3.836	4.138

Notes: a - $\overline{ITT}$=20.8°C Column duplicated; see text.

b - Not in original test data, supplied by linear interpolation.

Intensive Mode ARG, APG, and IPG depend upon temperature ITT, the Intensive Tracker Temperature, and (as opposed to the Global Mode situation) there do exist nearly adequate data for those Intensive Mode Gates. Table 2-13 presents Intensive Mode data for ARG, Table 2-14 presents data for APG, and Table 2-15 presents data for IPG. As discussed in subsection 2.4.1, we again duplicated the lowest ITT column, $\overline{ITT} = 20.8^{o}C$, to provide a ficticious $\overline{ITT} = 0^{o}C$ column. (Recall that bars here are to denote average temperatures over the period during which the calibration data were being taken.)

Referring to Table 2-2, we see that ARG and APG are never less than zero volts and that their upper limit is about +8 volts whereas IPG can range from about -4 to +4 volts. Suitable Engineering Units lower and upper limits respectively for these three gates are: 0. and 4.998 volts for ARG; the same for APG; and -0.924 and 3.659 volts for IPG.

2.4.6 The Receiver AGC Voltage RAGC

The parameter RAGC provides, through proper use of the calibration data, a measure of the signal level at the receiver in dBm. As in the waveform samplers, the double interpolation procedure [linear in both receiver temperature RRT (in ^{o}C) and in Engineering Units (volts)] will be used. Two separate RAGC tables are necessary, one for the Global Mode and one for the Intensive Mode of the altimeter. Among the several points to discuss for RAGC are: the pressure dependence of RAGC calibration, the difference in Intensive Mode calibration for Clean and for Clutter waveforms, and the saturation of the TAMS return signal simulator during testing at higher input powers.

First, it has been observed that there is a pressure dependence in the RAGC calibration. This is not unreasonable; some degree of physical flexing of waveguide sections might be expected to occur when the radar altimeter is put into a vacuum chamber simulating space pressures. Most of the other altimeter parameters are not sensitive to the environmental pressure but for RAGC it is important to use only calibration data obtained (at various temperatures) in an evacuated test chamber during "Thermal Vac" (T/V) testing.

Second, calibration data have been obtained in T/V for both Clean and Clutter waveforms. To discuss what is meant by "Clean" and "Clutter", we recall that these AGC calibration curves are obtained by injecting a repetitive pulse waveform into the altimeter's antenna port and measuring the resulting post-detection AGC voltage. Varying the input power and recording its level and the corresponding AGC voltage leads to a curve of AGC voltage vs. input power; this complete procedure is repeated for several different T/V chamber temperatures to produce a complete set of pre-flight AGC calibration curves.

The repetitive pulse waveform for these measurements was generated using a Video modulation waveform which approximated the average received power waveform expected during flight. Another set of AGC calibration curves was generated using, in addition to the modulating waveform just indicated, a noise source to modulate the rf phase and a second noise source to modulate amplitude. The set of AGC calibration curves generated with both noise sources <u>on</u> is referred to as the Clutter case while the set for both noise sources <u>off</u> is the Clean case. The Clutter case should provide a better approximation to the fluctuating and fading characteristics of the ocean backscattered return signal (assuming appropriate bandwidths of the noise sources) but, since the AGC voltage is derived from the (integrating) Plateau Gate, the presence or absence of zero-mean noise should on the average make no difference. Hence the Clean and Clutter AGC results should agree for either the Global or the Intensive Mode.

The Global Mode Level 4 Tests [4d] RAGC results for input power (Functional Units) of -60 dBm or lower are shown in Figure 2-5, separated according to temperature RRT, and it is seen that the Clean and Clutter calibration data do agree to within about 0.1 dBm except for the higher temperature case (and the altimeter is, we recall, expected to be relatively cold). The agreement to within a dB is of the order of the repeatability observed by GE (on these AGC measurements). However Figure 2-6 shows the results for RAGC in the Intensive Mode, and we see a consistent offset of about 3.6 dBm between the Clean and Clutter results in this case.

There is as yet no satisfactory explanation for the difference in the Clean and Clutter AGC calibrations in the Intensive Mode. The source of

Figure 2-5. Comparison of RAGC Calibration For Clean and Clutter Waveforms, Global Mode

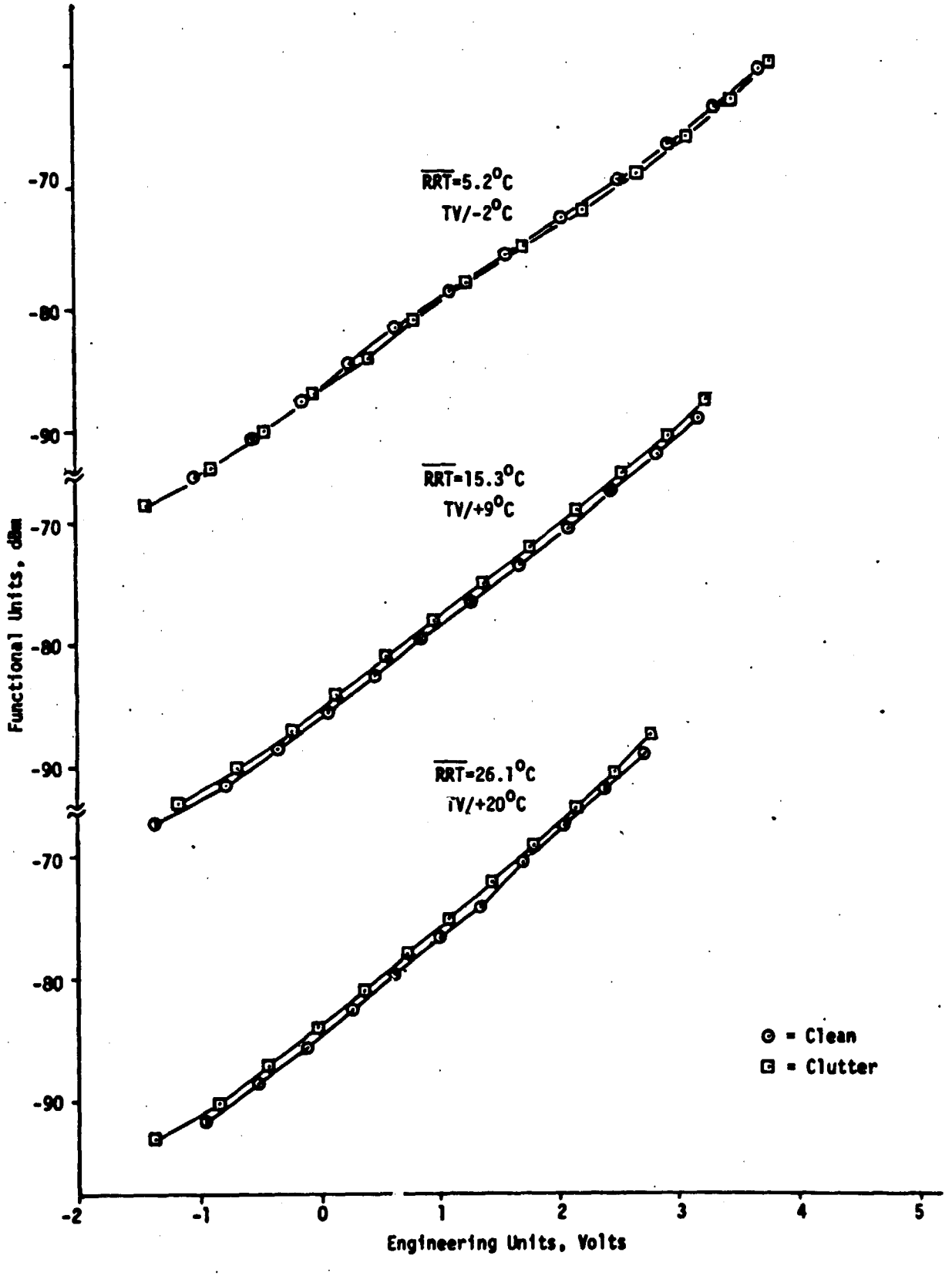

Figure 2-5 (Continued). Comparison of RAGC Calibration for Clean and Clutter Waveforms, Global Mode.

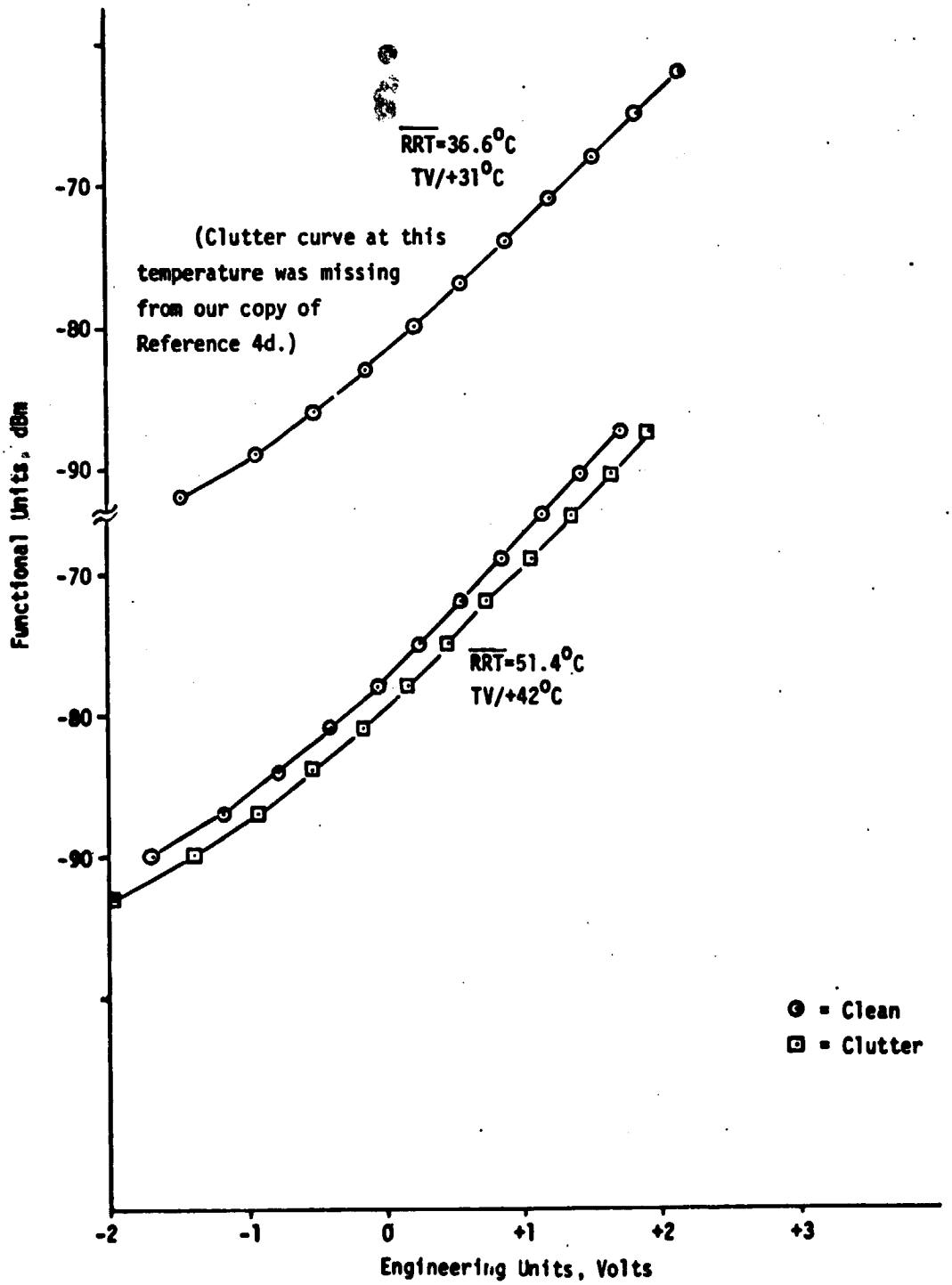

Figure 2-6. Comparison of RAGC Calibration for Clean and Clutter Waveforms, Intensive Mode

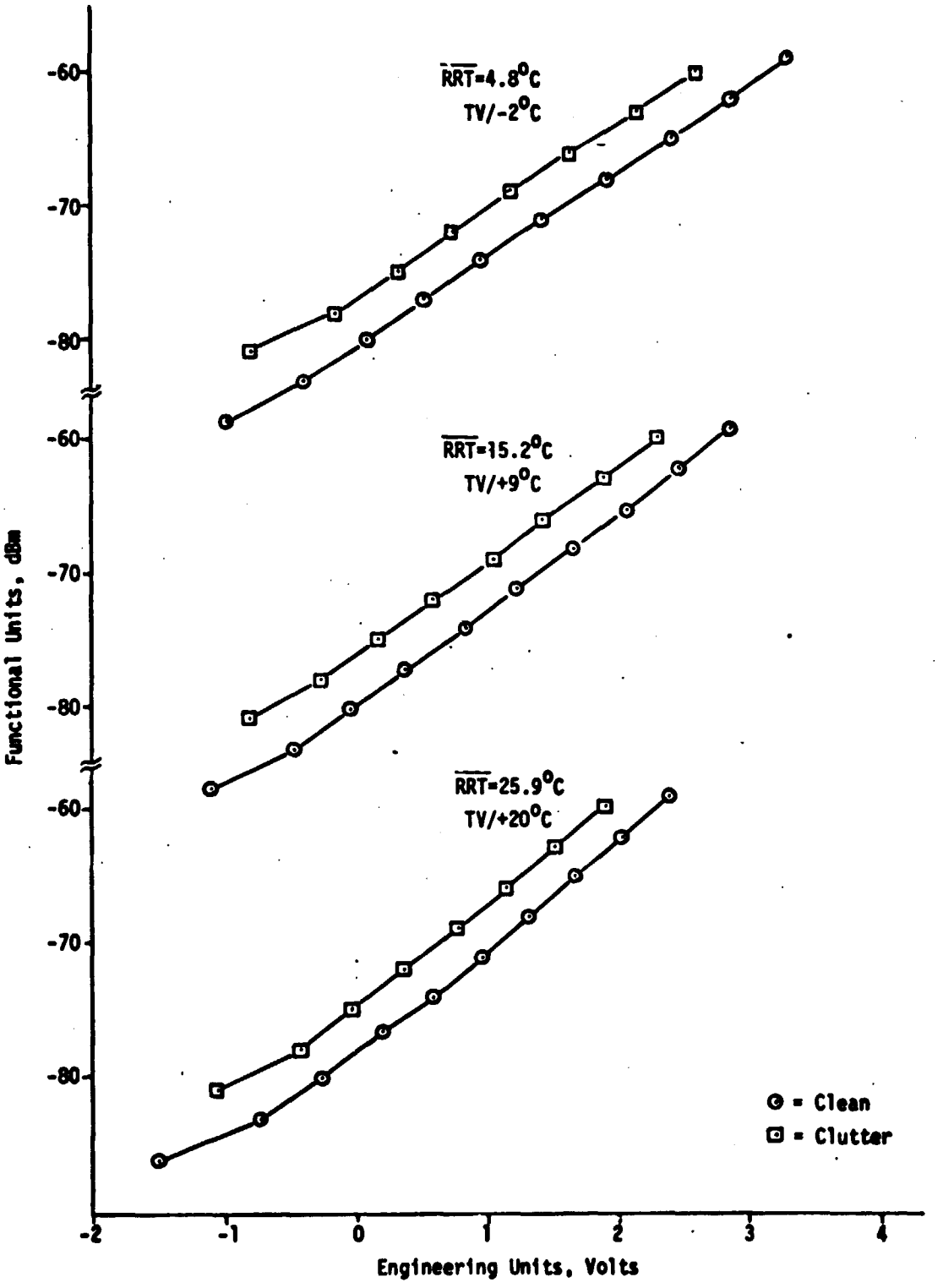

Figure 2-6 (Continued). Comparison of RAGC Calibration for Clean and Clutter Waveforms, Intensive Mode

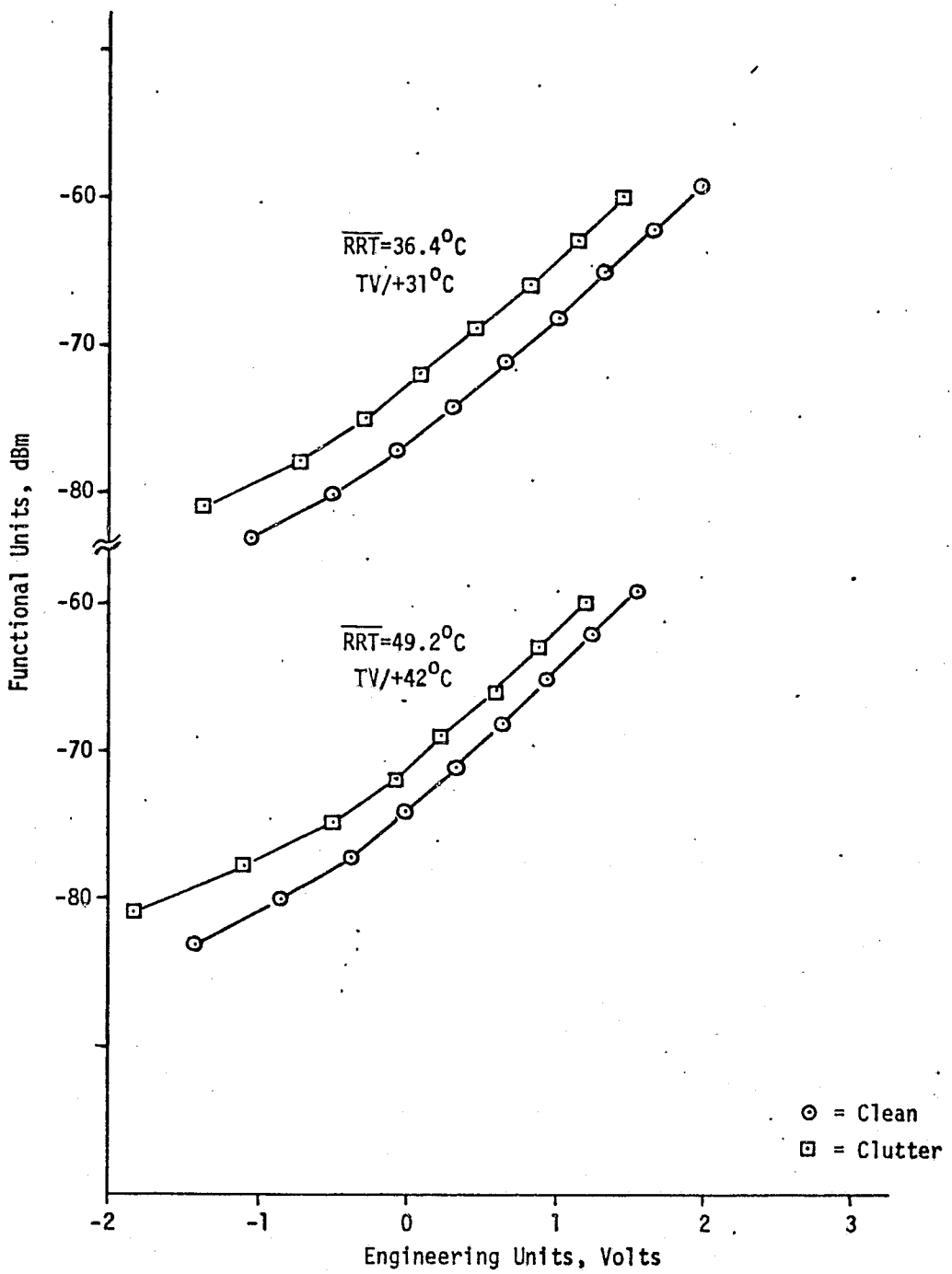

the problem may lie somewhere in the simulation of the return signal or in the actual measurement of peak power. We would recommend that the intact TAMS unit be made available for further testing with the Protoflight Model of the altimeter following a review and careful examination of the problem and after further discussions with E. L. Hofmeister at GE-Utica and other principals in the problem. For now it is necessary to arbitrarily choose one or the other, Clean or Clutter, for the altimeter AGC calibration data to be used in Wallops Flight Center processing.

We recommend here that the Clean waveform results be used for RAGC calibration, and the tables in this section are based on this choice. The reasons for this choice include: (1) the fact that the RAGC data available to us from the extended range, special tests (at APL, see next paragraph and footnote) were for Clean waveforms only; (2) the suspicion that the source of the problem lies somewhere in the Clutter signal generating or measuring procedure; and 3) the BIT/CAL Mode steps IF#1 and IF#2 use an internally-generated clean waveform and it may eventually be useful to be using clean waveform RAGC curves when we look in more detail at the BIT/CAL results. Note again that it is only for Intensive Mode results that the Clean vs. Clutter question is important, since there is effectively no discrepancy in the Global Mode.

Finally, the RSS (return signal simulator) within the TAMS [2] at GE began to saturate for levels greater than -60 dBm; this is why Figures 2-5 and 2-6 have been plotted only for data $\leq$ -60 dBm even though the calibration data in Reference 4d were taken for power up to about -39 dBm. This apparent saturation is an effect of the test procedure and not indicative of the altimeter itself.* To get around this limitation (because the IF step #1 within BIT/CAL should produce RAGC results corresponding to about -45 dBm), extended-range, special tests were carried out at APL** using a different rf chain. Unfortunately we have only data at ambient (room) temperature and pressure for these extended-range tests, so they

---

*This conclusion is based on various conversations with E. L. Hofmeister, C. L. Purdy, G. S. Brown, and others.

**The "Flight Model AGC Curve (Special Test, Extended Range)" special test data sheets, dated 13 November 1974, were obtained by correspondence with C. L. Purdy, NASA Wallops Flight Center.

must be compared only to ambient pressure and temperature tests at GE. The extended-range test results are plotted on Figures 2-7 and 2-8, and by comparing these to the GE Final Ambient test results, we see that to use the RAGC Functional Units (dBm) vs. Engineering Units (volts) calibration data, we should (1) use actual data at power levels less than -60 dBm and (2) use a straight-line-extrapolated results instead of TAMS-taken data for powers greater than -60 dBm. The straight line can be based on the last three or so data points for power $\leq$-60 dBm; this may be a rough recipe but it is the best we can do given the limitations of the data now at hand.

Tables 2-16 and 2-17 give the calibration data for RAGC based on the above considerations, and Figures 2-9 and 2-10 show the results plotted from these tables together with the original T/V data. Note that most of the entries in Tables 2-16 and 2-17 are obtained from linear interpolation between original pairs of data points; this has been for convenience in supplying a single set of Functional Unit values spaced 6 dB apart. In some cases, single linear extrapolations off the low power end of the tables have been performed in order to specify an appropriate Engineering Unit lower limit. The low-power end of these tables is somewhat suspect anyhow as some of these results were obtained under break-lock conditions in the testing. It may be that additional pre-flight calibration data are available for RAGC under vacuum and for a variety of pressures, and that Tables 2-16 and 2-17 can then be updated and corrected, but for now these two tables represent a best estimate based on data now available to us for the clean waveform AGC calibration.

As already noted in discussion of Table 2-2, there are two RAGC channels, high and low, in the telemetry system, with the high AGC channel having been a relatively recent addition. The distinction between high and low AGC channels is only important in converting from telemetry counts to Engineering Units; once a correct Engineering Units value is obtained, Table 2-17 for the Intensive Mode (or Table 2-16 for the Global Mode) is used to obtain Functional Units (dBm) regardless of whether the Engineering Units value was derived from the high or the low AGC telemetry channel.

Table 2-16. Flight Model Receiver AGC Voltage RAGC, Global Mode

		RAGC Output in Volts (Engineering Units)				
Test Environment		TV/-2°C	TV/+9	TV/+20	TV/+31	TV/+42
Test Average RRT		+5.2°C	15.3	26.1	36.6	51.4
Group B, Clean Triangular Signal Input in dBm (Functional Units)	-95.0dBm	-1.160V[b]	-1.300[b]	-1.470[b]	-1.950[b]	-2.400[b]
	-89.0	-0.316	-0.409	-0.588	-0.927[a]	-1.528
	-83.0	+0.484	+0.415	+0.205	-0.113[a]	-0.648
	-77.0	1.369	1.216	0.947	+0.574[a]	+0.045
	-71.0	2.314	2.025	1.651	1.228[a]	0.656
	-65.0	3.163	2.783	2.338	1.856[a]	1.241
	-59.0	3.890	3.483	2.993	2.479[a]	1.825
	-53.0	4.690[c]	4.210[c]	3.690[c]	3.110[c]	2.385[c]
	-47.0	5.490[c]	4.930[c]	4.370[c]	3.745[c]	2.955[c]
	-41.0	6.290[c]	5.650[c]	5.050[c]	4.370[c]	3.520[c]
	-35.0	7.090[c]	6.370[c]	5.730[c]	5.010[c]	4.095[c]
No. of runs averaged		3	1	1	1	3

(Engineering Units) Limits for RAGC, Global Mode: Upper Limit = +4.000V, Lower Limit = -1.100V

Unless otherwise noted, table entries have been obtained from linear interpolation between pairs of original calibration data points

Notes: a - Original data points.
b - Linear extrapolation to lower power than original data.
c - Linear extrapolation for input power greater than -60dBm.

Table 2-17. Flight Model Receiver AGC Voltage RAGC, Intensive Mode

		RAGC Output in Volts (Engineering Units)				
Test Environment		TV/-2°C	TV/+9	TV/+20	TV/+31	TV/+42
Test Average RRT		+4.8°C	15.2	25.9	36.4	49.2
Group C, Clean Rectangular Signal Input in dBm (Functional Units)	-95.0dBm	-2.705[b]	-2.922[b]	-3.712[b]	-3.212[b]	-3.724[b]
	-89.0dBm	-1.547[b]	-1.690[b]	-2.214[b]	-2.122[b]	-2.568[b]
	-83.	-0.389[a]	-0.458	-0.716	-1.032	-1.412
	-77.	0.522[a]	+0.397	+0.203	-0.058	-0.374
	-71.	1.426[a]	1.242	0.967	0.664	+0.330
	-65.	2.420[a]	2.090	1.686	1.332	0.947
	-59.	3.360[c]	2.889[c]	2.410[c]	1.976[c]	1.557[c]
	-53.	4.310[c]	3.699[c]	3.150[c]	2.613[c]	2.164[c]
	-47.	5.260[c]	4.509[c]	3.890[c]	3.251[c]	2.772[c]
	-41.	6.210[c]	5.319[c]	4.630[c]	3.888[c]	3.379[c]
	-35.	7.160[c]	6.129[c]	5.370[c]	4.526[c]	3.987[c]
No. of runs averaged		3	1	1	1	3

(Engineering Units) Limits for RAGC, Intensive Mode: Upper Limit = +3.900V, Lower Limit = -1.400V

Unless otherwise noted, table entries have been obtained from linear interpolation between pairs of original calibration data points

Notes: a - Original data points.
b - Linear extrapolation to lower power than original data.
c - Linear extrapolation for input power greater than -60dBm.

Figure 2-7. Comparison of GE Final Ambient and APL Extended Test Results, Global Mode, Clean Waveform

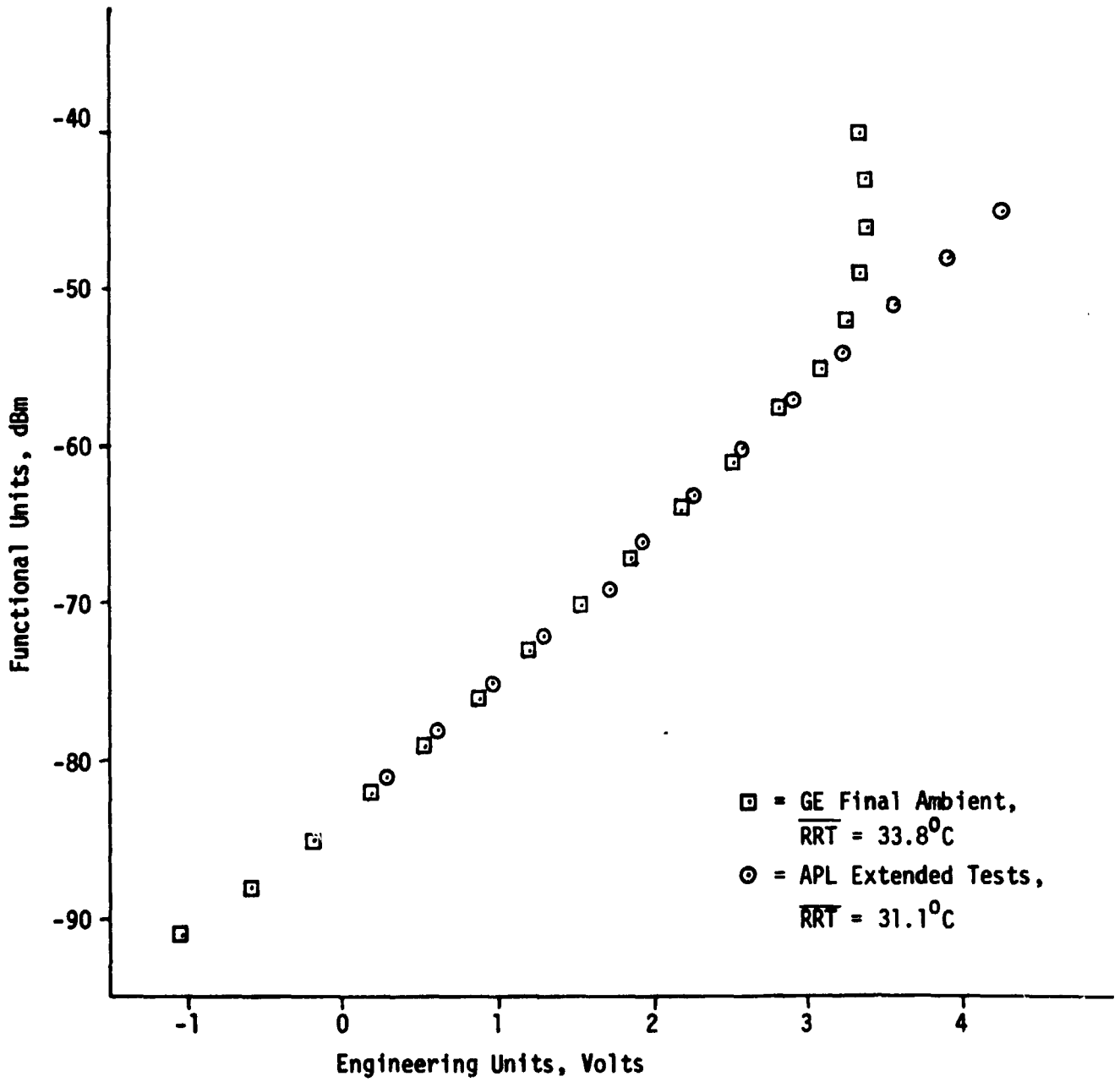

Figure 2-8. Comparison of GE Final Ambient and APL Extended Test Results, Intensive Mode, Clean Waveform

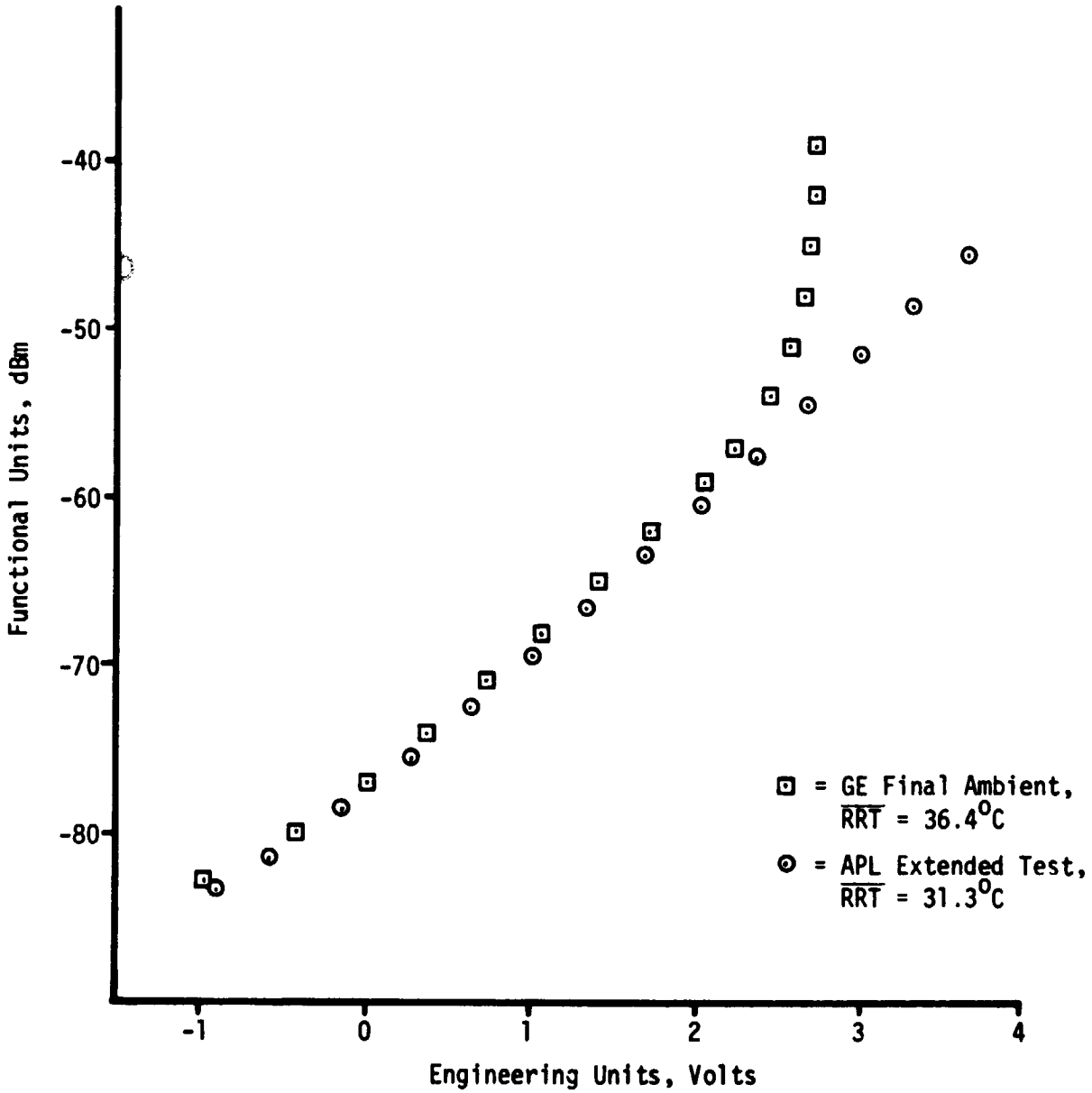

Figure 2-9. Calibration Curves For Receiver AGC Voltage RAGC, Global Mode (Line Segments are Based on Table 2-16 and Individual Symbols Are From Original Calibration Data.)

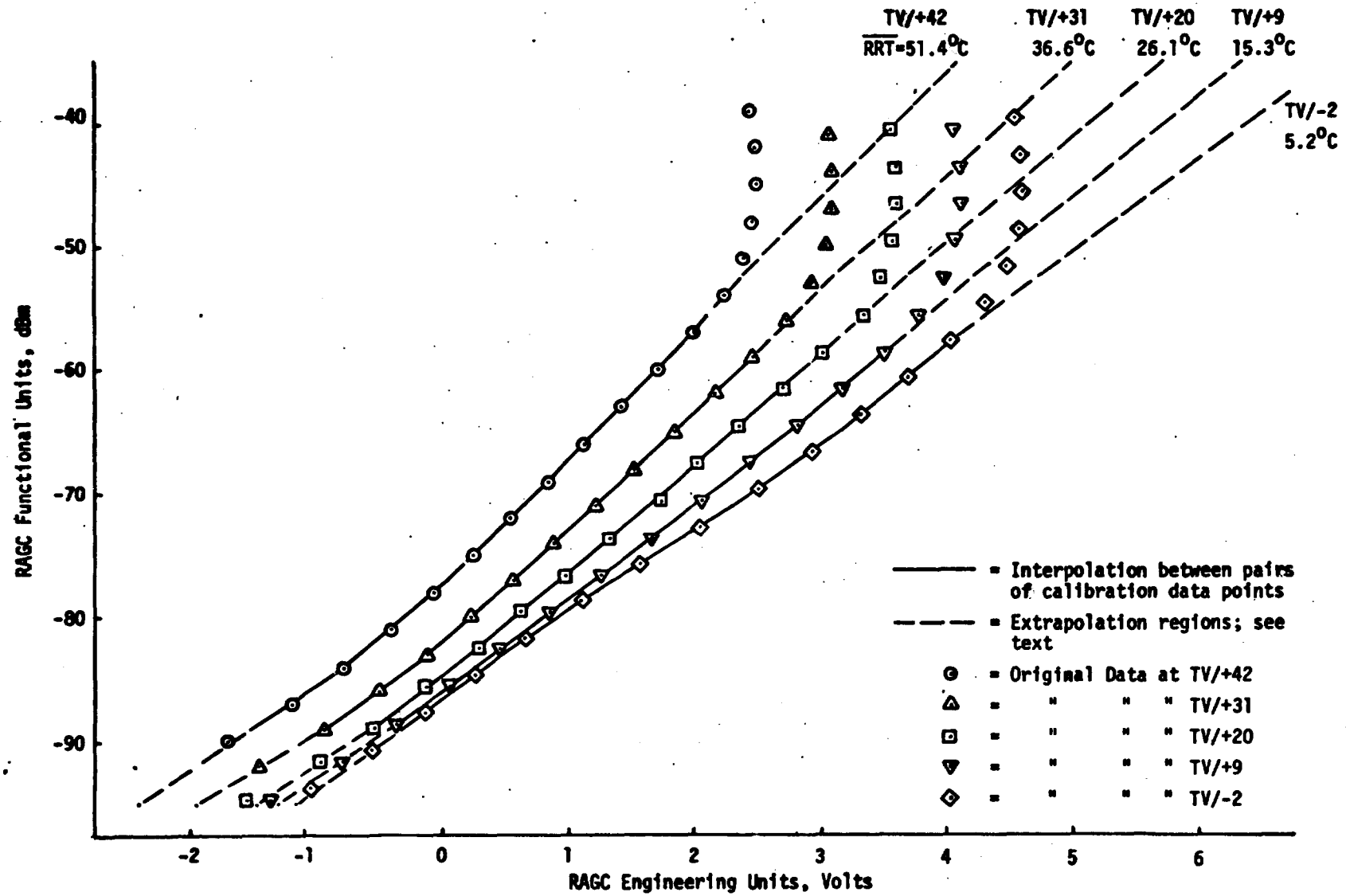

Figure 2-10. Calibration Curves For Receiver AGC Voltage RAGC, Intensive Mode (Line Segments Are Based on Table 2-17, and Individual Symbols Are From Original Calibration Data.)

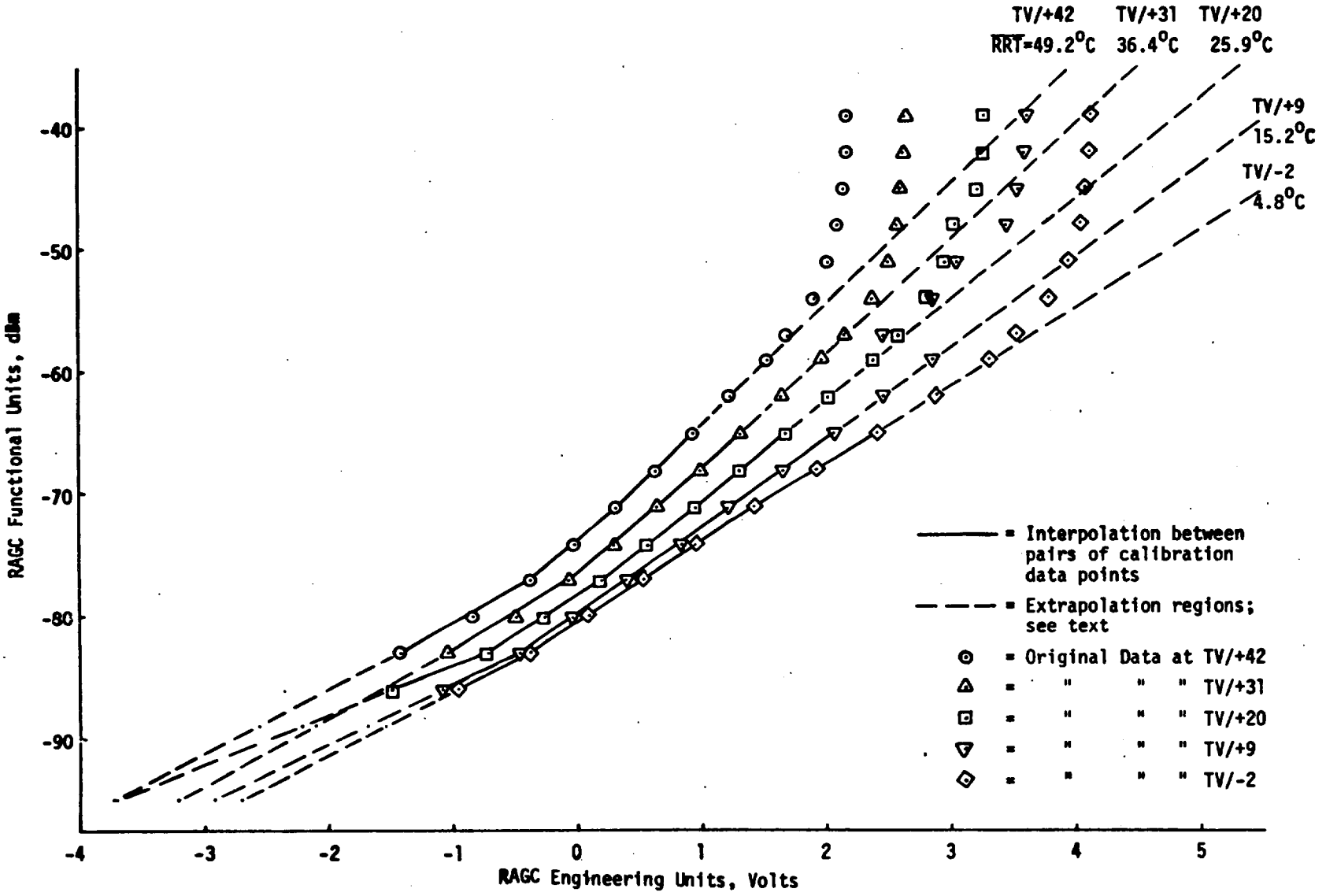

3.0 GEOS-C TIME-TAG PROCEDURES AND DATA PROCESSING CONSIDERATIONS

This section considers the time-delay effects associated with the altitude tracker, antenna-footprint, and illuminated area-to-satellite propagation delay. Time delays associated with the telemetry system are not considered here (i.e., the time within the frame at which the altitude buffer is read into the telemetry channel). Table 3-1 displays the composite timing corrections* now being used in conjunction with the NASA/WFC smoothed altitude data. Note that the composite time delay is approximately the midpoint of a major frame (e.g., one-half of 3.2 seconds in the case of Telemetry Mode 3 data). In the Wallops data processing for Telemetry Modes 1 and 2, the cumulative altitude values (10 per second) are further averaged, over 20 or 32 values respectively, to produce the smoothed altitude data (one per Major Frame).

The last (bracketed) quantity in the Table 3-1 composite time correction is the quantity to be discussed in the remainder of this chapter (specifically, 54 milliseconds in Telemetry Modes 1 and 2, and 4 milliseconds in Telemetry Mode 3). Section 3.1 will discuss the already implemented fixed time-tag corrections which should provide an adequate timing correction for surface features with spatial wavelengths $\geq$ 50 kilometers.

For data studies for which surface wavelengths of less than 50 kilometers are of primary concern, the fixed time-tag of correction of Section 3.1 will not be adequate and a data processing procedure is recommended which provides inherent time-tag correction (except for the propogation-path delay and telemetry-detail delay). Such a correction could be combined with other filtering procedures (e.g., minimum-variance estimation) to form a one-pass processing operation. These considerations for surface wavelength $\leq$ 50 km are presented in Section 3.2.

3.1 Fixed Time-Tag Correction

Need for the recommended time-tag corrections for the GEOS-C data (the quantities in brackets in Table 3-1) arises largely because of the time

---

*These data were obtained in March 1975 from R. Dwyer of Computer Science Corporation, Falls Church, Virginia.

Table 3-1. Timing Corrections Implemented at NASA/WFC for Each Telemetry Mode

Telemetry Mode	Altitude Entries Per Major Frame	Time Correction (Time in Milliseconds, T=Major Frame Start Time)
Mode 1	20/Frame	T + 20(51.20256) - 1(5.120256) - 0.1984 - 9.5(20)(0.5120256) - [54.0] = T + 867.4
2	32	T + 32(51.20256) - 10(0.5120256) - 0.1984 - 9.5(20)(0.5120256) - [54.0] = T + 1481.9
3	320	T + 32(51.20256) - 30(0.5120256) - 0.1984 - 5.120256 - [4.0] = T + 1613.8

delay inherent in the .1 second averaging operation performed by the GEOS-C altitude processor. Since the altitude word read out of the TM Channel constitutes an arithmetic average of altitude tracking loop accumulator values, the midpoint of the altitude data base is backward in time by roughly one-half the averaging period. An additive .001 second time delay which is also present is the time delay of the tracking loop itself in the geoidal long-wavelength limit.

Based on currently available information the altitude measurement process can be approximated in block diagram form as shown below where $H(j\omega)$ is the frequency domain (Fourier) transfer function*; the second block (the Averager) is not present in Telemetry Mode 3.

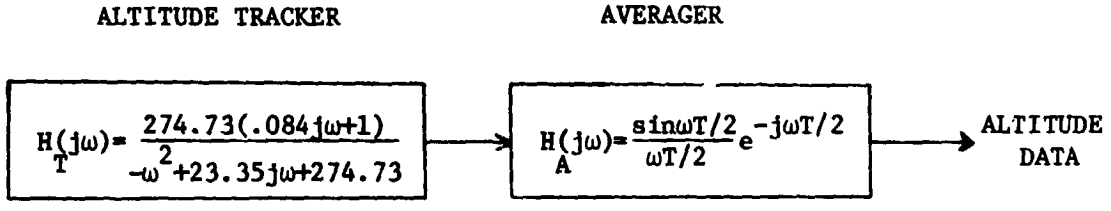

The corresponding time-domain impulse-response characteristics are shown in Figures 3-1 and 3-2. As shown in these characterizations, a particular altitude value represents contributions from a large number of past values; a given value is not centrally weighted since the tracker cannot be anticipative. As will be discussed in Section 3.2, if desired a non-anticipatory restriction can be removed in computer (non-real-time) data processing. The fixed-value time correction which is developed in the following paragraphs is considered adequate for most altimeter data applications.

The altitude tracker transfer function can be expressed in polar form as

$$H_T(j\omega) = |H_T(j\omega)| \exp\left(-j \tan^{-1} \frac{.084\omega^3 + .27308\omega}{.9614\omega^2 + 274.73}\right) ;$$

*Although the Global and the Intensive Mode tracker gates have different widths, their gains have been adjusted so that the loop transfer function is the same for both tracker modes, according to E. L. Hofmeister.

Figure 3-1. Weighting Function Sequence (Impulse Response) of Tracking Loop [Figure Supplied by E. L. Hofmeister, February 1975].

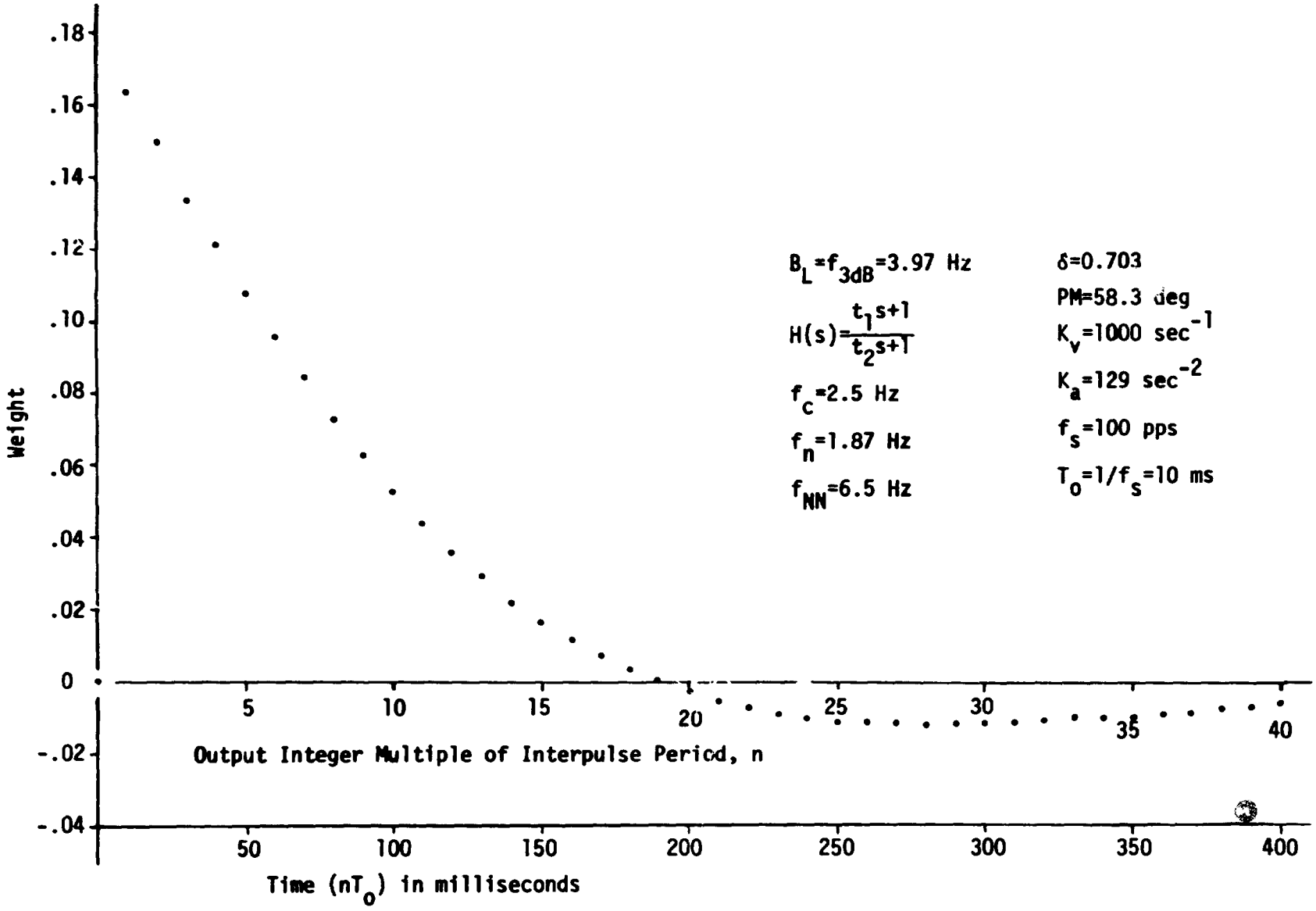

Figure 3-2. Weighting Function Sequence (Impulse Response) of Tracking Loop
[Figure Supplied by E. L. Hofmeister, February 1975].

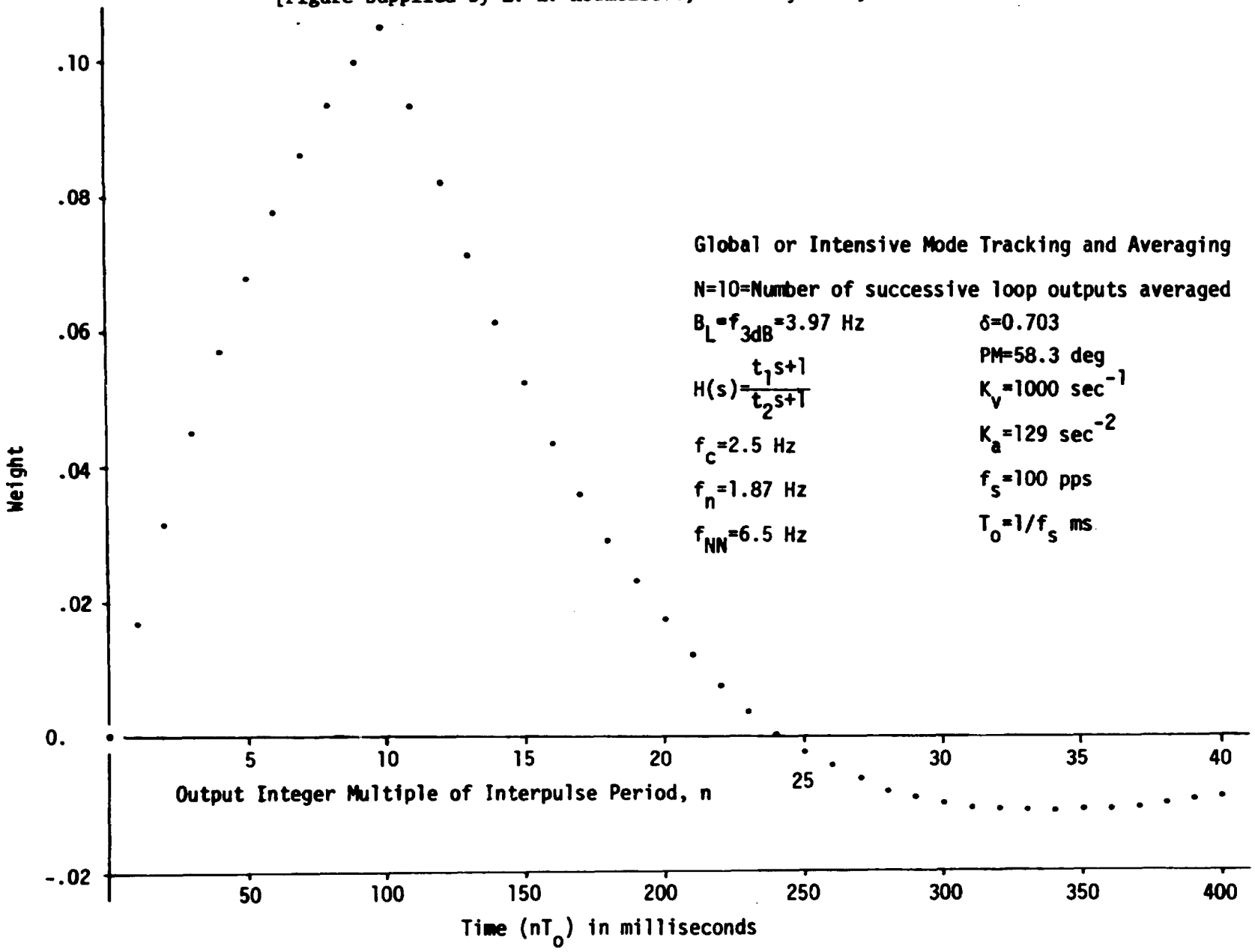

similarly,

$$H_A(j\omega) = |H_A(j\omega)|e^{-j\omega T/2} ,$$

where the averaging period T is .1 sec. Since an idealized linear phase-shift device will have a transfer function of the form,

$$H(j\omega) = |H(j\omega)|e^{-jt_o\omega} ;$$

by analogy* a frequency range can be established over which the altitude data may be considered to be derived from a fixed-time delay system. Using this analogy, the time delay t_o is given by

$$t_o = \frac{1}{\omega} \tan^{-1} \left[\frac{.084\omega^3 + .27308\omega}{.9614\omega^2 + 274.73} \right] + \frac{T}{2} .$$

This expression is evaluated in Table 3-2 for the intensive mode with frequency in Hz, ω in radian/sec, wavelength in km (assuming a ground track velocity of 7.4 km/sec), and time delay t_o in milliseconds. Table 3-2 shows that

1) the altimeter output data behaves essentially as a fixed time delay system for surface wavelengths equal to or greater than ~ 50 km, with a time delay of ~ 51 milliseconds**, and
2) the time delay of the on-board averaging operation is the dominant effect for the long wavelength case (its time delay alone accounts for 50 ms and the residual delay is the appropriate delay to be associated with the 100/sec altitude data.
3) a time delay of .003 sec should be added to these values, to account for the delay between the transmitted pulse timing event and the pulse incident on the Earth's surface.

---

*This is the delay relatable to monochromatic conditions; under an assumption of "weak dispersion", the time delays would be $d\phi/d\omega$, where ϕ is the angle variable and the two approaches yield the same result as $\omega \to 0$.
**This is essentially the value of t_o as $\omega \to 0$, i.e. $t_o = T/2$.

Table 3-2. Altitude Tracker Time Delay

Frequency in Hz	ω, in Radians/sec	Wavelength, in km	Delay, t_o, in Milliseconds
74.000Hz	464.96	0.1km	53.325ms
24.667	154.99	0.3	59.654
14.800	92.991	0.5	65.533
10.572	66.422	0.7	70.919
8.222	51.662	0.9	75.755
7.400	46.496	1.0	77.947
2.467	15.499	3.0	86.126
1.480	9.299	5.0	70.798
1.057	6.642	7.0	62.518
0.822	5.166	9.0	58.367
0.740	4.650	10.0	57.057
0.247	1.550	30.0	51.714
0.148	0.930	50.0	51.255
0.106	0.664	70.0	51.127
0.082	0.517	90.0	51.075
0.074	0.465	100.0	51.059
0.037	0.233	200.0	51.010
0.025	0.155	300.0	51.001
0 019	0.116	400.0	50.998
0.015	0.093	500.0	50.997
0.012	0.078	600.0	50.996

3.2 Time-Tag Correction For Short-Wavelength Features.

As discussed in Section 3.1, characteristics of the altitude tracker cause the exact time delay to be a function of surface wavelength under observation. This behavior arises because the altimeter is designed to be a quasi real-time device; it estimates current altitude value based only on current and past observations. Since all data studies will involve processing the surface profile information in a non-real-time sense, this dispersive time delay can be exactly corrected, in theory. In practice it can be corrected to the degree that the system response characteristics are known and are time-invariant.*

This section first discusses the nature of the numerical convolution procedure needed to compensate the time delay characteristics, and concludes with a discussion of "footprint" effects and observation random error considerations.

First consider the constraints on the smoothing functions that give the value of the smoothed function at the midpoint of the time interval. The output y(t) of a linear smoothing operation on input data x(t) by weighting coefficients w_i is given by

$$y(t) = \sum_{i=-k}^{k} w_i \, x(t + i\Delta t)$$

where Δt is the time interval between the equispaced samples. This may be written in the transform domain using a discrete Fourier transform $Y(j\omega)$ as

---

*We have received from E. L. Hofmeister at GE-Utica the tabulated values of weighting coefficients, etc., for the GEOS-C radar altimeter. These materials, dated 14 February 1975, represent the best values available as of the time of writing of the present report; these values were attached as Appendix A to an informal memorandum from L. S. Miller, Applied Science Associates, 20 February 1975. These are not attached to the present report because the effective tracker bandwidth will change if high sea-states or large attitude errors are present (these points were discussed in another informal memorandum from L. S. Miller to J. T. McGoogan, NASA/WFC, January 1975). Such effects can be assessed to some degree through examination of spectra of in-flight altimeter random error residuals.

$$Y(j\omega) = X(j\omega) \sum_{i=-k}^{k} w_i \, e^{ij\omega\Delta t} \, .$$

For a filtering function for which $w_i = w_{-i}$ this becomes

$$Y(j\omega) = X(j\omega) \left\{ w_o + \sum_{i=1}^{k} w_i \left(e^{ij\omega\Delta t} + e^{-ij\omega\Delta t} \right) \right\}$$

and since the term in parentheses is equal to $2\cos(i\omega\Delta t)$ the expression becomes

$$Y(j\omega) = X(j\omega) \left\{ w_o + 2 \sum_{i=1}^{k} w_i \cos(i\omega\Delta t) \right\}$$

where w_o is the central coefficient.

This form shows that the transform is a real variable (in contrast with the complex nature of the functions discussed in Section 3.1) and, as such, represents a time domain response corresponding to the midpoint of the smoothing interval. Note that the altimeter data has been filtered by the tracking loop and averager only over negative time indices

$$\sum_{i=-k}^{o} w_i \, x(t + i\Delta t)$$

and this time series may be converted to one that is centrally weighted by a subsequent convolution of

$$\sum_{i=1}^{k} w_i \, x(t + i\Delta t).$$

These results provide a method for compensating the time delay associated with the altimeter data: the weighting coefficients given in Figures 3-1 and 3-2 may be convolved with the 10 or 100 per second altitude data.

Next consider the result of multiple-pass convolutions with weighting coefficients u_i and v_i

$$y(t) = \sum_{i=-k}^{k} u_i \, x(t + i\Delta t)$$

and

$$z(t) = \sum_{i=-k}^{k} v_i \, y(t + i\Delta t)$$

In the transform domain these become

$$Z(j\omega) = U(j\omega) \; V(j\omega) \; X(j\omega)$$

which shows that these operations reduce to a single-pass operation, as long as the sampling events are equally spaced. [The composite weighting coefficients are the inverse transform of the product $U(\cdot)$ $V(\cdot)$.]

If the convolution over u_i is associated with the GEOS-C system characteristics and time-delay correction, the convolution over v_i may be related to smoothing algorithms designed to estimate (under some optimality criteria) surface undulation or slope information. This subject is next discussed with emphasis on the random error constraints imposed by the altimeter. Most of this material has already been reported [5], and is repeated here to make this chapter more nearly self-contained.

The analytical method and results to be discussed are as follows:

1. A procedure for filtering the GEOS-C altimeter data is first derived based on a minimum-mean-square error criteria. Its solution requires a mathematical description of the geoidal power spectral density; the one used is obtained from Skylab altimeter experimental data.

2. This quasi-optimal filter is then compared with the filter effect which arises from the nonzero spot-size of the altimeter (the so-called spatial filter effect). The spatial filter effect is found to be a relatively minor one compared to the short-wavelength cut off properties of the optimum filter (the filter response drops to one-half at ~ 40 km wavelength for the assumed altimeter measurement error characteristics) and computed spectra.

Figure 3-3 displays a power-spectral-density (PSD) plot for the Puerto Rican Trench region which was computed using Fast Fourier Transform methods and a Hanning type convolution window. The data base comprised SL-2, Pass 4, Mode 5 with 100 and 130 nanosecond pulsewidths (pulse compression was not functioning during SL-2). (For other details see Reference 5.) The Puerto Rican Trench data was used since we wanted to obtain PSD results for an anomalous region which should contain more energy in short-wavelength components than anomaly-free regions. The PSD so obtained, and data processing results derived therefrom, should represent the best opportunity for the altimeter to obtain information relating to short wavelength undulations and should yield an approximate upper bound on data processing requirements.

Referring to Figure 3-3, the dashed line corresponds to the density level for which a 5 Hz rectangular bandwidth, white noise spectrum would yield an rms level equal to 0.5 meters. The noise level shown in the calculated spectrum represents the Skylab altimeter noise level (1-2 meters rms). We will subsequently verify that the spatial filter function corresponds to considerably shorter wavelengths (less than 10 km) and that the calculated PSD is not contaminated by the altimeter footprint effect.

Note that the observed spectrum represents an asymptotic behavior which in the frequency parameter (f) is approximately f^{-4}. Kaula's model of one-dimensional spectral behavior decays as f^{-3} [6]. Since observable geoidal components are of much longer wavelengths than spatial filter effects, the data in Figure 3-3 may be interpreted as a cut through a two-dimensional spectrum. In wave-number space (k_x, k_y) a directional spectrum $S(k_x, k_y)$ with a k^{-4} behavior will yield a one-dimensional asymptotic behavior of k^{-3} (due to integration over the angular coordinate of the polar coordinate set).

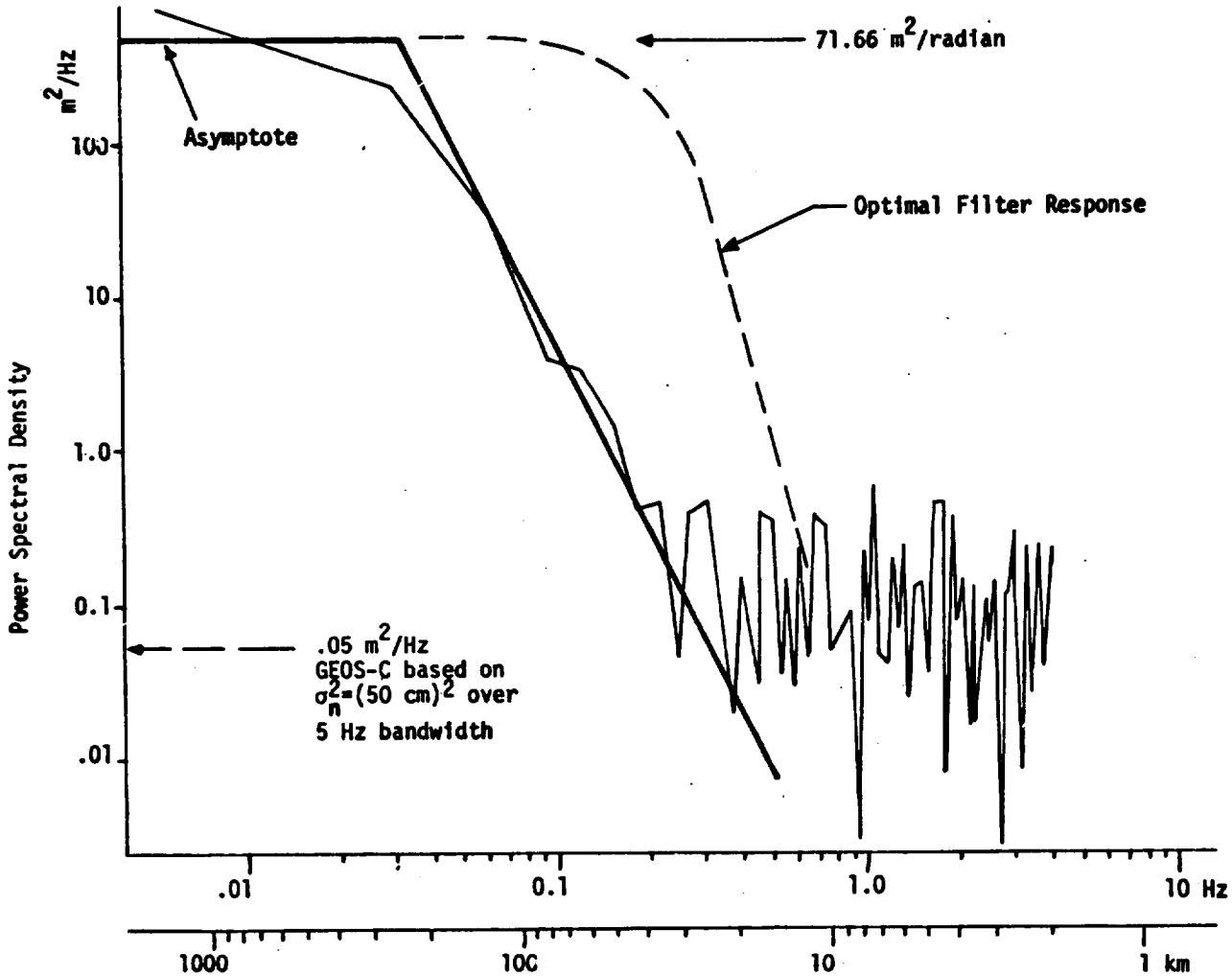

Figure 3-3. Geoid Undulation Spectrum of Puerto Rican Trench Area and Wiener Filter Transfer Function. [Figure Reprinted From May 1974 Report by L. S. Miller and G. S. Brown, Reference 5.]

Therefore, we feel that the observed spectrum depicts the proper theoretical behavior.

The optimization technique we use is the Wiener-Hopf formulation, which for the correlation functions $R(\cdot)$ of signal s and observation y, gives the optimum impulse response $h_o(t)$ as the solution to the integral equation

$$R_{sy}(\tau+\eta) = \int_0^\infty h_o(\mu)R_y(\tau-\mu)d\mu \ , \qquad \tau \geq 0.$$

For non-real-time processing, an estimate of a value at time t can be based on both past and future values. Therefore, the proper lower limit on the integrals is $-\infty$ and the integral equation becomes a convolution form which is readily solved by transform theory. For our purposes the form of the solution is

$$H(\omega) = \frac{S(\omega)}{S(\omega) + N(\omega)}$$

where $S(\omega)$ is the geoid undulation power spectrum and $N(\omega)$ is the additive noise spectrum. Since the altitude tracker has a noise equivalent bandwidth of ~ 5 Hz and a random error standard deviation of ~ 0.5 m, $N(\cdot)$ may be represented as a white noise spectrum with a density of $(.5)^2 m^2/5$ hz = .05 m^2/Hz or 7.96 x 10^{-3} m^2/radian. Using the break-point approximation (the asymptotes of which are shown in Figure 3-3) to $S(\omega)$ as [7]

$$S(\omega) = \frac{71.66 \cdot 6.554 \times 10^{-4}}{\omega^4 - .0512\omega^2 + 6.554 \times 10^{-4}} \ ,$$

the optimum transfer function is found to be

$$H_o(\omega) = \frac{5.9}{\omega^4 - .0512\omega^2 + 5.9006} \ .$$

This function is also shown in Figure 3-3. Note that the asymptote is twice as steep as the spectral decay. At the intersection of the break-point spectral approximation and the GEOS-C noise level (which occurs at ~ 22 km), $H_o(\omega)$ introduces an attenuation of ~ 12 dB. The 3 dB attenuation point occurs at ~ 40 km.

Figure 3-4 shows the computed spatial filter response function for the GEOS-C system. Note that the solution $[H_o(\omega)]$ given above effectively truncates geoidal data at considerably longer wavelengths than does the spatial filter effect (its 3 dB point occurs at ~ 10 km).

The optimal filter $H_o(\omega)$ has been inverse Fourier transformed through use of contour integration, and the normalized impulse response found to be

$$h(t) = e^{-0.8755t}(\cos 1.289t + 0.6792 \sin 1.289t), \text{ for } t>0.$$

Knowing that the optimal geodetic slope filter is the derivative of the optimum undulation filter, the impulse response for slope estimation is

$$\frac{d\,h(t)}{dt} = -0.8755\, e^{-0.8755t}(\cos 1.289t + 0.6792 \sin 1.289t)$$

$$+ e^{-0.8755t}(.8755t \cos 1.289t - 1.289 \sin 1.289t), \text{ for } t>0.$$

The undulation filter impulse response will be an even function of time, whereas the slope filter impulse response will be an odd function. Both response functions are shown in Figure 3-5.

Results of analyses such as the above will vary somewhat depending on the spectral characteristics assumed; however, the results given are considered to be indicative of the degree of smoothing required and the resolution achievable with the GEOS-C geoidal data. For ocean surface topographic studies similar conclusions apply; a 1-3 second smoothing interval will probably be required to profile features of major circulation systems such as the Gulf Stream. These factors argue that the simple, fixed time-tag correction of Section 3.1 will be adequate in most cases.

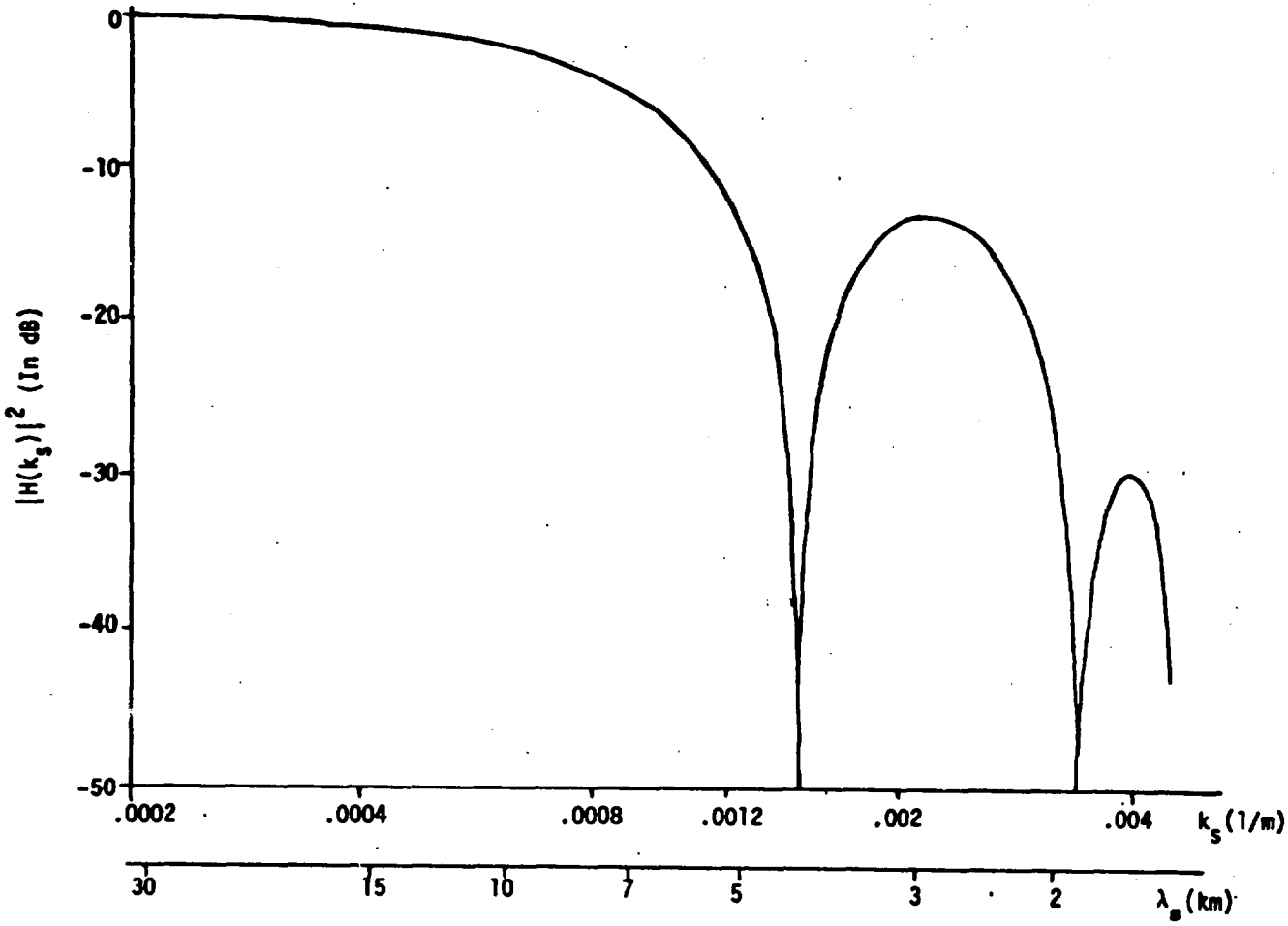

Figure 3-4. GEOS-C Intensive Mode Spatial Filter Transfer Function for Calm to Moderate Seas. [Figure Reprinted from May 1974 Report by L. S. Miller and G. S. Brown, Reference 5.]

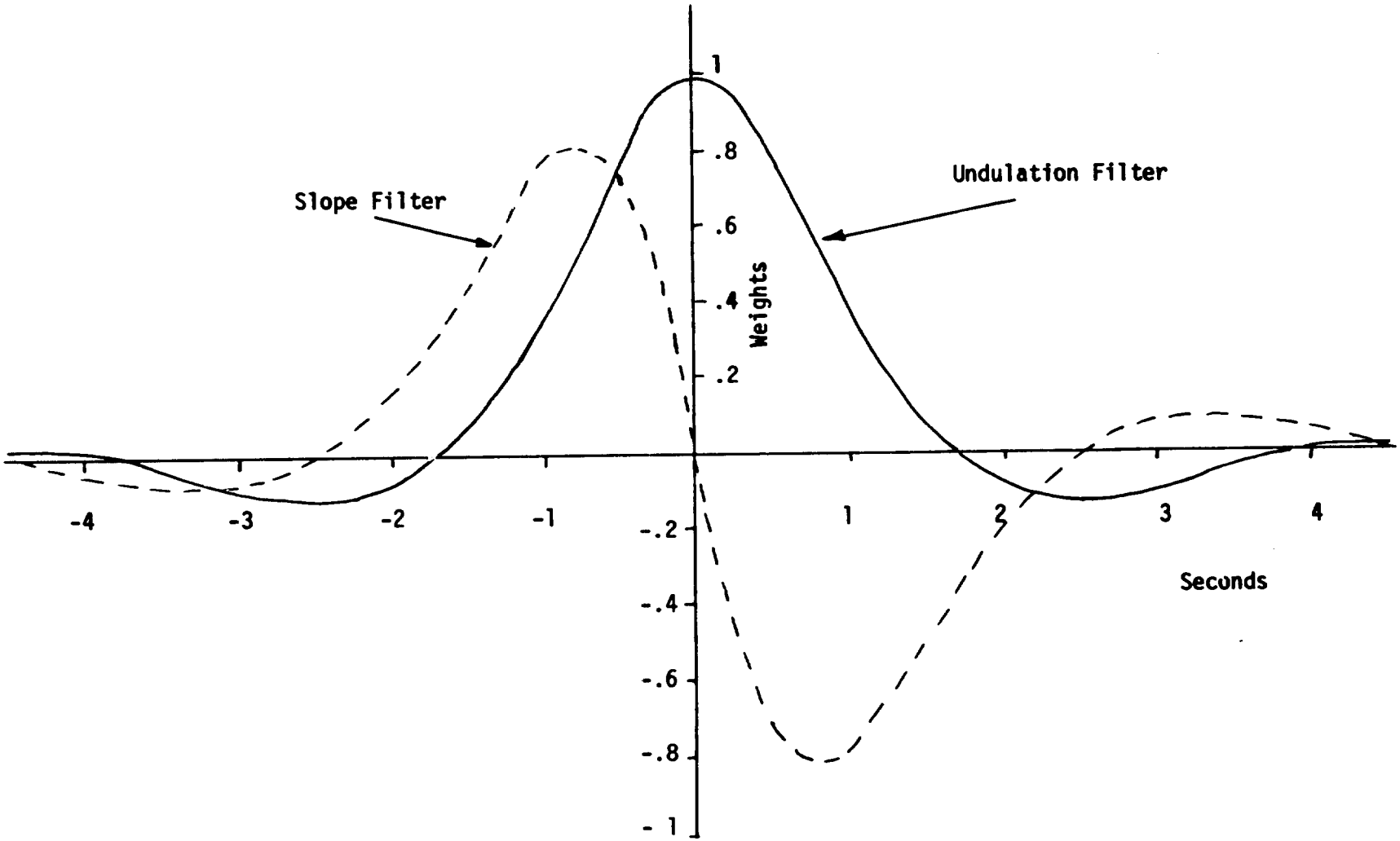

Figure 3-5. Derived Weighting Functions for Geoidal Data Processing. [Figure reprinted from May 1974 Report by L. S. Miller and G. S. Brown, Reference 5.]

4.0 ESTIMATION OF OFF-NADIR ANGLE (USING AASG AND APG)

During study of the Skylab altimeter data, it was found that the off-nadir angle of the altimeter could be determined accurately from the shape of the average return [8]. The accuracy of this technique resulted from the beamwidth limited operation of the altimeter (in the 100 ns pulse-width mode) and required inspection of the average return in the plateau region where beamwidth and pointing angle effects were dominant.

The procedures developed for Skylab can not be directly applied to the GEOS-C altimeter because the signal processor design does not provide for high speed Sample and Hold gates located sufficiently far into the plateau region of the return* to detect the changes induced by pointing errors. However, the General Electric Company proposed an alternate technique [9] whereby an integrating gate (called the Attitude/Specular Gate) would be located in that time portion of the return sensitive to variations in the pointing angle. The Attitude/Specular gate's output would be compared to the Plateau gate's output to determine the pointing angle. The preliminary analysis by GE was incomplete in that it did not account for the integrating behavior of the Attitude/Specular and Plateau gates. An analysis by ASA [5] included the effects of the integrating gates and provided a control curve which could be used to determine the pointing angle given the average output of the Attitude/Specular and Plateau gates.**

This chapter presents the derivation of the control curves and also obtains the estimated pointing angle errors due to the statistical nature of the gate outputs. Finally, there is a discussion of the effects of such practical factors as gate nonlinearities, saturation, temperature dependence, and receiver noise effects; however, systematic or bias errors are not considered.

Figure 4.1 is a simplified block diagram of the GEOS-C radar altimeter receiver for discussion of the attitude estimation process.

---

*This statement applies to the Intensive mode. For the Global mode, no point sampling of the average return is accomplished.

**A subsequent memorandum, "Interim Report on Attitude Estimation," by L. S. Miller, 1 August 1974, which was sent to Wallops Flight Center personnel, provided an estimate of the error involved in this technique for the Global Mode.

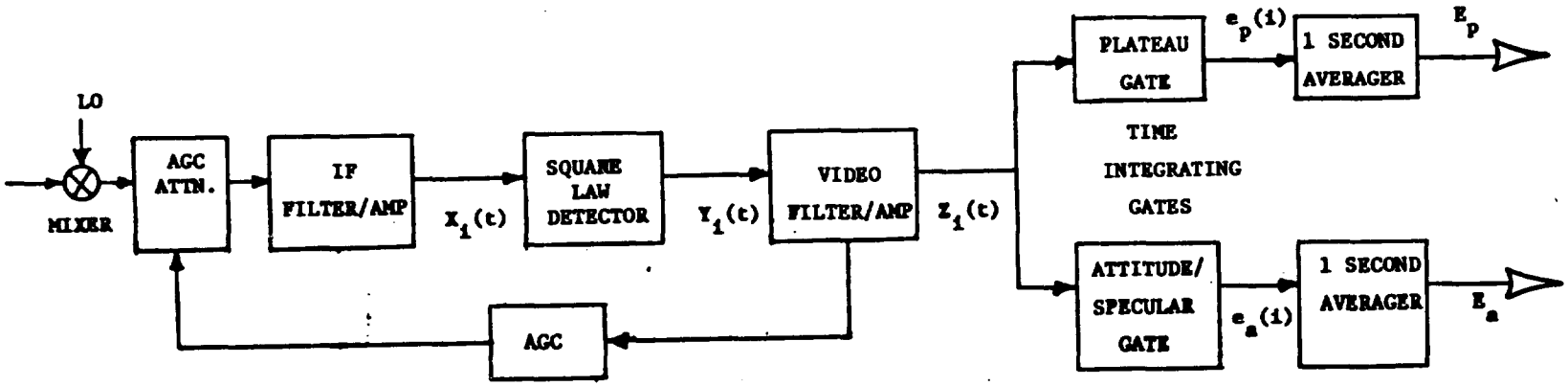

Figure 4-1. A Simplified Block Diagram of the GEOS-C Radar Altimeter Receiver Pertinent to the Attitude Estimation Process.

The output of the IF filter/amplifer, which also contains the pulse compression network in the case of the Intensive Mode (IM), may be represented as

$$X_i(t) = X_{c_i}(t) \cos \omega_o t - X_{s_i}(t) \sin \omega_o t \quad , \tag{4-1}$$

where ω_o is the IF center frequency and $X_c(t)$ and $X_s(t)$ are independent, zero mean, Gaussian random variables with a time-varying variance equal to $KP_r(t)$ (i.e., the average return power times a constant). Squaring (4-1) and regrouping terms yields, for the output of the square law detector,

$$Y_i(t) = \frac{1}{2}\left[X_{c_i}^2(t) + X_{s_i}^2(t)\right] + \frac{1}{2}\left[X_{c_i}^2(t) - X_{s_i}^2(t)\right] \cos 2\omega_o t$$

$$- X_{c_i}(t) X_{s_i}(t) \sin 2\omega_o t \quad . \tag{4-2}$$

Since the video filter/amplifier has a low-pass characteristic with a bandwidth much less than $2f_o$, the output of the video filter is approximately

$$Z_i(t) \approx \frac{1}{2}\left[X_{c_i}^2(t) + X_{s_i}^2(t)\right] \quad , \tag{4-3}$$

where the subscript i denotes the $i^{\underline{th}}$ return. Apart from the constant K which depends upon how the AGC is designed to normalize $Z_i(t)$ and neglecting receiver noise, the mean and standard deviation of $Z_i(t)$ are both equal to $P_r(t)$. Expressions for the mean and variance of the output of the integrating attitude/specular gate are given by

$$\bar{e}_a = E\left\{e_a\right\} = G_a \int_{\text{Gate}} \bar{Z}(t)dt \quad , \tag{4-4}$$

and

$$\sigma^2(e_a) = \text{Var}\left\{e_a\right\} = G_a^2 \int_{\text{Gate}}\int E\left\{Z_i(t_1)Z_i(t_2)\right\} dt_1 dt_2 - (\bar{e}_a)^2$$

where the bar denotes an ensemble average, and corresponding expressions

apply to the integrating Plateau gate. The factors G_a and G_p are gains of the Attitude/Specular and the Plateau gates with nominal values of $G_a \approx 20$ and $G_p \approx 10$.* Since $\bar{Z}_i(t) = KP_r(t)$ we need only know $KP_r(t)$ in order to determine the average output of the two gates. For the Intensive Mode (IM), an inspection of preflight test data indicates that the system point target response is adequately approximated by a Gaussian function. A good approximation of the average return power [5] is thus given by

$$P_{r_I}(t) = \hat{P}_{r_I}\left[\frac{1}{2} + \frac{1}{2}\,\mathrm{erf}\left(\frac{t-t_o}{\sigma_i\sqrt{2}}\right)\right] e^{-\frac{4c}{\gamma h}\cos 2\xi t}\, I_o\left(\frac{4}{\gamma}\sqrt{\frac{c}{h}}\sin 2\xi\sqrt{t}\right) \qquad (4\text{-}5)$$

The time shift in the argument of the error function is a result of using a Gaussian point target response. It must be inserted in order not to have the integrated point target response occur in time before the flat sea impulse response. For numerical purposes, t_o may be taken to be $2\sqrt{2}\,\sigma_i$. The other factors appearing in (4-5) are defined by:

$\sigma_i = 0.425 * PW_i$ (where PW_i is the width of the Intensive Mode system point target response as measured between the - 6dB points, post-video),

$\hat{P}_{r_I}$ = Peak of average return power in the Intensive Mode,

c = Speed of light,

$\gamma = 2.895 \sin^2(BW/2)$ (where BW is the 3dB beamwidth of the one-way antenna power pattern),

h = Altimeter height above mean sea level, and

ξ = Pointing angle of the altimeter antenna relative to nadir.

In computing $\bar{e}_a$ and $\bar{e}_p$, a further simplification can be made in (4-5). Since both the Plateau and Attitude/Specular gates are far removed from the leading edge of the average return, the factor

$$\frac{1}{2}\left[1 + \mathrm{erf}\left(\frac{t-t_o}{\sigma_i\sqrt{2}}\right)\right] \approx 1 \quad ,$$

*From private communication with E. L. Hofmeister, August, 1974.

and thus for computational purposes,

$$P_{r_I}(t) \approx \hat{P}_{r_I} e^{-\frac{4c}{\gamma h}\cos 2\xi\, t} I_o\left(\frac{4}{\gamma}\sqrt{\frac{c}{h}}\sin 2\xi\sqrt{t}\right) \qquad (4\text{-}6)$$

For the Global Mode (GM), it is impractical to assume that the shape of the point target response will be Gaussian because the IF and Video bandwidths are relatively wide compared to the 200ns pulse length. Of course, the true shape of the 200ns point target response should be obtained from scope photos of the video output during GM Bias portion of the BIT/CAL sequence, but we do not yet have such photos. For purposes of this computation, we assume that the point target response of the Global Mode (GM) may be best approximated by a 200ns rectangular pulse; thus, the average return power is given by

$$P_{r_G}(t) = \hat{P}_{r_G} F(t)\, e^{-\frac{4c}{\gamma h}\cos 2\xi\, t} I_o\left(\frac{4}{\gamma}\sqrt{\frac{c}{h}}\sin 2\xi\sqrt{t}\right), \qquad (4\text{-}7)$$

where

$$F(t) = \begin{cases} 0 & t \le 0 \\ t/T_p & 0 \le t \le T_p \\ 1 & t \ge T_p \end{cases}, \qquad (4\text{-}8)$$

and T_p is equal to 200ns. For the computation of $\bar{e}_p$ and $\bar{e}_a$, we can set $F(t) = 1$ since we will be integrating over a time domain which starts after 200ns.

To compute the variance of the Plateau and Attitude/Specular gates outputs, it would appear from the second equation in (4-4) that we must know the post-video nonstationary autocorrelation function of $Z(t)$, i.e., $E\{Z(t_1)Z(t_2)\}$. As will be shown below it is only necessary to know the predetection nonstationary autocorrelation function. Using (4-3), we have

$$E\left\{Z(t_1)Z(t_2)\right\} = \frac{1}{4}\left\{E\left[X_c^2(t_1)X_c^2(t_2)\right] + E\left[X_c^2(t_1)X_s^2(t_2)\right] + E\left[X_s^2(t_1)X_c^2(t_2)\right] + E\left[X_s^2(t_1)X_s^2(t_2)\right]\right\}$$

and the "1" subscripts have been dropped for compactness.

Since $X_c(t)$ and $X_s(t)$ are independent, zero-mean, Gaussian random variables, this reduces to [10],

$$E\left\{Z(t_1)Z(t_2)\right\} = \frac{1}{4}\left\{2E\left[X_c^2(t_1)\right]E\left[X_c^2(t_2)\right] + 2E\left[X_c^2(t_1)\right]E\left[X_s^2(t_2)\right] + 4E^2\left[X_c(t_1)X_c(t_2)\right]\right\},$$

or

$$E\left\{Z(t_1)Z(t_2)\right\} = K^2\left[P_r(t_1)P_r(t_2) + R_x^2(t_1,t_2)\right] \qquad (4\text{-}9)$$

where $R_x(t_1, t_2)$ is the predetection nonstationary autocorrelation function of the in-phase (or quadrature) component of the backscattered signal. The variance of the gate output is thus

$$\text{Var}\ (e_a) = \iint_{\text{Gate}} R_x^2(t_1,t_2)dt_1dt_2 \quad . \qquad (4\text{-}10)$$

For $R_x(t_1,t_2)$ we use the basic result of Berger's work [11] which we modify to account for pointing angle effects and operating modes. For the Intensive Mode we assume that the ambiguity function of the transmitted signal is approximately Gaussian (when time sidelobe filtering is included). We further assume that this is the dominant shaping factor relative to post-detection video filtering effects. Thus, for $R_x(t_1,t_2)^2$, we have

$$R_{x_I}^2(t_1,t_2) \approx P_{r_I}\, e^{-\frac{(t_1-t_2)}{4\sigma_i^2} - \frac{4c}{\gamma h}\cos 2\xi\, t_2}\, I_o\left(\frac{4}{\gamma}\sqrt{\frac{c}{h}}\sin 2\xi\sqrt{t_2}\right) \cdot \frac{1}{2}\left[1 + \text{erf}\left(\frac{t_1/2 + t_2/2 - t_o}{\sigma_p\sqrt{2}}\right)\right] \qquad (4\text{-}11)$$

As noted previously, we can neglect the [1+erf(•)]/2 term because in the range of integration it is essentially unity. For the Global Mode, the situation is much more complicated since the bandwidth of the IF filter is

about eight times larger than the matched filter bandwidth of the transmitted pulse (due to the necessity of accommodating drift in the magnetron center frequency). However to make the mathematics more tractable, we assume that the ambiguity function of the transmitted Global Mode pulse may be approximated by a Gaussian with $\sigma_g = (.425*200)$. The autocorrelation function is thus

$$R^2_{x_G}(t_1,t_2) \approx P_{r_G} e^{-\frac{(t_2-t_1)^2}{4\sigma_G^2} - \frac{4c}{\gamma h}\cos 2\xi\, t_2} I_o\left(\frac{4}{\gamma}\sqrt{\frac{c}{h}}\sin 2\xi\sqrt{t_2}\right) \cdot F(t_1/2 + t_2/2) \qquad (4\text{-}12)$$

where $F(\cdot)$ is defined by equation (4-8). As before we can neglect $F(\cdot)$ in integrating $R^2_{x_G}(t_1,t_2)$ over the Plateau and Attitude/Specular gates because $F(\cdot) = 1$ over these ranges of integration.

Using the expressions for average received power given by equations (4-6) for IM and (4-7) for GM, we can compute the average output of the integrating gates. Similarly, using the formulations developed for the predetection autocorrelation functions (equations 4-11 and 4-12), we can determine the variance of the average output of the integrating gates. However, the estimation function, Δ, from which we determine the pointing angle, is based on knowing the pulse-by-pulse outputs of the integrating gates averaged over one second. That is referring to Figure 4-1, the estimation function is defined here as

$$\Delta = 1 - \frac{E_a/G_a}{E_p/G_p} \qquad (4\text{-}13)$$

where E_a and E_p are one-second averages of the Attitude/Specular and Plateau gate outputs and we include the gain ratio to compensate for different gate gains. More specifically, they are defined as follows,

$$E_a = \frac{1}{N}\sum_{i=1}^{N} e_a(i)$$

$$E_p = \frac{1}{N}\sum_{i=1}^{N} e_p(i) \qquad (4\text{-}14)$$

where N is the number of independent pulses received in a one second interval; for the Intensive Mode $N=N_I=100$, and for the Global Mode $N=N_G=1600$. By the Central Limit theorem, we know that E_a and E_p will be essentially Gaussian with mean and variance given by

$$\bar{E}_a \approx \bar{e}_a \qquad \bar{E}_p \approx \bar{e}_p$$

$$\mathrm{Var}(E_a) \approx \frac{\mathrm{Var}(e_a)}{N} \qquad \mathrm{Var}(E_p) \approx \frac{\mathrm{Var}(e_p)}{N} \qquad (4\text{-}15)$$

The density function of Δ is determined by the joint density function of $(E_a G_p / E_p G_a)$. This density function can be derived by the methods given in [12], but it is so complicated that the mean and variance of Δ cannot be obtained in any closed form. An alternate approach to computing the mean and variance of Δ is to expand $(1-E_a G_p/E_p G_a)$ in a Taylor series about $E_a=\bar{E}_a$ and $E_p=\bar{E}_p$ and only retain the significant terms [Ref. 12, page 212]. This procedure is valid only when the probability masses of E_a and E_p are very concentrated near their center of gravity $\bar{E}_a$ and $\bar{E}_p$, and $(1-E_a G_p/E_p G_a)$ is smooth in the vicinity of this point. Reference 13 indicates the order of error this approximation can lead to when the above assumptions are violated. Because of the degree of variance reduction brought about by the one second averaging, we can safely apply this latter approach to computing the mean and variance of Δ. Using the formulas developed in [12], we have

$$\bar{\Delta} \approx 1 - \frac{G_p}{G_a}\,\frac{\bar{E}_a}{\bar{E}_p}\left\{1 + \frac{\mathrm{Var}(E_p)}{(\bar{E}_p)^2}\right\} \qquad (4\text{-}16)$$

$$\mathrm{Var}(\Delta) \approx \frac{G_p^2}{G_a^2}\left[\frac{\bar{E}_a}{\bar{E}_p}\right]^2\left[\frac{\mathrm{Var}(E_a)}{(\bar{E}_a)^2} + \frac{\mathrm{Var}(E_p)}{(\bar{E}_p)^2}\right] \qquad (4\text{-}17)$$

It will be noted that (4-16) differs from the previous results obtained for the estimator function $\bar{\Delta}$ [5, 9 , and the memorandum cited as a footnote on page 87. This disparity results from the assumption, inherent in previous analyses, that

$$\bar{\Delta} = 1 - \frac{G_p}{G_a} E\left\{\frac{E_a}{E_p}\right\} = 1 - \frac{G_p \bar{E}_a}{G_a \bar{E}_p} \qquad (4\text{-}18)$$

In other words the second equals sign in (4-18) is only valid to the extent that the ratio of the variance of E_p to the squared mean of E_p is much less than one (see equation 4-16). As will be shown, this neglect of the second term inside the brackets in (4-16) is essentially valid for both modes. The reason for the gain ratio in (4-16) is that previous analyses have assumed that each integrating gate had equal gain but whereas this is not the case for the actual hardware. Furthermore, it is necessary to insert this factor in our analysis so that the results for $\bar{\Delta}$ will be in agreement with the present data analysis scheme in force at WFC.

Equations (4-16) and (4-17) may be simplified through the use of equation (4-15). That is,*

$$\bar{\Delta} = 1 - \frac{G_p}{G_a} \frac{\bar{e}_a}{\bar{e}_p}\left[1 - \frac{\mathrm{Var}(e_a)}{N[\bar{e}_a]^2}\right] \qquad (4\text{-}19)$$

$$\mathrm{Var}(\Delta) = \frac{G_p^2}{G_a^2}\left[\frac{\bar{e}_a}{\bar{e}_p}\right]^2 \left[\frac{\mathrm{Var}(e_a)}{N[\bar{e}_a]^2} + \frac{\mathrm{Var}(e_p)}{N[\bar{e}_p]^2}\right] \qquad (4\text{-}20)$$

Using the previously developed expressions for the quantities in (4-19) and (4-20), $\bar{\Delta}$ and $\mathrm{Var}(\Delta)$ can be numerically evaluated.

Figure 4-2 is a plot of $\bar{\Delta}$ as a function of ξ for the Intensive Mode. Table 4-1 compares the results obtained from equation (4-19) with the approximate results given by (4-18).

---

*It should be noted that $N=N_I=100$ or $N_G=1600$ depending upon which Mode is considered.

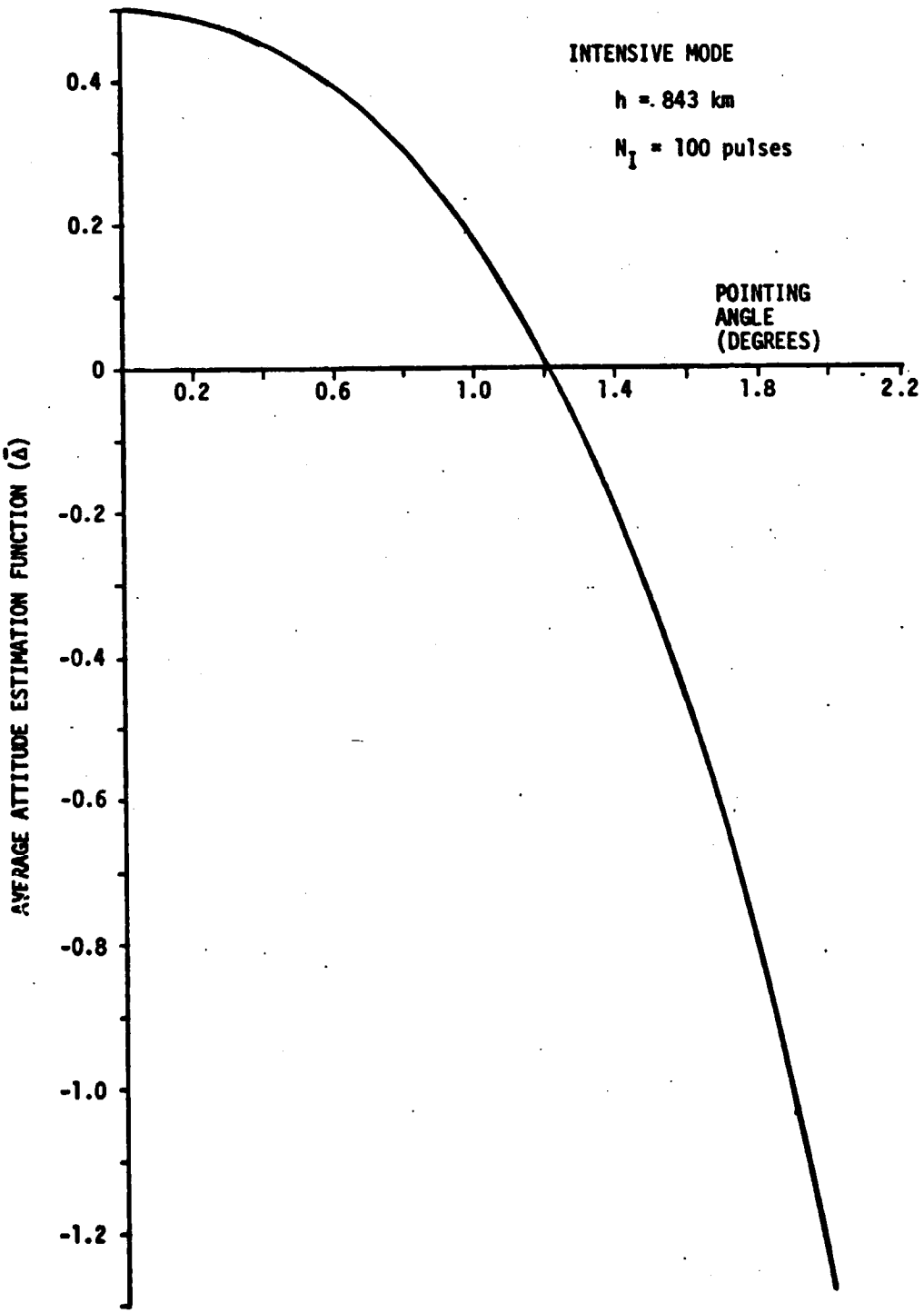

Figure 4-2. $\bar{\Delta}$ As a Function of ξ for the Intensive Mode.

TABLE 4-1

Comparison of Approximate and Exact Values of $\bar{\Delta}$ for the Intensive Mode, N=100, h=843 km.

ξ (DEGREES)	$\bar{\Delta}$ (EXACT) (EQ. 4-19)	$\bar{\Delta}$ (APPROX.) (EQ. 4-18)
0	.498	.502
0.2	.486	.49
0.4	.451	.455
0.6	.392	.396
0.8	.302	.307
1.0	.178	.184
1.2	.013	.021
1.4	-.210	-.191
1.6	-.477	-.464
1.8	-.831	-.814
2.0	-1.28	-1.258

From Table 4-1, we see that the largest difference occurs at 2 degrees but it is less than 2% and therefore may be neglected.

Figure 4-3 shows $\bar{\Delta}$ as a function of ξ for the Global Mode while Table 4-2 is a compilation of the results for the exact case. There is no comparison made between the exact and approximate formulations for $\bar{\Delta}$ because they are essentially the same. This is due primarily to the increase in N from 100 for the Intensive Mode to 1600 for the Global Mode as a result of the pulse burst operation.

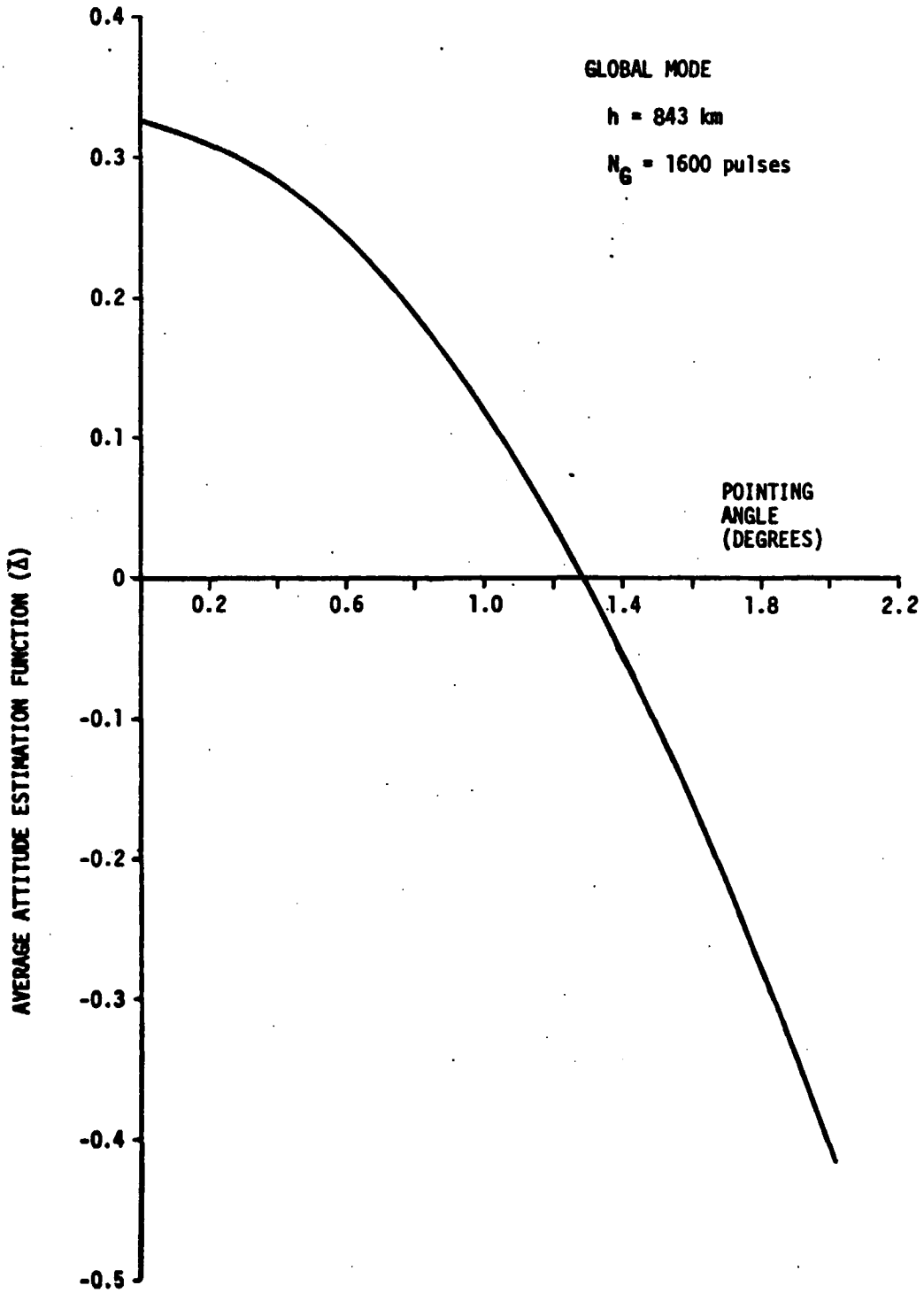

Figure 4-3. $\bar{\Delta}$ As a Function of ξ for the Global Mode

TABLE 4-2

Tabulation of Exact Values of $\bar{\Delta}$ as a Function of the Pointing Angle ξ, Global Mode.

ξ (DEGREES)	$\bar{\Delta}$ (EXACT) (EQ. 4-19)
0	.325
.2	.309
.4	.284
.6	.243
.8	.187
1.0	.117
1.2	.035
1.4	-.058
1.6	-.164
1.8	-.280
2.0	-.409

In order to determine how accurately the curves in Figures 4-2 and 4-3 will enable one to infer ξ from $\bar{\Delta}$, we must investigate how the variance of Δ depends on ξ. A plot of the standard deviation of a ten-second average of Δ computed from equation (4-20) is shown in Figure 4-4 for both the Intensive and Global Mode. The fact that sixteen times as many pulses are averaged per second in the Global Mode as in the Intensive Mode clearly shows the Global Mode to have a lower error. If we translate this standard deviation of Δ into the equivalent error in ξ, using the curves in Figures 4-2 and 4-3, we obtain the curves in Figure 4-5. The results shown in this figure clearly indicate that the Global Mode has a lower statistical error for $\xi \lesssim 0.8^{\circ}$ and that both modes have approximately the same error for $0.8 \leq \xi \leq 2.0^{\circ}$. It is interesting to note that under the assumptions we have made (constant gain integrators, no saturation, no receiver noise), this process will yield a one sigma error of less than 0.1° for $\xi \geq 0.2^{\circ}$ for both modes. This may seem somewhat optimistic since the beamwidth of the antenna is rather large. However, it must be remembered that the Attitude/Specular gate is located far into the plateau region of the return (700ns from the start of the leading edge) and thus is relatively sensitive to changes in pointing angle. It is also interesting to note the near

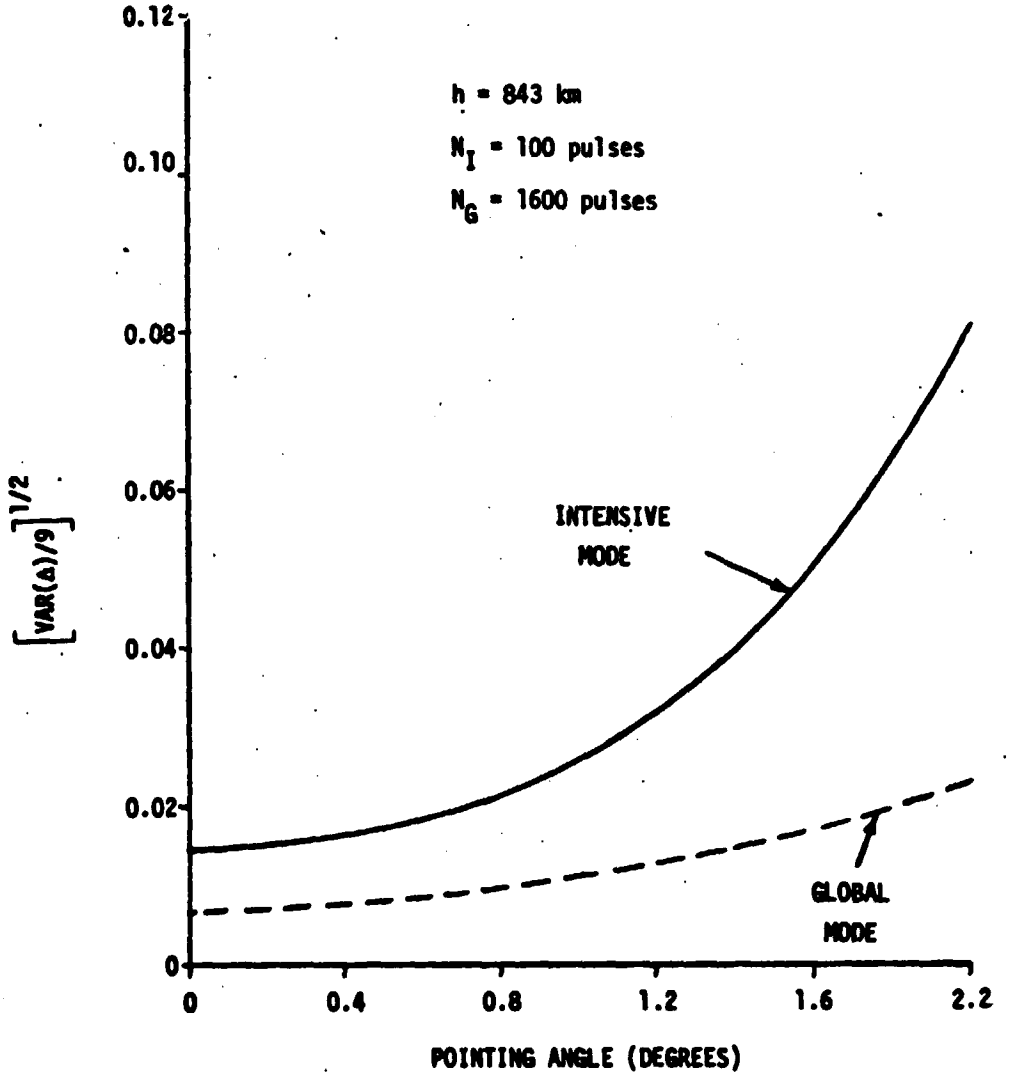

Figure 4-4. Ten Second Standard Deviation of Δ for Both Modes

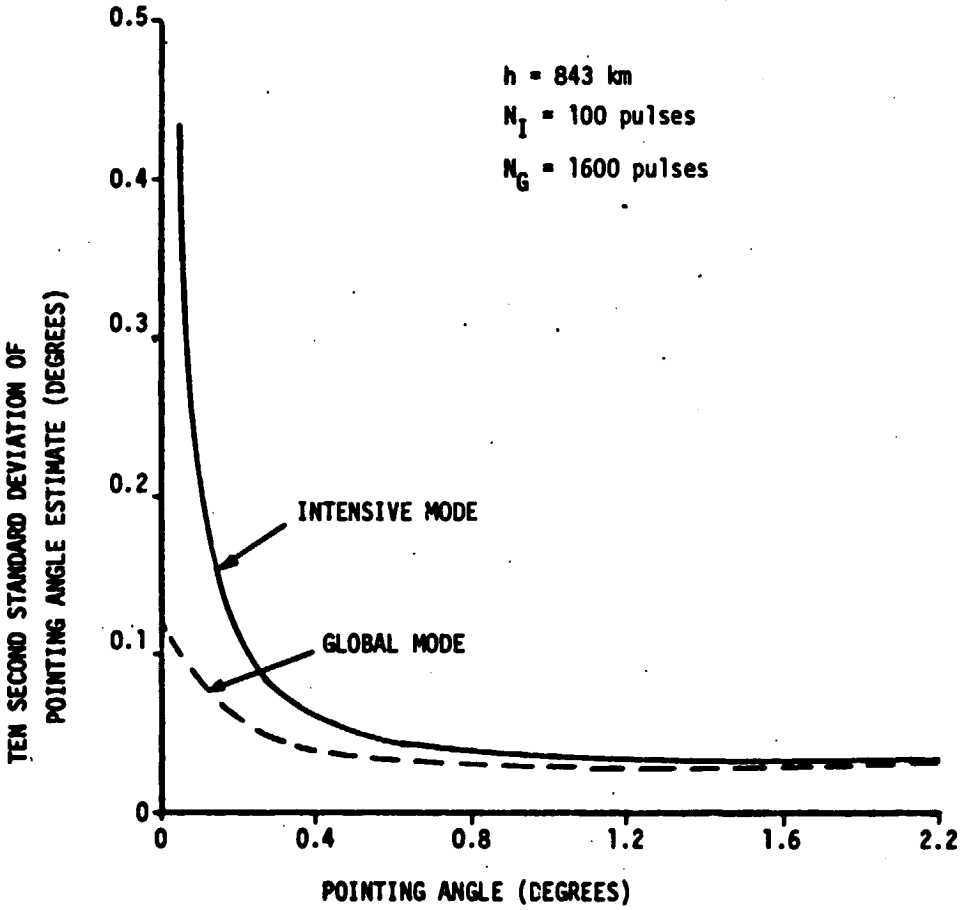

Figure 4-5. Approximate Standard Deviation of the Estimated Pointing Angle Based on a Ten Second Averaging Period.

equality in angle estimation error between the Intensive and Global modes, especially since the Intensive Mode achieves its low error via a very sharp dependence of $\bar{\Delta}$ on ξ (see Figure 4-2) while the Global Mode error is small due to its increased number of samples per second. In terms of the nomenclature employed by NASA/WFC, the ten second average value of Δ will be given by

$$\bar{\Delta} = 1 - \frac{\overline{AASG}}{\overline{APG}}$$

where the bars denote a ten second average.

Up to this point we have assumed a rather simplistic model of certain parts of the receiver. Such factors as receiver noise, integrating gate nonlinearity and gate saturation are of primary importance. For a pointing error of less than one degree, the loss in return power will be less than 3.5 dB and this implies that we can probably ignore receiver noise in the Global Mode. However, when the pointing error approaches two degrees, the received power drop will be about 14 dB, which implies that we can no longer ignore receiver noise even in the case of the Global Mode. The primary effect of receiver noise will be to increase the variance of Δ or the error bounds on our estimation curves. Receiver noise will probably cause the curves in Figure 4-5 to reach a minimum at about one degree and then start a more pronounced increase as ξ approaches two degrees. We caution that receiver noise effects will depend to a large extent upon what value we assign σ^o. For this reason, noise effects are best deferred until we have some data on near-nadir values of σ^o from Skylab.

As evidenced by the tabulations and curves presented in an earlier chapter of this report, the gains of the Attitude/Specular and Plateau gates are neither constant nor linear. For this reason it may prove to be more tractable to compute $\bar{\Delta}$ and $\mathrm{Var}(\bar{\Delta})$ using these nonlinear gains rather than trying to compensate for them by data processing. The problem here boils down to one of determining how far we can carry our analysis to account for nonlinear gate gains.

Another problem related to the integrating gates is that they also saturate beyond a certain input value. Unfortunately, this saturation point

is only about a factor of two or three above the mean operating voltage. This effect will also have to be accounted for in our revised analysis (this effect will be also dependent upon the value of σ^o which the system "sees").

In the case of the Global Mode we face an additional problem which involves a lack of calibration data on how the gain of the Plateau gate depends upon temperature. That is, at the present time we only know the gain of the integrating gate at room ambient temperature, and it is doubtful that the Protoflight and Flight units are matched closely enough to permit the use of additional Protoflight test data. However, it is felt that previous test data (not recorded in the EPTP) on the Flight unit can be useful in solving this problem. Since all of this data has been microfilmed by the Applied Physics Laboratory, it should be obtainable.

Finally, it would seem only fair to point out that the error estimates given in Figure 4-5 are optimum in the sense that they represent a lower bound. When practical hardware considerations are accounted for it is anticipated that these error estimates could increase by at least a factor of two.

5.0 POSSIBLE USE OF GROUND-BASED TARGETS TO OBTAIN ADDED IN-FLIGHT CALIBRATION DATA

This section heuristically examines the feasibility of using a ground-based passive reflector or active transponder as a means of obtaining additional in-flight calibration information on the GEOS-C system. With the envisioned concept, the (active or passive) target transponder would be located at an elevated, over-water site (such as the Chesapeake Coast Guard tower) and preferably very close to a ground-track intersection. In operation the return signal would first appear as a non-fluctuating point target response superimposed on the plateau region of the sea-scattered signal; as the satellite traversed over the target site the point-target response would move from the plateau region to the ramp region and into the noise-only region and then reverse this sequence after the satellite passed over the (active or passive) target. The degree to which this target response was moved time-wise ahead of the sea echo would be determined by the height of the target and its time delay characteristic (which could be made adjustable, in the case of the active device, by using coaxial delay lines).

This feasibility study was motivated by a consideration of the potential advantages of such a calibration source. Some of these are:

1. direct calibration of the point-target response of the complete satellite system,
2. calibration of the linearity and simularity characteristics of the waveform samplers and the degree of dc offset between samplers, and the other gate functions,
3. measurement of the radar altimeter's antenna pattern in one plane,
4. provide information relating to overall system performance (transmitter power, receiver noise level) based on signal-to-noise time-history of the point-target response,
5. information on sea state dependent tracker bias in a restricted sense, (the active or passive target cannot be situated in deep water ocean conditions) and,
6. provide sampled waveform data relative to absolute σ^o measurement.

5.1 Size of Corner Reflector Needed to Produce a "Point Target" Response Usable for System Calibration (Passive Reflector Method).

Using the radar equation for received energy E,

$$E = \frac{P_t\ t\ \lambda^2 G_t^2 \sigma}{(4\pi)^3\ R^4} \quad ,$$

and the equation for radar cross section σ of a corner reflector of side dimension a,

$$\sigma = \frac{4\pi\ a^4}{3\lambda^2} \quad ,$$

and equating the received energy to the receiver noise energy using $E = KT \cdot F \cdot SNR$; the required corner reflector dimension "a" is

$$a = R \left[\frac{3(4\pi)^2\ KT \cdot F \cdot SNR}{P_t t G_t^2} \right]^{1/4} = 8 \text{ meters or } 26.25 \text{ feet}$$

when

$R = 10^6$ meters

$KT = 4.11 \times 10^{-21}$ joules (for $T = 298^{\circ}K$)

$SNR = 10$ (signal-to-noise ratio)

$F = 10$ (receiver noise figure)

$P_t = 2.5 \times 10^3$ watts (peak transmitted power)

$t = 1.2 \times 10^{-6}$ sec. (nominal 12 ns pulse from 100:1 pulse compression)

$G_t = 4000$ (36 dB) = GEOS-C antenna gain

This dimension, a, is too large for practical consideration.

5.2 Use of a Paraboloid and a TWT (Active Transponder Method)

To avoid pulse decoding it is necessary to provide an rf signal level at the ground-based receiver of at least -80 dBm to override TWT thermal noise.

The range equation for two antennas is

$$P_r = \frac{P_t G_t G_R \lambda^2}{(4\pi R)^2}$$

where P_r = received power
G_t = GEOS-C antenna gain
G_R = Ground based antenna gain

Solving for G_R required for P_r = -80 dBm yields

$$G_R = .31$$

This result shows that gain of the ground antenna can be selected on other bases. For example, in order to avoid alignment and main-lobe intercept sensitivity, if a ~ two foot dish is used (i.e., the GEOS-C type hardware)

$$P_r = 10^{-5} \text{ watts}$$

or -20 dBm

Similar computations show that a TWT chain with a total gain of ~ 40 dB would be required to provide an rf signal level in the radar altimeter of ~ -80 dBm. Note that this choice of parameters leads to a 1/4 power beam intercept period of ~ 6 sec.; that is, the signal will be 6 dB below its peak value at ~ 3 sec. before (or after) time of closest approach. In general, the transponder signal level desired would be approximately that of the back-scattered signal level and it might be desirable to use the received signal in conjunction with a time delay so that the transponder signal could, at times, be programmed to appear only in the noise region, to ensure that the range tracker and AGC functions of the altimeter are not affected by the transponder signal. (The time delay necessary for this is only a few tens of nanoseconds shorter than the altimeter pulse-to-pulse period.)

In summary, the simple, inexpensive approach of using a passive reflector is found not to be a viable option and the active systems will require one or two antennas, rf devices such as circulators, traveling wave tubes, power supplies, non-regeneration circuitry, and some degree of self-actuation

and/or programmed control. Component costs for the transponder would be in the range of 10 - 20 thousand dollars. The value of such a device is totally dependent on how well the GEOS-C satellite system functions in orbit. Under certain failure-mode or malfunction assumptions the added calibration data would perhaps salvage the mission; under other failures the calibration data might not be very useful. Because of these factors, it is recommended that the subject be reconsidered after the satellite data analyses are available from the 90 day post-launch evaluation period.

APPENDIX A. ASA MEMORANDUM ON ALTIMETER TESTS, 17 OCTOBER 1974

The memorandum reproduced below is provided as a summary, for the record, of testing still unaccomplished as of October 1974. Some of the data have since been obtained, notably the "extended AGC range" data (at least for ambient pressure and temperature), but this memorandum should be useful in considering the merits of possible post-launch testing on the Protoflight altimeter. (The memo's Reference is listed as Reference 1 of this report.)

Memorandum

October 17, 1974

TO: H. R. Stanley
C. L. Purdy

FROM: L. S. Miller
G. S. Brown

Subject: Response to APL Letter TSSD-4664 "Calibration Test Data and Format"

Reference: "GEOS-C Radar Altimeter System Calibration and Evaluation Test Data Requirement," dated 22 Jan., 1974

Attachment 1 to this memorandum summarizes our estimate of the minimum level of testing necessary to support reasonable requests for GEOS-C investigators for data from the radar altimeter. If these tests cannot be conducted on the flight hardware, we feel very strongly that they should be run on the back-up hardware, even if this entails post-launch testing.

APL's letter tends to mention only those tests in Reference 1 which overlap, or can be at least partially satisfied by data from tests already planned by GE and APL; other test data requests tend to be ignored.

The tests called out in Attachment 1 reflect attempts on our part to reduce remaining test requirements to a minimum and to modify tests requested based on information obtained since Reference 1 was prepared. We believe the time has come when further exchanges of documentation on the requested test data will serve no useful purpose. Our recommendation to NASA is that the tests in Attachment 1 be added to tests planned by GE and APL as documented required tests, and we will do all we can to help obtain this data.

1.1.1 We concur with the APL responses subject to the following caveat: It is not clear that their test data will yield absolute delay of the instrument. We understand that a hardware change is made between the BIT/CAL bias measurement and a data acquisition mode. This change comprises a gain change of the IF preamplifier (module A3) to increase attenuation of the receiver and to provide a form of pulse stretching so that the "12 ns rectangular" calibrate signal can be range tracked. Information is needed on the gain and delay changes involved and their temperature dependencies. (The gain data will be used in σ^o data processing activities.)

1.1.2, 1.1.3 The APL response covers only the waveform sampling and telemetry processes and routine AGC calibrations. The original test description lacked specificity and certain problem areas have since arisen. Table I shows the test data needed in these areas and paragraphs 1-4 below elaborate on the rationale for these tests.

1. Comparative calibration of waveform sampling circuits using clean and clutter waveforms.
   Experience with the Skylab altimeter sampled waveform data has demonstrated that a one-to-one relationship does not exist between 1) non-fluctuating and fluctuating waveforms, and 2) dc offset patterns obtained in calibration data steps and those observed when the S&H circuits are sampling receiver noise. These effects are well documented. Such problems may not exist in the GEOS-C hardware; however, at present there is no assurance that corrections indicated in BIT/CAL or prelaunch test data will be usable. Test data should be analyzed so that experimenters will be spared the effort and expense of individually finding out that the waveform calibration data is not usable - if such is the case.

2. 4 to 5 dB difference between IM clean and noisy AGC curves:
   Most recent thermal-vacuum test results on the Protoflight altimeter show a 4 to 5 dB separation between the AGC calibration curves (AGC voltage vs. receiver input power) for IM clean and noisy input waveforms. There is no theoretical argument to support this separation. (It may be that this is attributable to an incorrect measurement of input power or a problem with the technique employed to generate the

"noisy" chirped return.) This statement is supported by the fact that the GM clean and noisy AGC calibration curves are essentially identical. In discussions with GE personnel, it was speculated that the simulated noisy return at the input to the receiver could contain noise power outside the IF bandwidth of the altimeter. Thus, whenever a measurement of power at the input of the receiver is made, a reading is obtained which is higher than the altimeter receiver actually sees. The implications of this suspected measurement problem apply to much more than just the AGC calibration. If this speculation is correct, this means that all IM performance specification tests are being conducted at an input power level which is 4 to 5 dB <u>below</u> that required in the GE contract. Also if this problem is not resolved, there will be no way by which GEOS-C experimenters can obtain accurate estimates of σ^o (from IM data) since there will always be the question of whether to use the noisy or clean AGC calibration curves. We recommend that GE be made aware of the importance of finding the source of this discrepancy and correcting it. If they elect to continue their current procedures, this problem <u>must</u> be resolved during testing at APL. It should be noted that the check on out-of-band noise is very easy to accomplish and only involves the TAMS since this is where the noisy return is generated. A previously proposed in-flight experiment to resolve this problem has been invalidated by the requirement to wait 3.5 minutes from GM shutdown to IM turn-on (due to TWT heater warm-up).

3. <u>Extended AGC calibration range</u>.

All AGC curves generated by GE during acceptance testing of the altimeter are invalid for an input power level of greater than -60 dBm. This is due to the manner in which the simulated return signal is generated and the fact that there is a saturation of the RSS for a level of greater than -60 dBm. GE maintains that they do not (contractually) have to provide AGC data for an input power level of greater than -60 dBm since the maximum received power (as per the APL specification of σ^o = 20 dB at 0^o pointing error and minimum altitude) will be less than approximately -60 dBm. From an experimenter standpoint it is desirable to have valid AGC curves for

an input power level of greater than -60 dBm for two reasons. Although it is not anticipated that σ^o should exceed 20 dB, we still should have the capability to accomplish such a measurement should the occasion arise. The second and more important reason for extending the range of the AGC calibration curves to above the -60 dBm level is that we need an accurate measurement of the "received" power in the BIT/CAL Bias test. BIT/CAL Bias power is important for determining the health of the front end of the receiver (up to and including the mixer) and as an alternate means of determining σ^o. For example, if the mixer changes characteristics as the altimeter is operated, this would invalidate the pre-flight AGC curves and we would not be able to determine σ^o from the received and transmitted power data. On the other hand, if the AGC curves were extended to include "received" power levels present in the BIT/CAL Bias test, we could compute σ^o by taking the ratio of received power during data acquisition and BIT/CAL, therefore eliminating any dependency upon preflight measurements of receiver gain. For the above reasons, it is strongly suggested that both the IM and GM AGC calibration curves be extended to include an accurate measurement of "received" power in the BIT/CAL Bias test. It is furthermore suggested that this calibration be conducted at APL.

4. Test for linearity of sampled waveform data.

Examination of Skylab average return waveforms has demonstrated that, under certain conditions, the S&H gates do not have a large enough linear range to accommodate the fluctuation statistics of the AGC'ed waveform. This results in the standard deviation of a point on the waveform being less than the mean. Furthermore, this saturation effect also reduced the mean value resulting in an erroneous estimate of the average return waveform. To insure that this will not happen on GEOS-C, we suggest running IM Impulse Response Tests at input power levels of P_{RH} and P_{RN}. Furthermore, histograms for S&H gates located in the plateau region of the return should be constructed to determine if the voltages are in fact exponentially distributed. For the Protoflight Unit, raw data necessary to construct a histogram were obtained by GE during Level 4 testing at P_{RL} and P_{RN}. However,

as noted previously the actual input power-levels during these tests may be low by 4 to 5 dB. Thus, we suggest these tests be conducted at APL after the test power level is properly established.

1.1.4 This test cannot be performed at APL because internal test points are not available.

1.1.5 We concur with the APL response, assuming that the calibration discrepancies between noisy and clean inputs are resolved.

1.2,2.2.2 This test relates to system tracking jitter as a function of received signal level. From an experimenter viewpoint this is a very important test. The desired test data is shown in Table II.

1.3 No APL comment. We strongly urge that scope photos be obtained of all BIT/CAL waveforms (at the video test output jack) and these be compared to the S&H gate output voltages. This test can be accomplished at APL.

1.4 The APL response indicates they will accept responsibility for these tests.

2.2.1 (APL labeled 2.1.1) This is an NRL request.

2.2.2 (APL labeled 2.1.2) Discussed with 1.2 above.

2.2.3, 2.2.4 (APL labeled 2.2.1, 2.2.2) We concur with the APL response. The following data is available with the TAMS system:

ASSP 1 (IM TRK 0, IM TRK 8)
Tracking Loop Jitter (1 sample/pulse)
Altitude (1 sample/pulse)

ASSP 2 (IM TRK 8, IM TRK 16)
Tracking Loop Jitter (1 sample/pulse)
Altitude (1 sample/pulse)
Even Instantaneous S&H (1 sample/10 pulses)
Even Avg. S&H (1 sample/50 pulses)

ASSP 3 (IM TRK 16)
Altitude (1 Sample/pulse)
Odd Instantaneous S&H (1 sample/10 pulses)
Odd Average S&H (1 sample/50 pulses)

Comment: It is conceivable that under some conditions the tracking loop jitter may be sufficient to warrant pulse-by-pulse realignment of the return waveforms. In order to do this, it is essential that we know how the pulse-by-pulse tracking loop jitter voltage [V(Tj)] relates to the Digital Delay Generator time increment. In other words, how is V(Tj) related to the time increment by which the S&H gates are shifted? It should be possible to operate the altimeter/TAMS configuration in a IM TRK 0 mode and obtain pulse-by-pulse outputs of altitude and V(Tj), simultaneously. This would determine how V(Tj) is translated (by the accumulator) into a DDG step size. This testing should also be accomplished at APL.

2.3.1 Table I addresses this data requirement.

2.3.2, 2.3.3 Desirable tests at the module level - not mandatory.

2.4.1, 2.4.3 This data should be available from GE thermal vacuum tests. Both mean and variance data is desired.

2.5 Data available from subsystem tests and from tests given in Table I.

2.6 (APL labeled 2.5) We feel this is an extremely important test and one that can be readily accomplished.

TABLE I

IM and GM[1] TESTS

WAVEFORM	#1 WH-0 (waveheight "0") NOISY	#2 WH-10 NOISY	#3 WH-0 CLEAN
TEST COND.	VACUUM & TEMP. @ -10,0,+20,+40°C	Same	Same
INPUT POWER LEVELS	-50 dBm to break-lock in 4 dB steps	Same as #1	Same as #1
RECORDED DATA	AGC voltage Tracker time history AVG. S&H gates INST. S&H gates PLAT. & ATT./SPEC. gate ALL ALTIMETER TEMPERATURES SCOPE PHOTOS	Same as #1	Same as #1
PROCESSED DATA	1. Tracker variance 2. Averages and variances of all gates 3. Histograms of all gates 4. Tracking Loop ACF	Same as #1	Same as #1

1. GM TESTS same as IM except delete reference to S&H gate outputs.
2. Scope photos of input signals to S&H ckts are desired, using a high speed sampling scope with averaging. Otherwise use ns radar sampling scope, recorder, and computer averaging programs.

TABLE II

I-mode system tracking jitter test

	1st Test	2nd Test
Input Signal	TAMS generated Expanded-Clutter pulse WH-0 -80 to -100 dBm in 5 dB steps -100 to -110 dBm in 3 dB steps (RF power values)	TAMS group A, WHO-0 clean signal inserted at "IF Test Output"* test point, with signal levels adjusted to equal those present at this point in 1st Test. This will necessitate pre-test calibration of coupler to determine reverse coupling factor.
Recorded Data	1. Inst. S&H gate outputs 2. Tracker time history 3. Scope photos of video and "IF Test Output" (for qualitative indication of SNR)	Same as 1
Processed Data	1. Mean and variance of all S&H values 2. Tracker variance	Same as 1
Temp.	Ambient	Same

*If use of this test point for signal input purposes is impractical, the video input test point may be used, although this is a less desirable procedure.

APPENDIX B. SAMPLE PROGRAM FOR LINEAR-LINEAR INTERPOLATION

This appendix presents a sample FORTRAN program to carry out the linear-linear interpolation described in Section 2.2 and summarized by Figure 2-2 in this report. Figure B-1 shows the source program and the input data which produce the printed output of Figure B-2. Notice that the input data in Figure B-1 is the Flight Model altimeter Average Waveform Sampler #1 (ARS1) calibration data from Table 2-8.

In the main program, the calibration data are loaded into the arrays (and dimensions) VF(4,10),VE(4,10),NV(4), and T(4) by Subroutine FILL. VF and VE contain, respectively, the Functional Unit and Engineering Unit pairs (up to 10) at each of the (4) separate temperatures T(4); NV(4) specifies the number of FU,EU points at each temperature. The search routine SRCH1 and its subroutine SRCH2 require that the calibration data be arranged so that $T(1) \leq T(2) \leq T(3) \leq T(4)$ and that at each T(J) the Engineering Units be in the order $VE(J,1) \leq VE(J,2) \leq \cdots \leq VE(J,9) \leq VE(J,10)$; that is, there must be ascending ordering in temperature and Engineering Units. The Main Program call to Subroutine SRCH1(VE,VF,NV,T,4,10,TEMP,XJ,YJ,JF) returns a value for the Functional Unit YJ corresponding to the input Engineering Unit XJ and temperature TEMP as a result of the linear-linear interpolation within the above calibration data VE,VF,NV, and T; the 4 and 10 in the SRCH1 call are variable dimensions since we want to be able to use SRCH1 for different altimeter quantities whose calibration data tables will have differing dimensions. A flag JF is also returned from SRCH1 to the Main Program, with JF=0 if the input data pair (XJ,TEMP) lies within the calibration data.

SRCH1 finds the index of the pair of input EU vs. FU curves such that TEMP lies between this index and this index +1, and then calls SRCH2 to carry out the interpolation between FU,EU point pairs on each fixed-temperature EU vs. FU curve.

Notice that SRCH1 initially sets the flag JF (in the Main Program) to zero. JF is decreased by 10 if the input temperature TEMP is lower than the lowest calibration temperature T(1), and the T(1) curve for FU vs. EU is used. Similarly, JF is increased by 10 to TE... T(4) and the T(4) curve

APPENDIX B

Figure B-1. Sample FORTRAN Program and Input Data For Linear-Linear Interpolation.

```
      DIMENSION VF(4,10),VE(4,10),NV(4),T(4),
     1 XIN(30),YOUT(30),JFLOUT(30)
      CALL FILL(VE,VF,NV,T,4,10)
      TEMP=-30.
      XIN(1)=-2.25
      DO 5 I=2,30
    5 XIN(I)=XIN(I-1)+.25
      DO 10 I=1,5
      TEMP=TEMP+20.
      DO 15 J=1,30
      XJ=XIN(J)
      CALL SRCH1(VE,VF,NV,T,4,10,TEMP,XJ,YJ,JF)
      JFLOUT(J)=JF
   15 YOUT(J)=YJ
   10 WRITE (3,20) TEMP,(XIN(K),YOUT(K),JFLOUT(K), K=1,30)
   20 FORMAT(/' FOLLOWING (EU,FU,FLAG) FOR TEMP=',F7.3/(' ',
     1  4('(',F5.2,',',F6.3,',',I3,')' )))
      STOP
      END

      SUBROUTINE SRCH1(X,Y,NX,T,I1,I2,TI,XI,YI,JF)
      DIMENSION X(I1,I2),Y(I1,I2),NX(I1),T(I1)
      JF=0
      J=1
      TN=T(J)
      IF (TI-TN) 10,20,30
   10 JF=JF-10
   20 CALL SRCH2(X,Y,NX,I1,I2,J,XI,YI,JF)
      RETURN
   30 TO=TN
      J1=J+1
      TN=T(J1)
      IF (TI-TN) 40,50,60
   40 CALL SRCH2(X,Y,NX,I1,I2,J,XI,YI1,JF)
      CALL SRCH2(X,Y,NX,I1,I2,J1,XI,YI2,JF)
      YI=YI1+(YI2-YI1)*(TI-TO)/(TN-TO)
      RETURN
   50 J=J1
      GO TO 20
   60 J=J1
      IF (J.LT.I1) GO TO 30
      JF=JF+10
      GO TO 20
      END
```

Figure B-1. (continued) Sample FORTRAN Program and Input Data.

```
      SUBROUTINE SRCH2(X,Y,NX,I1,I2,J1,XI,YI,JFLAG)
      DIMENSION X(I1,I2),Y(I1,I2),NX(I1)
      J=1
      XN=X(J1,J)
      IF (XI-XN) 10,30,20
   10 JFLAG=JFLAG-1
   30 YI=Y(J1,J)
      RETURN
   20 NN=NX(J1)
   40 XO=XN
      J2=J+1
      XN=X(J1,J2)
      IF (XI-XN) 50,70,60
   50 YJ=Y(J1,J)
      YI=YJ+(Y(J1,J2)-YJ)*(XI-XO)/(XN-XO)
      RETURN
   60 J=J2
      IF (J.LT.NN) GO TO 40
      JFLAG=JFLAG+1
      GO TO 30
   70 J=J2
      GO TO 30
      END

      SUBROUTINE FILL(X,Y,NX,T,I1,I2)
      DIMENSION X(I1,I2),Y(I1,I2),T(I1),NX(I1)
      DO 20 J=1,I1
      READ (1,25) NJ,T(J)
   25 FORMAT(I5,F10.0)
      NX(J)=NJ
   20 READ (1,35) (X(J,K),Y(J,K), K=1,NJ)
   35 FORMAT(10F8.0)
      RETURN
      END
```

[Input Data for Above Program's Subroutine FILL]

```
    7   0.
-1.752  -.1     0.024   0.      1.754   .1      3.457   .2      4.975   .3
4.986   .35     4.998   .4
    7   20.
-1.752  -.1     0.024   0.      1.754   .1      3.457   .2      4.975   .2
4.986   .35     4.998   .4
    6   44.7
-1.655  -.1     0.017   0.      1.701   .1      3.232   .2      4.949   .3
4.998   .35
    7   63.1
-1.596  -.1     0.024   0.      1.765   .1      3.232   .2      4.653   .3
4.826   .35     4.998   .4
```

Figure B-2. Program Output from Sample Program of Figure B-1.

```
FOLLOWING (EU,FU,FLAG) FOR TEMP=-10.000
(-2.25,-0.100,-11) (-2.00,-0.100,-11) (-1.75,-0.100,-10) (-1.50,-0.086,-10)
(-1.25,-0.072,-10) (-1.00,-0.058,-10) (-0.75,-0.044,-10) (-0.50,-0.030,-10)
(-0.25,-0.015,-10) ( 0.00,-0.001,-10) ( 0.25, 0.013,-10) ( 0.50, 0.028,-10)
( 0.75, 0.042,-10) ( 1.00, 0.056,-10) ( 1.25, 0.071,-10) ( 1.50, 0.085,-10)
( 1.75, 0.100,-10) ( 2.00, 0.114,-10) ( 2.25, 0.129,-10) ( 2.50, 0.144,-10)
( 2.75, 0.158,-10) ( 3.00, 0.173,-10) ( 3.25, 0.188,-10) ( 3.50, 0.203,-10)
( 3.75, 0.219,-10) ( 4.00, 0.236,-10) ( 4.25, 0.252,-10) ( 4.50, 0.269,-10)
( 4.75, 0.285,-10) ( 5.00, 0.400, -9) (

FOLLOWING (EU,FU,FLAG) FOR TEMP= 10.000
(-2.25,-0.100, -2) (-2.00,-0.100, -2) (-1.75,-0.100,  0) (-1.50,-0.086,  0)
(-1.25,-0.072,  0) (-1.00,-0.058,  0) (-0.75,-0.044,  0) (-0.50,-0.030,  0)
(-0.25,-0.015,  0) ( 0.00,-0.001,  0) ( 0.25, 0.013,  0) ( 0.50, 0.028,  0)
( 0.75, 0.042,  0) ( 1.00, 0.056,  0) ( 1.25, 0.071,  0) ( 1.50, 0.085,  0)
( 1.75, 0.100,  0) ( 2.00, 0.114,  0) ( 2.25, 0.129,  0) ( 2.50, 0.144,  0)
( 2.75, 0.158,  0) ( 3.00, 0.173,  0) ( 3.25, 0.188,  0) ( 3.50, 0.203,  0)
( 3.75, 0.219,  0) ( 4.00, 0.236,  0) ( 4.25, 0.252,  0) ( 4.50, 0.269,  0)
( 4.75, 0.285,  0) ( 5.00, 0.400,  2) (

FOLLOWING (EU,FU,FLAG) FOR TEMP= 30.000
(-2.25,-0.100, -2) (-2.00,-0.100, -2) (-1.75,-0.100, -1) (-1.50,-0.088,  0)
(-1.25,-0.073,  0) (-1.00,-0.059,  0) (-0.75,-0.045,  0) (-0.50,-0.030,  0)
(-0.25,-0.016,  0) ( 0.00,-0.001,  0) ( 0.25, 0.013,  0) ( 0.50, 0.028,  0)
( 0.75, 0.043,  0) ( 1.00, 0.057,  0) ( 1.25, 0.072,  0) ( 1.50, 0.086,  0)
( 1.75, 0.101,  0) ( 2.00, 0.116,  0) ( 2.25, 0.131,  0) ( 2.50, 0.146,  0)
( 2.75, 0.161,  0) ( 3.00, 0.176,  0) ( 3.25, 0.191,  0) ( 3.50, 0.206,  0)
( 3.75, 0.222,  0) ( 4.00, 0.238,  0) ( 4.25, 0.254,  0) ( 4.50, 0.270,  0)
( 4.75, 0.286,  0) ( 5.00, 0.380,  2) (

FOLLOWING (EU,FU,FLAG) FOR TEMP= 50.000
(-2.25,-0.100, -2) (-2.00,-0.100, -2) (-1.75,-0.100, -2) (-1.50,-0.092,  0)
(-1.25,-0.077,  0) (-1.00,-0.062,  0) (-0.75,-0.046,  0) (-0.50,-0.031,  0)
(-0.25,-0.016,  0) ( 0.00,-0.001,  0) ( 0.25, 0.014,  0) ( 0.50, 0.028,  0)
( 0.75, 0.043,  0) ( 1.00, 0.058,  0) ( 1.25, 0.072,  0) ( 1.50, 0.087,  0)
( 1.75, 0.102,  0) ( 2.00, 0.118,  0) ( 2.25, 0.133,  0) ( 2.50, 0.149,  0)
( 2.75, 0.165,  0) ( 3.00, 0.181,  0) ( 3.25, 0.197,  0) ( 3.50, 0.213,  0)
( 3.75, 0.229,  0) ( 4.00, 0.245,  0) ( 4.25, 0.261,  0) ( 4.50, 0.277,  0)
( 4.75, 0.299,  0) ( 5.00, 0.364,  2) (

FOLLOWING (EU,FU,FLAG) FOR TEMP= 70.000
(-2.25,-0.100,  9) (-2.00,-0.100,  9) (-1.75,-0.100,  9) (-1.50,-0.094, 10)
(-1.25,-0.079, 10) (-1.00,-0.063, 10) (-0.75,-0.048, 10) (-0.50,-0.032, 10)
(-0.25,-0.017, 10) ( 0.00,-0.001, 10) ( 0.25, 0.013, 10) ( 0.50, 0.027, 10)
( 0.75, 0.042, 10) ( 1.00, 0.056, 10) ( 1.25, 0.070, 10) ( 1.50, 0.085, 10)
( 1.75, 0.099, 10) ( 2.00, 0.116, 10) ( 2.25, 0.133, 10) ( 2.50, 0.150, 10)
( 2.75, 0.167, 10) ( 3.00, 0.184, 10) ( 3.25, 0.201, 10) ( 3.50, 0.219, 10)
( 3.75, 0.236, 10) ( 4.00, 0.254, 10) ( 4.25, 0.272, 10) ( 4.50, 0.289, 10)
( 4.75, 0.328, 10) ( 5.00, 0.400, 11) (
```

is used. Similar increases or decreases in JF are performed by SRCH2 if the input EU value is high or low relative to the calibration data; however, SRCH2 increments JF by only ± 1. This allows us to determine from the single flag JF the two different types of out-of-calibration-range errors which can occur in the linear-linear interpolation.

REFERENCES

1. _____, "GEOS-C Radar Altimeter Systems Calibrations and Test Data Requirements," 16 January 1974, Applied Science Associates, Apex, N. C., prepared under Contract No. NAS6-2307 for National Aeronautics and Space Administration, Wallops Flight Center.

2. Roback, J. E. and E. L. Hofmeister, "Electrical Performance Test Procedure (EPTP): Volume I - Procedure, Revision B." 13 May 1974, General Electric Company, Utica, N. Y., prepared under Contract No. APL372165 for the Applied Physics Laboratory of the John Hopkins University, Silver Spring, Md.

3. Plonisch, I. and E. L. Hofmeister, "GEOS-C Flight Radar Altimeter: Level 1b Test (Pre-Vib, Post-Vib & Thermal Vacuum); Transmitter Peak Power Measurements (Pre-Vib and TAMS #1 Reference); and Special Tests [V(IF/C) and V(CL)]," 13 December 1974, General Electric Company, Utica, N. Y., prepared under Contract No. APL372165 for the Applied Physics Laboratory of the John Hopkins University, Silver Spring, Md.

4. Roback, J. E. and E. L. Hofmeister, "Electrical Performance Test
4a Procedure (EPTP): Volume II - Data Sheets, Revision B; Flight Radar
4b Altimeter," 13 December 1974, General Electric Company, Utica, N. Y.,
4c prepared under Contract No. APL372165 for the Applied Physics Laboratory
4d of the Johns Hopkins University, Silver Spring, Md. [Note - The EPTP data sheets have been separated into four volumes. These will be referred to either collectively as Reference 4 or individually according to the following: Reference 4 denotes Level 4 Test Data at VAC/-2°C; Reference 4b denotes Level 4 Test Data at VAC/+42°C; Reference 4c denotes Level 4 Test Data at Final Ambient (in TV Chamber); and Reference 4d denotes the AGC Data for Thermal Vacuum and Final Ambient].

5. Miller, L. S. and G. S. Brown, "Engineering Studies Related to the GEOS-C Radar Altimeter; Final Report for Task D," Applied Science Associates, Inc., Apex, N. C., May 1974, prepared under Contract No. NAS6-2307 for National Aeronautics and Space Administration, Wallops Flight Center.

6. Brown, P. D. and S. Vincent, "Power Spectrum of Geoid Undulation," Paper Presented at Am. Geophys. Union Meeting, San Francisco, Cal., December 1972.

REFERENCES (Cont.)

7. McGoogan, J. T., C. D. Leitao, L. S. Miller, and W. T. Wells, "SKYLAB S-193 Altimeter Experiment: Performance, Results, and Applications," Paper Presented at International Symposium on Marine Geodesy, Columbus, Ohio, 1974.

8. Brown, G. S., " A Closed Form Relation for the Average Return Waveform From a Near-Nadir Pointed, Short Pulse, Satellite Based Radar Altimeter," Paper Presented at the USNC/URSI Conference, Boulder, Colorado, Oct. 1974.

9. "GEOS-C Summary Phase I Technical Report, Volume I," 31 May 1972, General Electric Company, Utica, N. Y., Prepared under Contract No. APL372085 for the Applied Physics Laboratory of the Johns Hopkins University, Silver Spring, Md. See pg. 18 (System Performance Specifications).

10. Davenport, W. B. Jr. and W. L. Root, An Introduction to the Theory of Random Signals and Noise, McGraw-Hill Book Co., New York, 1958, page 168.

11. Berger, T., "Satellite Altimetry Using Ocean Backscatter," IEEE Trans. on Ant. & Propog., Vol. AP-20, pp. 295-309, May 1972.

12. Papoulis, A., Probability, Random Variables, and Stochastic Processes, McGraw-Hill Book Co., New York, 1965, p. 197.

13. Nitzberg, R., "Limitations Of a Variance Approximation," IEEE Trans. on Aerosp. & Elect. Vol. AES-8, pp. 246-247, March 1972.